

**POLITECNICO DI MILANO**

Master of Science in Mechanical Engineering

School of Industrial and Information Engineering



**A Novel Shape Display for Physical Interaction with  
Virtual Surfaces**

Supervisor: Prof. MONICA BORDEGONI  
Co-supervisor: Prof. UMBERTO CUGINI  
Ing. ALESSANDRO MANSUTTI

Graduation thesis of:  
LUCA PELLEGRINO  
ID 824061

Academic Year 2015 - 2016





## *Ringraziamenti*

*Vorrei esprimere la più profonda gratitudine al relatore della mia tesi, la professoressa Monica Bordegoni, per avermi dato la possibilità di affrontare un argomento a me così caro e per avermi seguito durante lo svolgimento senza mai limitare la mia passione di scegliere, provare, magari sbagliare, ma alla fine arrivare ad un risultato seguendo le mie idee.*

*Desidero inoltre ringraziare il professore emerito Umberto Cugini, nonché correlatore della mia tesi, per tutti i preziosi consigli e per le lunghe e costruttive discussioni, esperienze che porterò sempre con me nella mia carriera lavorativa.*

*Uno dei grazie più grandi lo devo al correlatore e ora anche amico Ing. Alessandro Mansutti per tutti questi mesi passati insieme a trovare soluzioni e per avermi saputo ricordare ogni giorno che per quanto sia emozionante fantasticare, bisogna sempre mantenere il senso pratico di tutto ciò che si progetta.*

*Non posso non ringraziare tutti i miei amici e tutte le persone a me care, Micol, Francesco L., Francesco C., Giacomo, Sal, Pietro, Riccardo, Pietro, Simone, Giorgio, Federico, Marco, Nicola, Mattia S., Mattia P. A tutti quanti, tutte le persone che ho incontrato fino a questo importante momento della mia vita, anche a voi che non ci siete più, a tutti voi devo un ringraziamento enorme, perchè avete contribuito a gettare le fondamenta della persona sarò e, nel bene o nel male, avete partecipato in questo successo, a voi devo la persona che sono oggi.*

*Infine, il ringraziamento più grande di tutti. A mia madre e mio padre, i genitori migliori che possano esistere. Mi avete sempre guidato e siete sempre stati al mio fianco, sostenendo tutte le mie scelte.*



# Contents

<b>List Of Figures</b>	<b>xii</b>
<b>Estratto della tesi</b>	<b>xvii</b>
<b>1 Introduction</b>	<b>1</b>
<b>2 Research Field Background</b>	<b>5</b>
2.1 Engineering Design Process . . . . .	5
2.1.1 Conceptual Design . . . . .	6
2.1.2 Traditional product design process . . . . .	7
2.1.3 Proposed product design process . . . . .	8
2.2 Surface Exploration . . . . .	9
2.3 Related Works . . . . .	10
2.3.1 Local Surface Display . . . . .	10
2.3.2 Full Shape Display . . . . .	11
2.4 Previous research context: SATIN system . . . . .	13
2.4.1 Issues and problems to solve . . . . .	14
2.4.2 New System Specification and architecture . . . . .	18
2.4.3 Attempt to re-engineering the SATIN . . . . .	19
<b>3 Design Strategy</b>	<b>23</b>
3.1 Problem definition . . . . .	24
3.2 Geometric formulation . . . . .	25
3.2.1 Input data: STL file format . . . . .	25
3.2.2 Managing and controlling virtual surfaces . . . . .	25
3.3 Analytical approach . . . . .	27
3.3.1 Polynomial regression . . . . .	27
3.3.2 Analytical description of the frame . . . . .	28

3.4	Surface-control points interaction . . . . .	34
3.4.1	NURBS curve ans strip control . . . . .	34
3.4.2	Accuracy of the approximation: degrees of freedom . . . . .	35
3.5	Surface displacement prediction . . . . .	36
3.5.1	Kirchhoff theory of plates . . . . .	37
3.5.2	Finite element method approach . . . . .	38
3.6	Final algorithm construction . . . . .	44
3.6.1	Definition of an error function . . . . .	44
3.6.2	Functioning principle . . . . .	47
<b>4</b>	<b>Physical Interface Design</b>	<b>51</b>
4.1	Initial considerations . . . . .	51
4.1.1	Reducing d.o.f. . . . .	52
4.1.2	Overview on actuating system . . . . .	52
4.2	Device structure and kinematic analysis . . . . .	55
4.2.1	Servomotor control . . . . .	58
4.2.2	x y and z actuating system . . . . .	59
4.2.3	$\theta_1$ and $\theta_2$ actuating system . . . . .	65
4.3	Components sizing . . . . .	65
4.3.1	Rack-pinion system for vertical degree of freedom . . . . .	66
4.3.2	Four bar linkage design . . . . .	68
4.3.3	Z servomotor bracket design . . . . .	69
4.4	Final model . . . . .	72
<b>5</b>	<b>Model Validation</b>	<b>75</b>
5.1	Numerical test . . . . .	75
5.1.1	Results discussion . . . . .	77
5.2	Prototyping . . . . .	82
5.2.1	Control board . . . . .	85
5.3	Experimental test . . . . .	86
5.3.1	Photogrammetry . . . . .	88
5.3.2	Accuracy of the experimental setup . . . . .	91
5.3.3	Evaluation protocol . . . . .	91
5.4	Example test . . . . .	92
5.4.1	Saddle shape . . . . .	92
5.4.2	Results discussion . . . . .	99
<b>6</b>	<b>Conclusions</b>	<b>103</b>
6.1	Future improvements . . . . .	106
	<b>Appendices</b>	<b>107</b>

---

<b>Appendix A</b>	<b>Experimental test results</b>	<b>109</b>
A.1	Test 1 . . . . .	109
A.2	Test 2 . . . . .	114
A.3	Test 3 . . . . .	119
<b>Appendix B</b>	<b>Algorithm implementation</b>	<b>125</b>
<b>Appendix C</b>	<b>Technical drawings</b>	<b>131</b>
<b>Bibliography</b>		<b>137</b>



# List of Figures

1.1	Engineering design process. . . . .	3
2.1	Traditional design process. . . . .	7
2.2	Proposed design process. . . . .	8
2.3	Concept of the SATIN system . . . . .	14
2.4	SATIN strip displacements . . . . .	16
2.5	Control points . . . . .	16
2.6	SATIN prototype . . . . .	17
2.7	Desktop version of the SATIN . . . . .	20
3.1	Components for the mathematical problem . . . . .	24
3.2	example and definition of an STL file . . . . .	26
3.3	Bézier surface with control points . . . . .	26
3.4	Variance decreasing with polynomial order . . . . .	29
3.5	Components for the mathematical problem: virtual surface . . . . .	30
3.6	Basic concept of shapeshifting patch and control points . . . . .	30
3.7	Single frame elements and control points coordinates . . . . .	31
3.8	Control points kinematic constraints and local deformed shape . . . . .	36
3.9	final control point configuration (in blue the 5 d.o.f.) . . . . .	37
3.10	Physical surface measures . . . . .	40
3.11	Ashby's diagram . . . . .	42
3.12	Honeycomb principal directions . . . . .	43
3.13	Components for the mathematical problem: physical surface . . . . .	44
3.14	Components for the mathematical problem: error function . . . . .	47
3.15	Algorithm . . . . .	48
3.16	Bilinear function for the frame . . . . .	49
3.17	NURBS approximation . . . . .	49
3.18	Honeycomb displacement prediction . . . . .	50
4.1	Frame positioning d.o.f. . . . .	53
4.2	Reduced d.o.f. number . . . . .	53

4.3	Degrees of freedom for a cartesian actuating system . . . . .	54
4.4	Degrees of freedom for a relative actuating system . . . . .	55
4.5	Concept of a quadrilateral element . . . . .	56
4.6	Kinematic chain in x-z plane . . . . .	56
4.7	Kinematic chain in y-z plane . . . . .	58
4.8	Schematic diagram of servo system [31] . . . . .	59
4.9	Block diagram of servo system [31] . . . . .	60
4.10	X-Y positioning . . . . .	61
4.11	Ball screw scheme . . . . .	62
4.12	Concept of x-y actuating system . . . . .	63
4.13	Direct motor coupling . . . . .	63
4.14	Spur geared transmission . . . . .	64
4.15	Vertical movement of the module . . . . .	64
4.16	Slope control: housing for $\theta_1$ . . . . .	65
4.17	Slope control: housing for $\theta_2$ . . . . .	66
4.18	Approximation for the $z$ rack-pinion coupling . . . . .	66
4.19	Tilting servomotor characteristics . . . . .	69
4.20	Module initial concept . . . . .	70
4.21	Module with bracket . . . . .	71
4.22	IPE beam nomenclature . . . . .	71
4.23	FEM analysis on IPE <i>H-section</i> beam . . . . .	72
4.24	IPE displacements . . . . .	72
4.25	Final concept of the tactile device . . . . .	73
5.1	Car bonnet . . . . .	76
5.2	Simplified shape of a generic car bonnet . . . . .	76
5.3	Initial undeformed configuration . . . . .	77
5.4	Polynomial surface interpolation . . . . .	77
5.5	Control strips approximation . . . . .	78
5.6	Comparison between control strips and virtual surface . . . . .	78
5.7	Finite element surface displacement prediction . . . . .	79
5.8	Error function: gap on nodal vertical displacement . . . . .	79
5.9	Error function: gap on first derivative in $x$ direction . . . . .	80
5.10	Error function: gap on first derivative in $y$ direction . . . . .	80
5.11	Error function: gap on second derivative in $x$ direction . . . . .	81
5.12	Error function: gap on second derivative in $y$ direction . . . . .	81
5.13	Error function: gap on mixed second derivative . . . . .	82
5.14	Components CNC machining . . . . .	84
5.15	Linear bearing housing within the nuts . . . . .	84
5.16	Simplified H-section IPE beam . . . . .	85
5.17	Assembly of a module . . . . .	86
5.18	Rack-pinion transmission system . . . . .	87
5.19	Regulation system . . . . .	87



5.20	Final prototype . . . . .	88
5.21	Control board and power supply housing . . . . .	88
5.22	Manual movement board . . . . .	89
5.23	Lynxmotion controller . . . . .	89
5.24	PWM signal relations . . . . .	90
5.25	Main parameters in camera acquisition . . . . .	90
5.26	Monkey saddle surface: $z = x^3 - 3xy^2$ . . . . .	93
5.27	Saddle CAD geometry . . . . .	93
5.28	Tactile device positioning . . . . .	94
5.29	Acquired photogrammetry mesh . . . . .	95
5.30	Median lines of control strips . . . . .	95
5.31	Experimental comparison on strip 1 . . . . .	96
5.32	Experimental comparison on strip 2 . . . . .	96
5.33	Experimental comparison on strip 3 . . . . .	97
5.34	Experimental comparison on strip 4 . . . . .	97
5.35	Experimental comparison on strip 5 . . . . .	98
5.36	Experimental comparison on strip 6 . . . . .	98
5.37	Experimental comparison on strip 7 . . . . .	99
5.38	Control points placement: positioning error in $x$ , $y$ and $z$ direction . . . . .	101
A.1	Small concave surface . . . . .	110
A.2	Device arrangement . . . . .	110
A.3	Test1: Experimental comparison on strip 1 . . . . .	111
A.4	Test1: Experimental comparison on strip 2 . . . . .	111
A.5	Test1: Experimental comparison on strip 3 . . . . .	112
A.6	Test1: Experimental comparison on strip 4 . . . . .	112
A.7	Test1: Experimental comparison on strip 5 . . . . .	113
A.8	Test1: Experimental comparison on strip 6 . . . . .	113
A.9	Test1: Experimental comparison on strip 7 . . . . .	114
A.10	Small convex surface . . . . .	114
A.11	Device arrangement . . . . .	115
A.12	Test2: Experimental comparison on strip 1 . . . . .	115
A.13	Test2: Experimental comparison on strip 2 . . . . .	116
A.14	Test2: Experimental comparison on strip 3 . . . . .	116
A.15	Test2: Experimental comparison on strip 4 . . . . .	117
A.16	Test2: Experimental comparison on strip 5 . . . . .	117
A.17	Test2: Experimental comparison on strip 6 . . . . .	118
A.18	Test2: Experimental comparison on strip 7 . . . . .	118
A.19	Wide convex surface . . . . .	119
A.20	Device arrangement . . . . .	119
A.21	Test3: Experimental comparison on strip 1 . . . . .	120
A.22	Test3: Experimental comparison on strip 2 . . . . .	120
A.23	Test3: Experimental comparison on strip 3 . . . . .	121

A.24 Test3: Experimental comparison on strip 4 . . . . .	121
A.25 Test3: Experimental comparison on strip 5 . . . . .	122
A.26 Test3: Experimental comparison on strip 6 . . . . .	122
A.27 Test3: Experimental comparison on strip 7 . . . . .	123
C.1 Mechanical slide . . . . .	132
C.2 C-section IPE beam . . . . .	133
C.3 Glide Plate . . . . .	134
C.4 Module exploded view: Bill Of Material (BOM) . . . . .	135

---

## Sommario

Lo sviluppo di nuovi prodotti è un processo a cui le aziende dedicano la maggior parte delle proprie risorse con l'unico scopo di massimizzare la soddisfazione del cliente, e il compito di reinventare prodotti fatti su misura dell'utente è affidata all'esperienza dei progettisti, i quali utilizzano gran parte del tempo a disposizione per creare modelli digitali tridimensionali, strettamente legati ad un aspetto visivo, per poi valutarli a valle della fase di realizzazione di un prototipo fisico. Qualora il concept non dovesse soddisfare i requisiti del progetto, i progettisti devono tornare alla fase di modellazione e adattare il modello digitale tenendo conto dei feedback, per poi costruire nuovamente un prototipo necessario per le valutazioni. Questo processo iterativo causa un eccessivo incremento dei tempi e costi di sviluppo del prodotto. Per migliorare la competitività delle aziende sarebbe conveniente spostare la fase di valutazione ed effettuarla simultaneamente con la fase di modellazione.

Pertanto, questa tesi mira a sviluppare un nuovo dispositivo, basato sull'idea di superfici in grado di cambiare la propria forma, e quindi capace di rappresentare varie superfici virtuali in modo tale da ridurre perdite di tempo e soldi legate alla costruzione di diversi prototipi. Come prima cosa, questo lavoro propone una trattazione matematica rigorosa per prevedere come una superficie fisica si possa deformare per adeguarsi ad una virtuale. È stato utilizzato quindi un approccio modulare innovativo basato sul concetto di punti e curvature di controllo. Uno degli aspetti più critici di questa ricerca è stata la scelta di una adeguata tipologia di materiale per la superficie fisica. È stato introdotto un modello ad elementi finiti adatto alla previsione della deformazione della superficie fisica, necessaria per costruire una funzione d'errore atta a minimizzare la differenza tra le componenti delle superfici virtuali e quelle fisiche, massimizzando quindi l'accuratezza della rappresentazione.

La fase di valutazione sperimentale è stata coadiuvata dalla costruzione di un prototipo semplificato del dispositivo progettato, utilizzato per confrontare il modello su forme semplici largamente utilizzate nel design di prodotto. Inoltre è stato affrontato un test numerico su una applicazione industriale reale. Il caso applicativo fa riferimento alla rappresentazione di un cofano d'automobile attraverso l'utilizzo di una formulazione con ampio insieme di variabili.

**Parole chiave:** display tattile, interazione fisica, dispositivi aptici, realtà virtuale, superfici virtuali



---

## Abstract

Development of brand new products is a process on which companies focus the majority of their resources in order to maximize customers satisfaction, and the capability of thinking up new products tailored on user desires relies on the experience of industrial designers which spend a lot of time in routine-based tasks. These design processes are based on the creation of 3D digital models, strictly related to the visual aspect, and finally evaluated after the construction of a mockup. Whether the concept doesn't fit the project requirements, product designers have to go back to the modeling phase and adapt the digital model entailing a new physical prototype for further evaluations. This iterative process leads to an overall increase of development costs. To improve companies competitiveness would be suitable to move backward the tactile evaluation and perform it at the same time of the modeling phase.

Hence, this thesis aims to develop a new device based on the idea of shape-shifting surfaces, able of rendering virtual surfaces in order to reduce losses of time and costs related to several concept construction. First of all, this work propose a rigorous mathematical model to predict the deformation of a physical surface needed to approximate the virtual one. An innovative modular approach based on points and curvatures control has been used. One of the most critical issue of this research field regards the choice of the physical surface. A finite element model has been used to predict the warping of the physical surface and to build an error function between virtual surface characteristics and physical ones that can ensure the maximum accuracy of the representation.

A simplified prototype has been built to test basic shape features commonly used in industrial design field. Moreover a numerical test on a real industrial application case has been performed. The case is related to the approximation of a car bonnet by the means of an extended variables set problem.

**Keywords:** shape display, physical interaction, haptics, virtual reality, virtual surfaces



## Estratto della tesi

Lo sviluppo di un nuovo prodotto è un processo estremamente complesso che si affida all'esperienza di progettisti ed ingegneri. Una larga parte di questo processo è dedicato all'invenzione di nuove curve di stile, le quali impatteranno significativamente sull'esperienza di utilizzo dell'utente.

Al giorno d'oggi i progettisti sono fortemente supportati da diversi strumenti, sia informatici che non, per la creazione e la valutazione di forme e superfici, e, sebbene questi strumenti siano largamente accettati da tutta la comunità dei progettisti, essi rimangono legati ad un aspetto strettamente visivo del progetto, ovvero ad un settore della *realtà virtuale* (VR). Al contrario i progettisti sono soliti scegliere un modo diretto di valutazione delle forme, prettamente tattile, pertanto essi hanno bisogno di *interagire fisicamente* con lo sviluppo delle curve in modo tale da verificare gli aspetti geometrici in maniera intuitiva e naturale. Per questo motivo il prototipo è un concetto imprescindibile nel processo di progettazione.

Come suggerito dall'approccio sistematico di Pahl & Beitz, la progettazione ingegneristica si svolge attraverso alcuni momenti essenziali, e lo sviluppo di nuove forme si posiziona a metà del *conceptual design* attraverso un processo iterativo partendo con la formalizzazione delle idee, fissate nella fase precedente (*tasks clarification*), attraverso schizzi e disegni manuali utilizzati poi per realizzare modelli digitali del prodotto in questione, i quali permettono ai progettisti di effettuare la prima ed importante valutazione visiva della forma e delle caratteristiche geometriche. Successivamente viene realizzato un modello fisico dell'oggetto, necessario per valutarne la fattibilità e i parametri globali di progetto; se poi questi parametri non dovessero essere soddisfatti, o anche se solo le forme stesse non dovessero raggiungere gli standard richiesti, allora il progettista riparte dai disegni per realizzare nuove forme digitali ed un nuovo prototipo. Quindi prima di raggiungere una rappresentazione finale del prodotto in analisi vengono svolti parecchi cicli di progettazione, che comporta la realizzazione di molti prototipi fisici. È importante sottolineare come, ogni volta che si rende necessario lo sviluppo di un prototipo, viene sottratto del tempo-macchina alla produzione e si presentano considerevoli tempi d'attesa e ritardi, quindi è evidente come questo processo iterativo abbia un impatto enorme sui tempi ed i costi di progettazione.

---

Per risolvere questo problema sarebbe necessario spostare la fase di valutazione tattile in modo tale da effettuarla simultaneamente con la fase di modellazione digitale e valutazione visiva, senza quindi una reale necessità di costruzione di un prototipo fisico, ma per riuscirci serve sviluppare un sistema capace di rappresentare in real-time le forme del modello digitale. La comunità di ricerca ha sviluppato diverse soluzioni a questo problema e alcune di esse sono state commercializzate come veri e propri dispositivi, però la maggior parte di essi sono basati su una valutazione a posteriori di una interazione puntuale e locale, o al più capaci di far interagire l'utente con la superficie virtuale tramite l'utilizzo di un solo dito, rappresentando quindi piccole porzioni dell'oggetto interessato. Queste interfacce quindi da considerarsi affidabili solo nel caso in cui l'aspetto in analisi sia una peculiarità locale mentre non possono essere considerati attendibili per una valutazione globale.

Alcuni tentativi atti a risolvere la questione sono stati condotti da soli gruppi di ricerca. Per esempio, Iwata et. al [16] nello sviluppo del progetto *FEELEX* hanno disquisito di un superficie deformabile guidata dal controllo di pin verticali, ma è evidente che questa tecnica di approccio al problema comporta forti limitazioni nel campo delle possibili superfici virtuali rappresentabili. Metodologie simili sono state proposte dall'università TU di Monaco di Baviera [18] e dal Massachusetts Institute of Technology [23]. Per quanto riguarda il campo dei dispositivi a risoluzione variabile, sono stati condotti degli studi dal gruppo di ricerca KAEMaRT del Politecnico di Milano durante lo sviluppo del sistema *SATIN* (nel contesto del progetto europeo EU-IST-FP6 SATIN) e successivamente da Bordegoni, Covarrubias et. al [10], necessari all'esplorazione di oggetti virtuali, mantenendo però l'implicita limitazione di un dispositivo per l'analisi della curvatura locale, in grado di rappresentare le sole traiettorie identificate da un piano di taglio attraverso l'uso di una strip geodetica.

Lo scopo di questa tesi è quello di proporre un nuovo e più profondo approccio al campo dei dispositivi per la rappresentazione di superfici complete e di sviluppare un prototipo di dispositivo in grado di soddisfare tutte le caratteristiche necessarie alla rappresentazione di molteplici superfici. Questo approccio intende favorire l'eliminazione di attività ripetitive ed iterative e la riduzione delle procedure necessarie al lancio di un nuovo prodotto sul mercato, incoraggiando l'innovazione e sviluppo di nuove frontiere per la progettazione ingegneristica, fino ad arrivare alla possibilità di sviluppare nuovi prodotti industriali progettati su misura per gli utenti. In particolare, questa tesi intende dimostrare che l'utilizzo di una modellazione matematica intelligente può a tutti gli effetti migliorare le prestazioni di rappresentazione e flessibilità dell'applicazione, infatti una scelta sbagliata del modello approssimante e del metodo di ottimizzazione potrebbe sfociare in problematiche legate all'eccessivo onere computazionale in termini di tempo, limitando quindi il vantaggio di rimuovere i suddetti processi iterativi.

La progettazione di questo moderno dispositivo sarà incentrata sulle principali caratteristiche necessarie ad ottenere un apparato utilizzabile anche in piccoli



---

studi di progettazione o addirittura da singoli utenti. Quindi risulta evidente come le caratteristiche principali di questo dispositivo devono essere la possibilità di personalizzazione, facilità di trasporto, la espandibilità del sistem ed un prezzo relativamente contenuto, mantenendo in ogni caso elevate prestazioni di rappresentazione delle superfici virtuali. Il fatto di poter essere trasportato facilmente risulta necessario per ottenere un dispositivo direttamente integrabile in un comune spazio di lavoro, senza rivoluzioni drastiche delle condizioni lavorative, ed inoltre un costo relativamente basso porterà ad ottenere un sistema conveniente e facilmente combinabile con le tipiche modalità di lavoro. Per quanto riguarda gli aspetti di personalizzazione e espandibilità, necessari per andare incontro alle differenti realtà industriali delle aziende, essi saranno garantiti da un approccio alla progettazione di tipo modulare. Infine, per quanto riguarda le prestazioni di rappresentazione, lo studio del dispositivo deve essere portato avanti ponendo particolare attenzione ai raggi di curvatura in prossimità dei punti di controllo i quali, come affermato in studi precedenti [37], hanno un forte impatto sulla qualità del risultato. L'efficacia di questo criterio sarà verificata su un caso applicativo di una tipica situazione industriale. Qualora la valutazione effettuata su un piccolo prototipo dovesse mostrare risultati apprezzabili, un caso applicativo confermerà definitivamente che il modello proposto ha reali possibilità di affermarsi come la tecnologia del futuro.

Le attività sono state organizzate come segue:

- **Capitolo 2:** Il capitolo introduce gli argomenti principali di questa tesi. Intende descrivere come gli umani percepiscono il senso del tatto e quale sia il ruolo delle forme nella percezione umana, cosa sia l'esplorazione di superfici e come un dispositivo di rappresentazione superfici complete possa perfezionare la fase di *conceptual design*. Viene inoltre presentato un breve stato dell'arte.
- **Capitolo 3:** Nel capitolo viene presentata una possibile formulazione analitica del problema in cui ci si concentra sulla definizione di una funzione d'errore necessaria a massimizzare l'accuratezza dell'approssimazione. Inoltre viene proposto un nuovo approccio basato sul controllo delle curvature.
- **Capitolo 4:** Nel capitolo viene discussa una possibile soluzione per il dispositivo fisico e il dimensionamento dei relativi componenti.
- **Capitolo 5:** Descrizione della fase sperimentale, sia dei test numerici che dei test sul prototipo. In aggiunta viene riportata una breve discussione dei risultati ottenuti.
- **Capitolo 6:** Il capitolo presenta una ampia discussione finale dei risultati ottenuti e possibili sviluppi futuri della tematica



# 1

## Introduction

Development of a new industrial product is an extremely complex process relying significantly on the experience of designers and engineers. A huge part of this process is dedicated to think up new kind of styling curves which will have the very first impact on user experience.

Nowadays designers are highly supported by many tools, such as computer aided ones, for shape creation and evaluation and, although this tools are widely used in the product design community, they remain strictly related to the visual side of the project and to the *Virtual Reality* (VR). However, designers usually choose a direct way of shape evaluation granted by means of the sense of touch. Indeed they need to *physically interact* with the products evolving shapes in order to check their geometric features in a natural and intuitive manner. Therefore a physical prototype is a necessary part of the design process to deal with.

As suggested by Pahl & Beitz systematic approach, engineering design passes through some important stages (cf.figure 1.1) and the development of new surfaces settles in the middle of the *conceptual design* where an iterative process takes place: it begins with the formalisation of the ideas fixed in the previous phase (tasks clarification) with hand drawings and free sketching. Those are used to

create digital models of the products that allow the designer to perform the visual evaluation of the shape and its geometric features. Then the physical mock-up is built to check the feasibility and overall project parameters and if the model doesn't meet the requirements a new concept has to be developed. Hence, before reaching a final product representation, several loops are carried out and thus several physical prototypes are developed during the design process. Moreover, each time a physical mock-up is required, project lead time is affected by stops and delays, then it's easy to see why this iterative loop has a strong impact on development time and costs.

To overcome this issue is necessary to move backwards the tactile evaluation in order to allow the designers to perform it simultaneously with the modelling phase and without a real need of a physical mock-up. To achieve this goal, it is necessary to develop a system capable to render in real-time the shape of the digital model. The research community has developed several solutions and some of them have also been introduced as commercial devices. However, the majority of these devices are based on point-based interaction, or are able to allow users to interact with *virtual surfaces* only with a single finger, or are able to render only small portions of virtual shapes. All of those interfaces are useful whether the aim of the analysis is the local feature while they cannot be considered as suitable one for a global evaluation.

Some attempts to find a solution with a patch display has been carried out by many research group. For example, Iwata et. al [16] in the project FEELEX have discussed about a deformable surface guided by vertical pins, but this problem approach has a strong limitation in representable surfaces range due to fix resolution of the display. Similar approaches has been proposed by TU München university [18] and Massachusetts Institute of Technology [23]. Variable resolution shape display has been studied also by the research KAEMaRT Group of Politecnico di Milano university with the development of the SATIN system (in the framework of the EU-IST-FP6 SATIN project) and then by Bordegoni, Covarrubias et. al [10], to achieve the exploration of virtual object but with the implicit limitation of a local shape display able to represent only trajectories traced by the geodesic strip.

The purpose of this thesis is to propose a new and wider approach to the patch tactile displays field and to develop a prototype able to fulfill the required features necessary to render a surface. This approach will promotes the elimination of routine-like tasks, the reduction of time-to-market procedures encouraging the innovation and future paths of engineering design, leading to new, user-inspired, industrial products. Furthermore this thesis wants to demonstrate that the usage of a smart mathematical methodology can actually improve the rendering performance and the flexibility of the applications, indeed a wrong choice of the approximating model and optimization method may come out with expensive computational time or limit the output to non-implicit surfaces. Same steps of previous studies has been followed to establish the layout of this dissertation. The

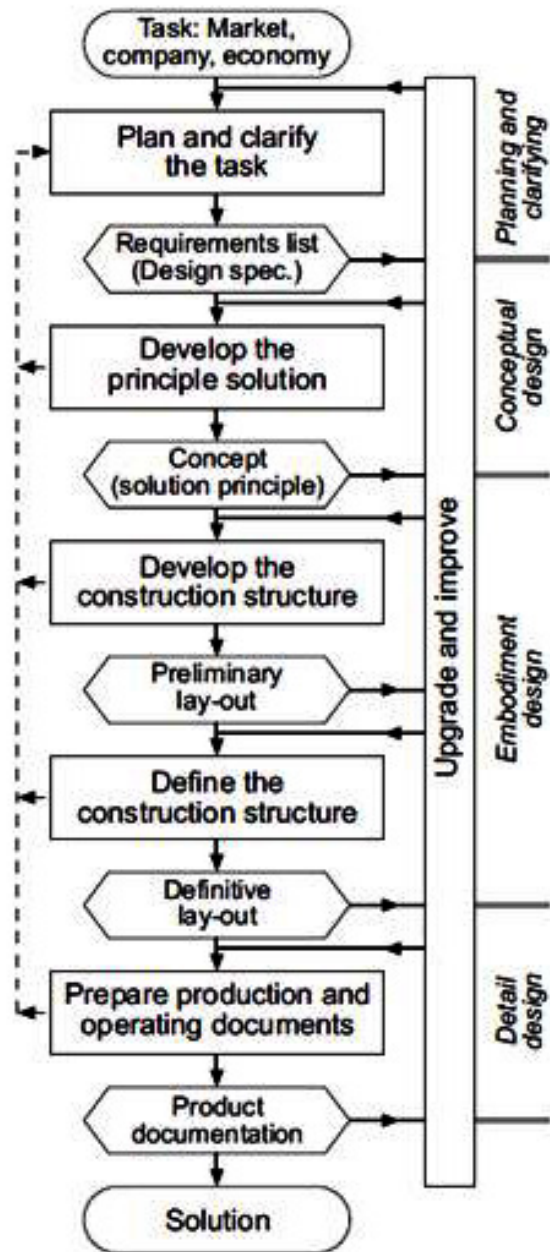


Figure 1.1: Engineering design process.

design of this brand new system will be focused on the main features needed to obtain a device that can be used also by small design studios or by a single user. So the tactile display has to be portable, customisable, expandable, relatively low cost, and has to ensure high performance rendering. The portability characteristic will ensure to obtain a device directly usable in a common workspace, and the low cost feature will lead to an affordable system that can be combined to typical working routine (i.e. no invasive change in working conditions). For what concerns the customisation and expandability aspect, necessary to meet different working reality conditions, it will be obtained by means of a modular approach. Regarding the rendering performance, tactile display design has carried out paying attention to curvature radii beside control points which, as stated in previous studies [37], have a strong impact on output quality. The effectiveness of this approach will be checked with an example of typical industrial situation: whether the evaluation on a small prototype will show appreciable results, a use case will definitely confirm that the model has real chances to establish as the future leading technology.

The activities will be organized as follow:

- **Chapter 2:** This chapter introduces the main topics of this thesis. it describes how humans perceive sense of touch and what is the shape role in human perception, what surface exploration is and how a patch display can improve engineering conceptual design. A brief state of the art will also be presented.
- **Chapter 3:** An analytical formulation for the problem will be given. The focus is on the formulation of an error function needed to maximize the approximation accuracy. Furthermore, a new approach based on curvature control will be proposed.
- **Chapter 4:** In this chapter will be discussed a possible solution for the physical device and its components design.
- **Chapter 5:** Description of the experimental phase, of the prototype construction and a brief discussion and comparison of results.
- **Chapter 6:** A final discussion on achieved results and possible future implementation.

# 2

## Research Field Background

This chapter specifies and introduces main topics related to this work:

- Brief introduction to engineering design process
- Surface exploration

After that a state of the art of tactile displays will be presented, showing also the methods and tools with whom they interact with VR environments.

### **2.1 Engineering Design Process**

The mechanical design of a product consists in the solution of a design problem from the assignment to final product design. As suggested by Pahl [33] (and with reference to the above mentioned figure 1.1), design process work flow of mechanical product can be divided in the following main phases:

- Planning and task clarification

- Conceptual design
- Embodiment design
- Detail design

The first step is necessary to clarify the given tasks in detailed way and collect information about the requirements that have to be fulfilled by the product. The input is often based on a customer specification. The result of this activity is the requirement list, on which the subsequent phases should be based on. In the conceptual design step usually is determined the principle solution(concept) that can be represented in the form of a final mock-up. After the concept, the design process follows with the embodiment design step: starting from the concept, it aims to define rough structural dimension of the product, in accordance with technical, economic and aesthetic considerations. All of these tasks consist in the detailed design, whose specifications and information are formalized in technical documentation for production.

### 2.1.1 Conceptual Design

The activities in the preliminary and conceptual phases differ from the latter detailed design work [43]. Detailed design requires to employ generally well-established tools to solve problems which have been well-specified in form or structure beforehand. The conceptual phase concerns the problem of coming up with new ideas or new solutions to older problems. Good conceptual design means innovation, and an innovative design comes about when one deliberately tries to create one. The issue in conceptual design theory is to understand the processes which lead to innovation and to create tools which generate such step changes in function of an orderly and repetitious basis. Processes for conceptual design are currently typified by "Buhl's Seven Steps" which are shown in table 2.1.

STEP	DESCRIPTION
<b>Recognition</b>	Recognize that a problem exists and decide to do something about it
<b>Definition</b>	Define problems in familiar terms and symbols. Dissect into sub-problems. Determine limitations and restrictions
<b>Preparation</b>	Compile past experience in the form of data, ideas, opinions, assumptions
<b>Analysis</b>	Analyse preparatory material in view of defined problems and evaluation that could bear on the problem
<b>Synthesis</b>	Develop a solution, or solutions, from developed information
<b>Evaluation</b>	Evaluate possible solutions. Verify and check all facets of the solution. Reach a decision
<b>Presentation</b>	Plan a strategy for convincing others and carry it out

Table 2.1: Buhl's steps to conceptual design



It's easy to understand that in the last evaluation step settles the above mentioned iterative process, where designers need a proper mock-up for the geometric, aesthetic and functionality features of the concept. The figure 2.1 shows up the traditional iterative product design process, and in figure 2.2 is established the new layout that this thesis aims to confirm as the future leading process, moving backward the tactile evaluation and thus saving time and money spent on the mock-up.

### 2.1.2 Traditional product design process

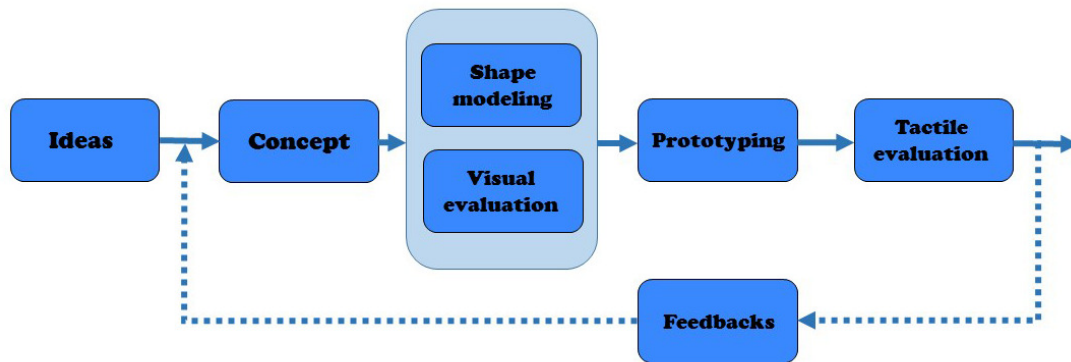


Figure 2.1: Traditional design process.

The design process of products, especially for what it concerns shape and geometric feature of a product, could be ideally divided into five different moments, referring to figure 2.1:

- **Concept design:** starting from the clarified ideas leading the project, designers contrive the product concept with basic features and bring it to life with some free sketching, which show the main characteristics of the shape.
- **Shape modelling:** The modelling phase, where the shape of the product is represented by using IT tools like CAD models. Here the designer manages the shape and the overall features thanks to different kinds of software tools, obtaining a 3D digital model of the product. Designers at this moment make the very first evaluation of the product only by the visual channel. The digital model, actually, can be represented only by means of a visualisation system. This task is performed simultaneously with the shape-modelling phase and requires an implicit loop process to meet the concept requirements.

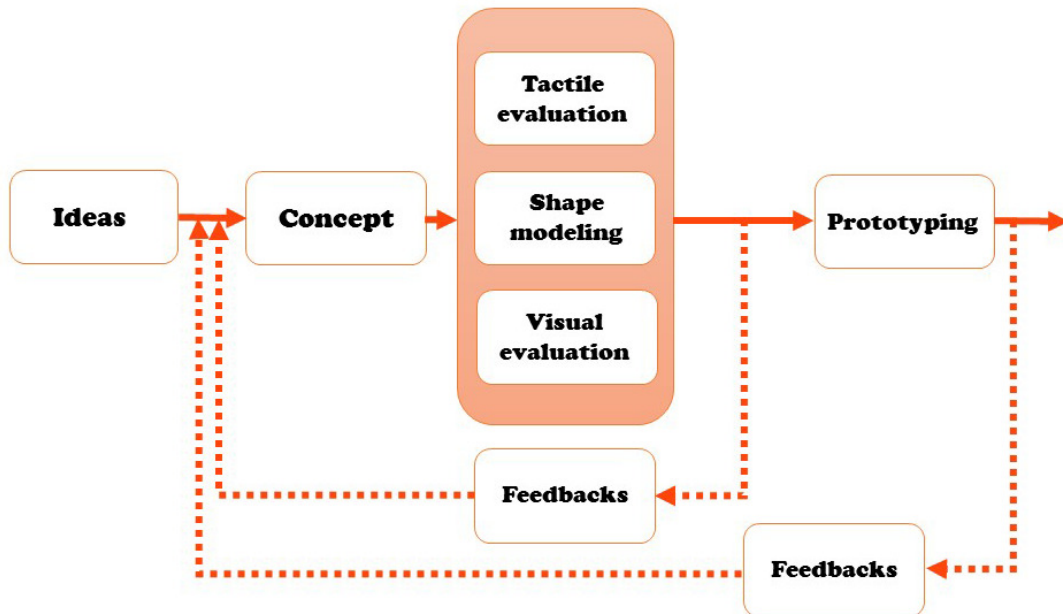


Figure 2.2: Proposed design process.

- **Prototyping:** Thanks to the wide spreading of rapid prototyping based techniques like 3D printing technology, it is possible for the designers to obtain a physical prototype of the digital model in a few hours. However, the prototype that can be obtained could be expensive and it is typically made of a material that is not the one of the final product, and it is not flexible in case one desires to change the shape, color, material and texture. Here comes the real need of low cost and flexible techniques to overcome the limits imposed by the mock-up, and here *Virtual Reality* and the *patch display* will concur the most.
- **Evaluation:** The final evaluation phase, where a multisensorial analysis is made, in particular the tactile one (is experimentally verified that touch has the bigger impact on people very first impression [21],[44]). This final evaluation give in output all the economical, aesthetic, functionality and geometric feedbacks needed by the designer to improve their concept.

### 2.1.3 Proposed product design process

The new proposal consists in moving backward the tactile evaluation and therefore perform it during the shape-modelling stage. To achieve this goal it can be used a display for surface inspection proposed in literature, but since now there

is no device that can actually fit a wide range of surfaces. Indeed, purpose of this thesis is to develop a device (i.e. a patch display) able to fulfil this task. With the new proposed approach designers can truly cut down the waste of time and money, since there is no need to build many prototypes to end up with the ultimate concept. Absurdly, it might be used only a final prototype but, since there are too many factors affecting the model (e.g. economical and production constraints) there is the need of a second feedback phase, where the prototype can be evaluated only on the non-mechanical side, and this could definitely reduce the prototyping stage to only few mock-up.

## 2.2 Surface Exploration

According to Okamura et. al [32] Haptic exploration is an important mechanism by which humans learn about the properties of unknown objects. Through the sense of touch, we are able to learn about characteristics such as object shape, surface texture, stiffness, and temperature. Unlike vision or audition, human tactile sensing involves direct interaction with objects being explored, often through a series of exploratory procedures (EP) [22]. These procedures are outlined as:

- **Lateral motion** - associated to surface texture evaluation. The skin is passed across a surface, producing shear forces.
- **Pressure** - associated to compliance or hardness evaluation. Force is exerted on the object against a resisting one; e.g. by pressing onto the surface, bending the object or twisting it.
- **Static contact** - associated to apparent temperature evaluation. The skin surface is held in contact with the object surface, without motion; typically a large surface, like the whole hand, is applied.
- **Unsupported holding** - associated to weight evaluation. The object is held while the hand is not externally supported.
- **Enclosure** - associated to global shape evaluation. The fingers are usually moulded closely to the object surface.
- **Contour following** - associated to exact shape evaluation. Skin contact follows the gradient of the object's surface.

It is therefore possible to say that touch sense plays an important role in human perception. Indeed some studies led on congenitally blind infants [39] states that "The specificity of exploratory behaviour suggests that the infants interest in the gradient texture surface is focused on texture-properties and not on other properties of the surface" due to an increasing frequency in fingering and rubbing

across test sections, and according to [40], infants show up a manipulative behavior whether the objects they are approaching is a completely new one. Thus there is enough evidence that touch sense affect the very first impression of object comprehension both on shape and texture perception level. In this thesis is discussed only the role of shape. Furthermore it's important to underline how previous studies stated that during a new surface exploration, users prefer employing their palm instead of fingers and that the minimum perceivable curvature error between two similar object arises between 5% and 10%. This last value it's a very important parameter which will be the main base of comparison of this work.

## 2.3 Related Works

As mentioned above, Tactile interaction consists in providing the user of a *Virtual Reality* environment with sensations related to touch, mainly during the evaluation and the manipulation of virtual objects. In some cases the term tactile is used to refer to mechanical stimulation of the skin, which -together with the kinaesthetic sense- creates the haptic feedback. For these reasons, the tactile devices are strictly related to the haptic interfaces. Hereafter are presented some of the previous works related to *surface displays*.

### 2.3.1 Local Surface Display

Local surface displays are those devices, which present to the user a local, oriented surface, instead of just a single point of contact. This surface may be either mounted on a full-contact force feedback display or on a position controlled robot. The surface may be either at or selectable from a limited number of optional sides of an interface block, each carrying a generic shape like a ridge or a valley. There are a few experimental devices such as the following:

- **De la Torre Haptic shape display:** An haptic illusion explored by Hayward and Robles de la Torre [13] in years 2000. The device is equipped with a plate, where the user slides the finger in order to perform lateral linear motions. Through the introduction of lateral forces the device is able to provide the illusion of a bump during lateral motion. This illusion works on a smaller size scale than the Morpheotron illusion.
- **McGill Morpheotron:** In 2001 Hayward et al. [14] have developed at the McGill University the Morpheotron device that consists in a free running carriage with a tilting surface. Thanks to this device, Hayward has demonstrated it is possible to create an illusion of curvature, even with a linear motion, by tilting a finger platform surface. The Morpheotron is not a real

VR device, but it has proved that tilting contributes to the perception of shapes. It is an example of the potential usefulness, although limited in this case, of haptic illusions.

- **VisHap:** This system [48], developed by the Johns Hopkins University in 2003, proposes to overcome a common issue of almost all point-based tactile devices. that is the need of the user to be attached to the haptic device during whole time of the test, even though force feedback is not always being rendered. A camera vision system tracks user's hand and the device is slaved to it. When contact is made, the force feedback is applied by means of impedance control.
- **Stanford contact location display:** The device developed by Provancher et al. [35] in 2005 is based on a Phantom device connected with finger contact thimble. This is equipped with a small cylinder suspended beneath the users fingertip. The cylinder can rotate freely or be prevented from rotating, using a small brake, to portray rolling or sliding contact, respectively. This cylinder is moved under the thimble, giving the finger the impression that the surface under the thimble has a certain orientation. The impression of sliding or rolling the finger over a curved surface can be created in one direction only. The roller is driven by an actuator strapped to the users arm, by means of a push-pull rod connecting to the thimble on the finger.
- **The Pantograph MKII:** Another device developed by Hayward et al. in 2005 is known with the name Phantograph [36] and its improved version Phantograph MKII [5]. This interface is a two degrees of freedom planar, parallel mechanism pantograph, which is equipped with a plate where user can slide the finger performing planar movements. By means of controlling tangential interaction forces it is possible to control the fingertip deformations and provide tactile sensations that give the illusion to explore a real surface.
- **Percro Fingertip display:** The researchers of the Perceptual Robotics Laboratory of Scuola Superiore Sant'Anna in 2007 have developed a device [42] made up of a supporting haptic interface and a fingertip display. Thanks to the combination of these two kinds of interfaces the obtained device is able to provide both kinaesthetic and local tactile cues at the level of the fingertip.

### 2.3.2 Full Shape Display

Full shape displays are interfaces able to render a spatial continuous surface with whom users can interact by using any part of their hand. These devices usually

allow them to test the rendered shape by means of a free hand modality. This means that the user is not obliged to wear a device, neither to hold tools affecting the evaluation. The aim of full shape displays is to present and render a portion of surface leaving the user free to decide where and how to explore it. Some of the most important works led on this theme are presented hereafter.

- **Digital Clay:** Researchers, in the year 2000, of the Georgia Institute of Technology did a theoretical study [41] on a desktop full controllable mesh surface by using a high number of multiple collocated spherical joints, which can be combined to obtain a formable crust. It could be commanded in order to render desired shapes or be deformed by the user.
- **Feelex:** The device has been developed at the University of Tsukuba in 2001 [16] and is a 2.5D crust concept, which is made up of 6 x 6 arrays of vertical pins under a rubber screen. The pins are driven by ball screw actuators. In addition, by means of vertical translation, they deform a 200 x 200 mm flexible rubber membrane. In this way the device allows the user to touch the surface and feel its shape.
- **SATIN:** This haptic interface has been developed within the context of the EU-funded project IST-FP6-SATIN developed in 2010 [4], which has been followed by other versions aiming at improving the initial concept. These devices consist in a plastic flexible strip, which is bended and twisted by a finite number of control modules. As a general concept, the strip is the tangible version of a line in a 3D space. It can be thought as leaning on the surface of a geometric model, which has to be touched and explored for being evaluated. The strip deforms itself and represents trajectories, which are controlled by a finite number of nodes, named control points. These trajectories can be freely explored by the users.
- **Relief:** This shape display [23], developed by the researchers of the MIT Media Lab in 2010, is a desktop device able to render and animate three-dimensional surfaces. It allows users to touch digital models like geographical terrain in an intuitive manner. The deformable surface is actuated by an array of 120 motorized pins, and each pin is also able to detect user input as pulling and pushing. The device is scalable and based on open-source hardware and software components.
- **Super-thin 3D form display:** The device developed by the University of Tokyo [28] in 2011 is a 3D shape display which integrates a simple visualisation system with a novel and super-thin interface. The thickness of this system is below 1.0 mm, and this system can generate 30.0 mm stroke. The researchers have achieved this thickness by using a mechanical system that consists of a (Shape Memory Alloy) SMA materials- coil and a single

leaf spring. Thanks to this feature the device is lightweight and portable. As regards the visualisation system, it has been obtained by means of a projector mounted on top of the shape display.

- **Formable Object:** In 2013 a new concept has been developed by the researchers of the Institute of Automatic Control Engineering of TUM [18]. It is a full surface display composed of a matrix of servo-actuated nodes. The Formable Object project can be mounted on the end-effector of a robotic arm, which allows displaying basic shapes like cylinders or spheres. It can be further extended so as to cover larger interaction areas.

## 2.4 Previous research context: SATIN system

A tactile interface enables user to interact with and feel a wide variety of virtual objects by using the palm of their hand. Although is possible to find in literature several ideas for a tactile device, nowadays there are some issues that has not been solved, those are:

- wide portion of area to be represented
- continuity of the surface
- range of representable surface

In fact, both local and full shape display doesn't answer to those problem requests. For this reason the aim of this thesis is to develop a system that could fix those issues and will enable designers to simultaneously see and touch virtual shapes of products. By means of a visual and tactile representation, the designer will be able to evaluate various properties of the shape, as its dimension, proportion, geometrical features and physical characteristics. The tactile evaluation should be a natural interaction with the shape, where designers can touch and explore a shape manually through free hand interaction. The main advantage of this new way of evaluating the shape concept is that visual and tactile evaluation can be performed at the same time, in a much convenient and effective way. On the basis of the results of shape evaluation, the digital shape can be changed, and evaluated again. This work proposes a tactile display allowing designers to touch a virtual surface through a continuous touch of curves lying on the product shape. The tactile display is developed on the basic idea of the SATIN system, that has been already developed in previous research, and which is described in the following section. The solution for a patch-like full shape display that will be presented next will improve and encourage the development of new products based on user's needs, following the tendency of the big enterprises, that is to be competitive in the market with the capability to develop products tailored on the specific customer requirements with a short lead-time.

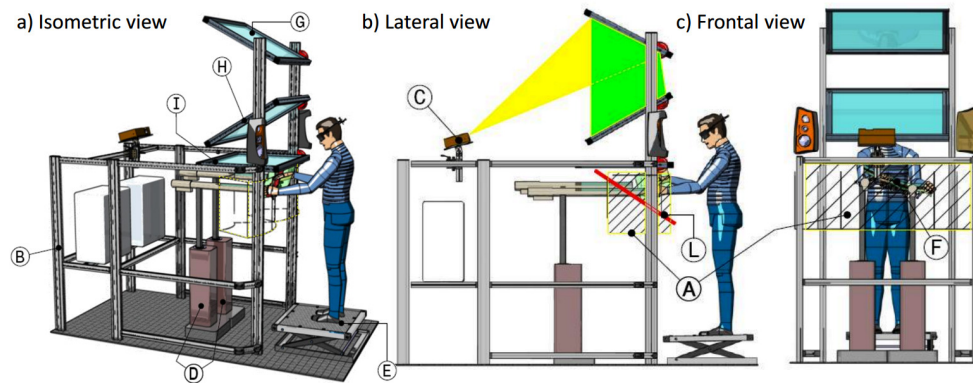


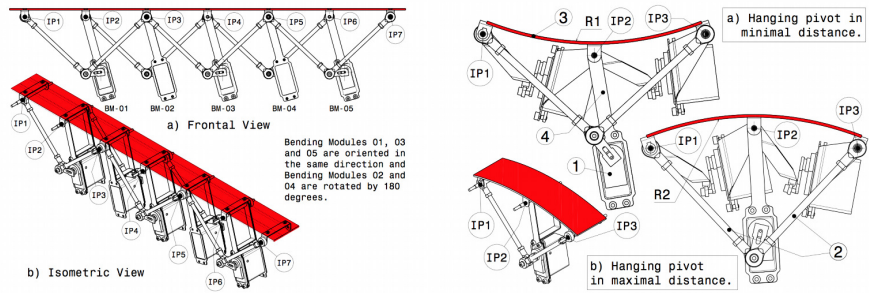
Figure 2.3: Concept of the SATIN system

### 2.4.1 Issues and problems to solve

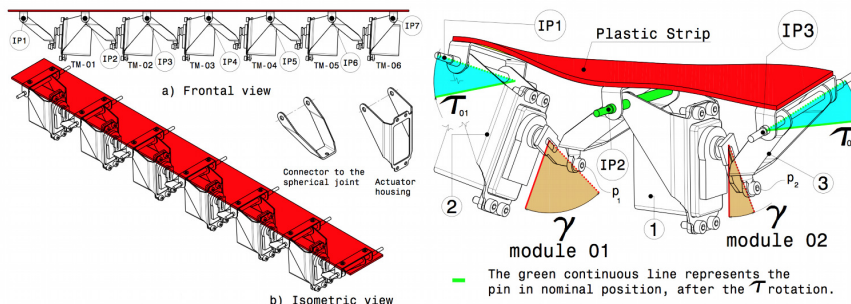
This Section described the SATIN system that has been developed in the context of the EU-funded project IST-FP6 SATIN, and the issues and problems outlined and subsequently addressed in the present research. The research presented in this thesis is the natural prosecution of the SATIN project. In actuality, having as a starting point the knowledge and know-how acquired during the project by the researchers at the KAEMaRT group, it has been possible to identify the limits of the system, and to define the research path to follow in order to develop an innovative and novel system, much performing and better usable than the previous one. The SATIN project consists of a working station for the evaluation of and interaction with virtual prototypes of products. It is mainly made up of: 1) a tactile interface, 2) a stereoscopic visualization system, 3) a system for sound rendering. The tactile interface consists of a flexible strip placed in the space by two MOOG HapticMaster devices. The strip imitates the bend typically used by designers to perform style evaluation of physical mock-ups of concept products. A 3D visualization of the surface is superimposed on the physical model by means of a retro-projected stereoscopic visualization system. This consists of a DLP projector, a mirror, a half-silvered mirror and a rear-projection screen (figure 2.3). The projector is located in a position that is above and on the back with respect to the haptic system (C). This position allows the user to stand in front of the visualisation system without the problem of creating a shadow with her/his head, thus occluding the image projected by the projector. The display system is also designed in a way that its components do not interfere with the haptic workspace (A). So, the user can freely move her/his hands within the interaction space, and is able to interact with the system by grabbing and manipulating the physical interface (F), which is positioned under the half-silvered mirror. The two haptic devices (D) are positioned under the visualisation system. The stereo image deriving from the projector is reflected on the mirror positioned on top of



the layout (G). The image is projected straight to the overhead projection plane, which is a rear-projection screen (H) that has been previously angled in order to correct the distorted image. The user sees the mirrored image in the virtual plane where the 3D image is created through the half-silvered mirror (I). This configuration offers good image visualisation and also allows us to control the sense of depth. If the rear-projection screen is located near to the half-silvered mirror the user perceives the virtual object near as well; if the rear-projection screen is located far from the half silvered mirror the user perceives that the virtual object is far as well. A frame (B) supports the components and a platform (E) is used to accommodate the users height. All the components are equipped with regulation systems. These allow us to easily relocate and adjust the position and orientation of the virtual image plane (L). In order to increase the perception of the 3D image, the user is provided with stereoscopic glasses. These glasses are tracked so that the projected image is always coherent with the orientation of the users point of view. This tracking has been made possible by using the Opti-Track system, which is provided with three cameras, placed on the upper part of the whole structure. The tactile system is made up of a flexible strip that is bended and twisted (figure 2.4a and figure 2.4b) so it has to be able to render a portion of a virtual surface, which physically represents the digital model of the product. In order to obtain the desired deformation, the strip is moved by relative servo-actuated mechanisms. They control the strip by means of parallel equidistant sectors, which correspond to the control points of the rendered surface.



(a) Bending mechanism



(b) Twisting mechanism

Figure 2.4: SATIN strip displacements

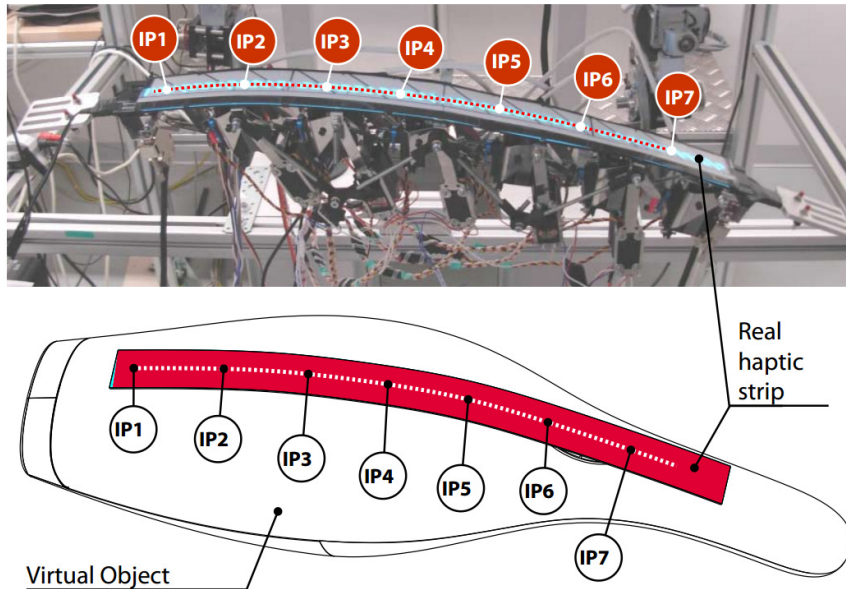


Figure 2.5: Control points

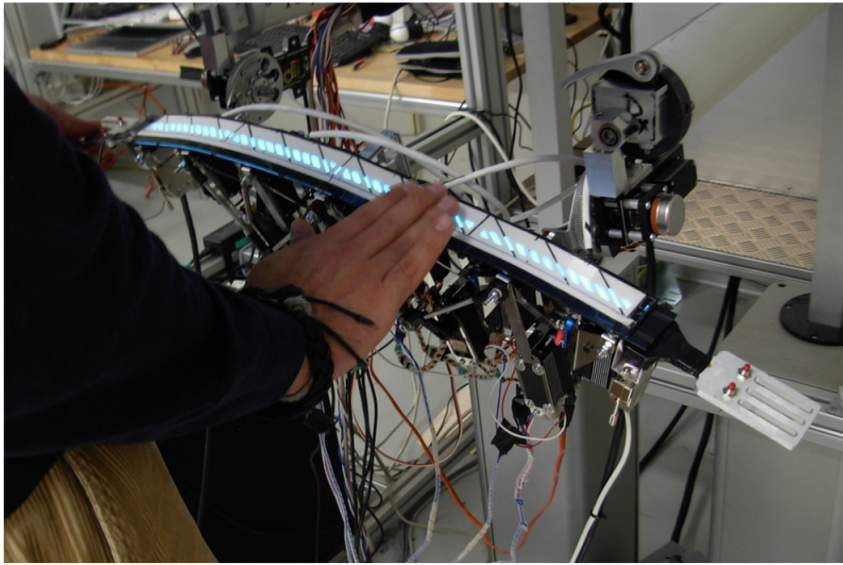


Figure 2.6: SATIN prototype

The SATIN system is extremely innovative. However, it has some limits, which make difficult its effective adoption in a design studio. By analysing the criticalities of the system, it is possible to identify issues related to:

- **Size:** The system is bulky and it is difficult to move it around. The huge proportion of the system is imputable to the necessity of using a structure for mirror displacement of the retro-projection system, to the frame of tracking system and the placement of two cumbersome MOOG-HapticMaster devices.
- **Costs:** The entire system is very expensive from an implementation point of view
- **Customisation:** The system, as it has been conceived, results to be poorly flexible in terms of implementation and adaptability to the users needs. The system is not only a fixed working station requiring a big amount of space, but it has also limitations related to the use of the tactile interface, which is composed by eight modules in standard configuration. It has been, indeed, conceived to be partially customized for what concerns its size. However, it presents limitations due to the relative nature of the actuation systems. In order to customize the length of the strip, according to the kind of the surface to render, it is necessary to add or remove some modules of the strip itself. This is first of all an activity that requires efforts and time. Moreover, it is not possible to add an infinite number of modules because, after a certain number, the system will not be able to sustain its weight.

- **Rendering performances:** This limitation is related to the tactile device, which has been developed within the context of the project. Also in this case, the limit relies in the relative placement of the actuation mechanisms. This means that the distance between the control points of the surface cannot be lower than 90 mm, that distances cannot be varied and the system can't represent curvature radii lower than 185 mm.

<b>SATIN system</b>	
Overall dimension	2600x2100x1280 [mm]
Number of control points	9
Distance between control points	90 mm
Realtime regulation	NO
Minum radius of curvature	185 mm
Modularity	NO
Portable	NO
Implementation costs	High

Table 2.2: SATIN system specifications

The main characteristics of the SATIN system are shown in table 2.2. The characteristics and corresponding values are used to define the requirements of the system that will be developed in this research work, and which will allow us to compare the values and evaluate the characteristics and performances of the new system.

### 2.4.2 New System Specification and architecture

According to the issues described in the previous Section, the system will have to comply with the following general specifications:

- It has to be low cost, so as to be affordable for a large number of design studios or even for single designers.
- It has to be in a desktop and portable version. This is because it will ease the introduction of the system in the everyday working life as it happens for a mouse or a keyboard.
- It has to be compliant with as many commercial software applications for surface modelling as possible.
- It has to be modular, so as to be customized according to the kind of surfaces with whom the designer and/or the design studio usually deals.
- it has to be performer in terms of the potentiality of representing a surface. Indeed, the system has to be able to render real surfaces with curvature radii lower than 90 mm. This will be an improvement compared with the devices that are currently available.

In order to satisfy the system requirements a full shape display has been developed; it takes cues from the know-how acquired within the development of the SATIN system with regard to the modalities of interaction with the virtual surface. Indeed, the system developed is of type "free hand". This device is able to modify its shape so as to mimic the shape of the surface to represent. Consequently, it enables the users to choose where to freely explore the virtual surface through the sense of touch, as it commonly happens with a real object. For this reason the approach of a full shape display, based on patch elements, seems to appear more effective than a geodesic strip one.

### 2.4.3 Attempt to re-engineering the SATIN

A first attempt to overcome the issues introduced by the SATIN system has been managed by A. Mansutti [25] [26] in 2014 when he developed a desktop and modular version of the geodesic strip. His approach aimed to define an overall length for the haptic strip and then insert any number of modules underneath just to control the twisting and the bending effects needed to warp the strip like the shape that derives from the intersection of the cutting plane and the virtual surface. In the proposed device five degrees of freedom has been used to define the control points placement in a Cartesian space, three for the relative rotations and two dedicated to the bending and twisting control, in which every motor has been directly housed in the respective degree of freedom, and for the linear movements a rack-pinion transmission system has been used. Mansutti's dissertation was the starting point for this thesis: and the same idea of control points placing has been introduced to guarantee the proper device movements,

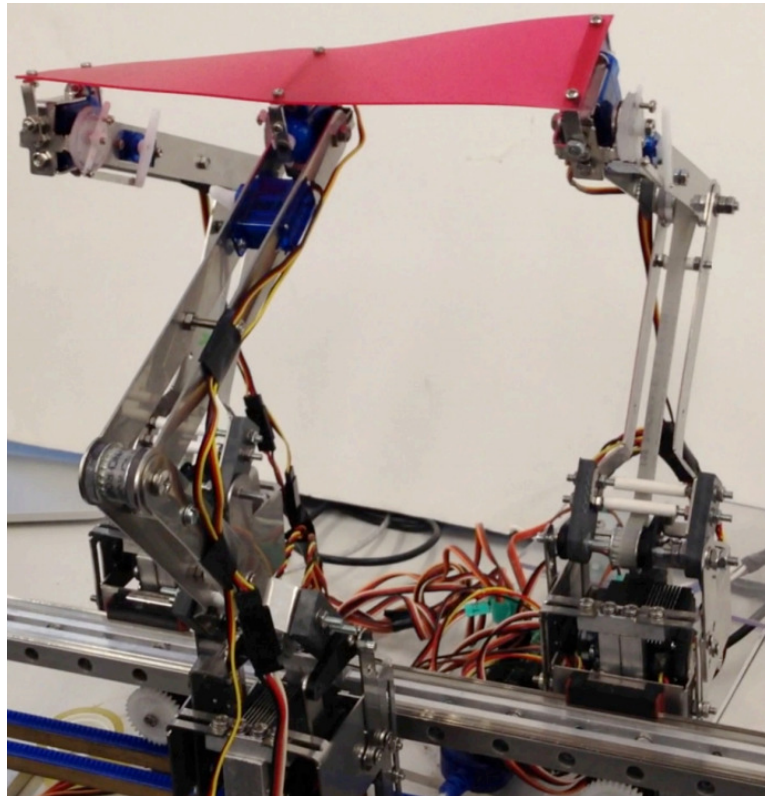


Figure 2.7: Desktop version of the SATIN

and the twisting and bending effects controlled for the geodesic strip has been introduced in the proposed patch display to carry out the local curvature control.

Referring to figure 2.7 the main features of this device are subdivided as follows:

- **Control points:** developed prototype integrates three modules with direct actuation system. This is the minimum number of modules that are needed to control the deformation of the strip. Thanks to the modular configuration of the system, it is possible to add a higher number of modules. Actually, there is not a maximum number of modules, since this value depends on the length of the longitudinal rail, which can be selected according to the kind of surfaces to render.
- **Curvature radius:** short distance between control sectors and the possibility of modifying in realtime this distance allows a minimum curvature radius of 30 mm. This value corresponds to the resolution of the system, and allows users to render a large range of smooth surfaces. Concerning the accuracy of the rendering, the possibility to select the best position for the control points by means of the developed control algorithm, ensures the capability to control the elastic deformation of the plastic strip. Indeed, deforming the strip by means of the control sectors placed in particular points ensures the best configuration available for managing the strip behaviour.
- **Modularity:** The system in charge of managing the control points along transversal plane consists of modules with absolute configuration. These modules can be replicated, and it is possible to decide how many modules to include in the desktop station according to the characteristics of the surface to render.





# 3

## Design Strategy

This chapter shows the main approach used to develop a solution to the leading subjects of the thesis:

- Settling the entire problem
- Dealing with the input data available to designers
- Assessment of a mathematical model to define where the control points will be placed and how they will relate to the physical surface
- Taking into account the large displacements of the physical surface

while a device proposal will be explored on the following chapter. In the first section will be given an exhaustive explanation of the data a designer uses to generate a virtual surface and starting from those will be detailed a mixed analytical-numerical solution to predict the behaviour of the physical surface, with the help of a finite element problem definition in which will be faced a general material selection to overcome the large displacements issue.

### 3.1 Problem definition

Aim of the problem is to find a proper way to describe how it is possible to use a physical surface to mimic a virtual shape. In order to accomplish this it is necessary to define a mathematical model for the problem in question and its component that will be examined in depth from the next section. Firstly we need to take into account the common work routine that every designer have and therefore the instruments they usually implement in the shape modelling, for this reason the first two steps consist in

- Describing the typical designer instruments in order to settle the starting point of the analysis
- Finding a proper model to mathematically describe their instruments

Achieving a mathematical description of those inputs it's then possible to focus on a method to describe the physical surface behaviour instead. Taking into account a modular approach to solve this issue, we need to introduce

- A model to describe the positioning of the points that will control the surface deformation, and how they interact with it
- A possible method to increase the model accuracy
- A choice and a mathematical description of the physical surface material

Finally, having a proper description for the above mentioned components it is possible to settle a function that will describe the main differences between physical and virtual surfaces, indeed final step of this problem is to

- Build an error function that, when properly minimized will give as an output the set of variables for the current problem

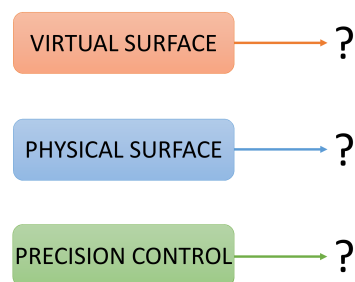


Figure 3.1: Components for the mathematical problem

## 3.2 Geometric formulation

In the process of developing a new product, industrial designers have at their disposal a wide set of instrument made available by the *information technology* (IT). To produce new kind of product shape they follow two principal ways:

- drawing their ideas by means of *computer aided design* (CAD) softwares, and using the techniques imposed by the geometrical modelling
- starting from a points cloud obtained with reverse engineering process (e.g. photogrammetry or laser scanner) and then modify the existing shape to meet new product requirements

In any case, whatever is the path followed, the final output of the process is a file containing all the informations necessary to the description of the virtual surface.

### 3.2.1 Input data: STL file format

Since every CAD software has their own file format with proprietary encoding, but they still need to interface each other and with other software packages, a universal language is widely used to share data among them; This universal language is called STL [49] file format by *3D Systems* company and is a file format native to the stereolithography CAD softwares and has several after-the-fact acronyms such as Standard Triangle Language and Standard Tessellation Language. STL files describe only the surface geometry of a three-dimensional object without any representation of color, texture or other common CAD model attributes and this format specifies both ASCII and binary representations. An STL file describes a raw unstructured triangulated surface by the unit normal and vertices (ordered by the right-hand rule) of the triangles using a three-dimensional Cartesian coordinate system. As shown in figure 3.2 an STL file can contains all the points necessary to describe a surface and, obviously, the more points it contains the more accurate will be the description.

### 3.2.2 Managing and controlling virtual surfaces

The idea behind the control of a surface is explained by the geometrical modelling with the usage of low computational burden mathematical methods (i.e. Bézier surfaces), ruled by a set of control points that can accomplish completely different surface shape with only one model. In geometrical modelling, a *control points* is a member of a set of points used to determine the shape of a spline curve or, more generally, a surface or higher-dimensional object. As it's possible to see on figure 3.3 usually the control points are not on the virtual surface and then it's not possible to make an analogy with physical surface control, but this idea will be the

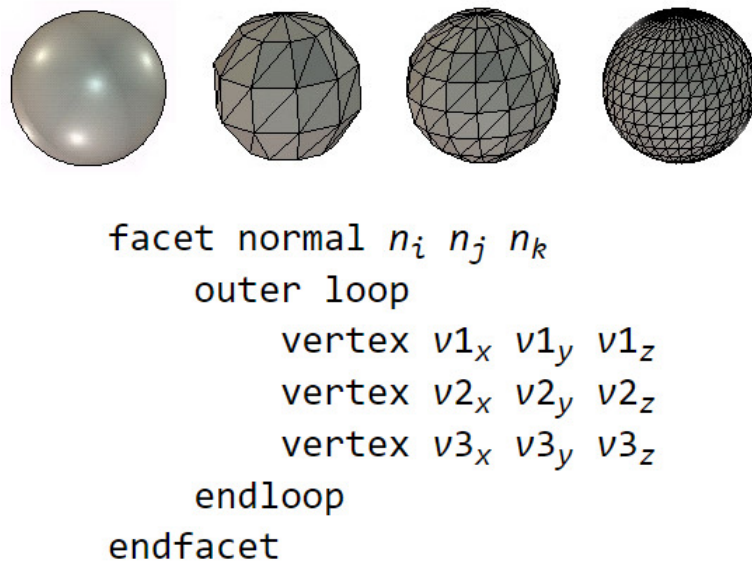


Figure 3.2: example and definition of an STL file

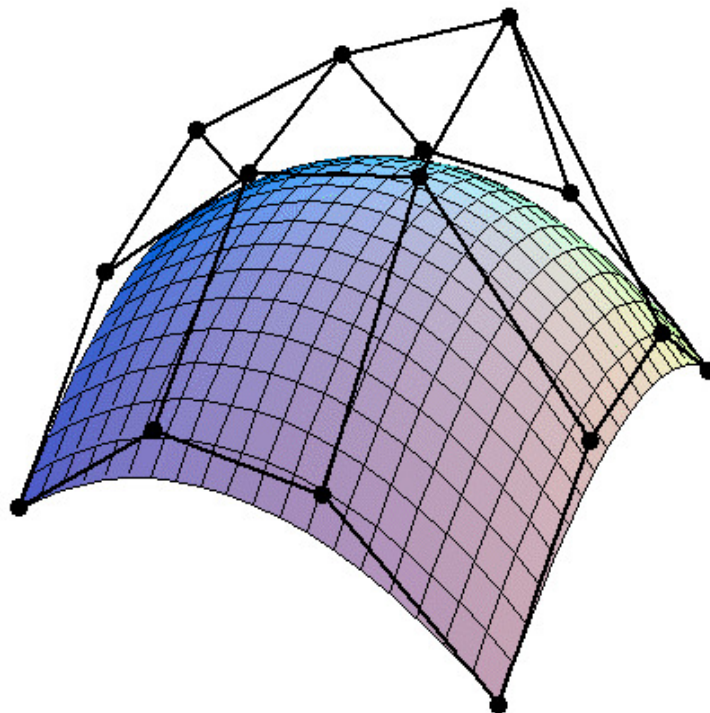


Figure 3.3: Bézier surface with control points

basis of the model suggested in this work. Starting from this idea it's possible to think a surface as a grid made of rectangular elements that can approximate the surface, at which corners there are the control points, and keeping them on the physical surface they will somehow interact with it to minimize an error function among the virtual and physical surface.

### 3.3 Analytical approach

Explained the idea behind the approach proposed it's easy to understand the need of an analytical approach to solve the problem, i.e. to state an analytical error function, but the only datas available at this stage is the set of points defined by the STL file outcoming the CAD software. For this reason it's necessary to appeal for a mathematical method which starting from a set of points it is able to give as an output an analytical function for the demanded surface. Among the many methods we can find in literature, a polynomial fitting is surely one of the most flexible and the one that could ensure a low computational cost for the further analysis.

#### 3.3.1 Polynomial regression

Polynomial regression is a form of linear regression in which the relationship between the independent variable  $x$  and the dependent variable  $y$  is modelled as an  $n$ th degree polynomial. Polynomial regression models are usually fit using the method of least squares, in which the best fit in the least-squares sense minimizes the sum of squared residuals, where residual being the difference between an observed value and the fitted value provided by a model. Starting from the structured data given by the STL file, it's possible to make a preprocessing centering and scaling them [46] to improve the effectiveness of the regression. After that we can write down the equation of polynomial surface

$$f(x,y) = \sum_{m=k=0}^l p_{mk}x^m y^k \quad (3.1)$$

where  $l$  is an integer major or equal than zero and  $p_{mk}$  is the polynomial coefficient. For example a polynomial of second degree will have the following shape:

$$f(x,y) = p_{00} + p_{10}x + p_{01}y + p_{20}x^2 + p_{02}y^2 + p_{11}xy \quad (3.2)$$

The premise of polynomial regression is that a data set of  $n$  paired  $(x,y,z)$  members:  $(x_1,y_1,z_1), (x_2,y_2,z_2), \dots, (x_n,y_n,z_n)$ . The essence of the method is to reduce the residual  $R$  at each data point

$$R_i = z_i - p_{00} - p_{10}x_i - p_{01}y_i - p_{20}x_i^2 - p_{02}y_i^2 - p_{11}x_iy_i \quad (3.3)$$

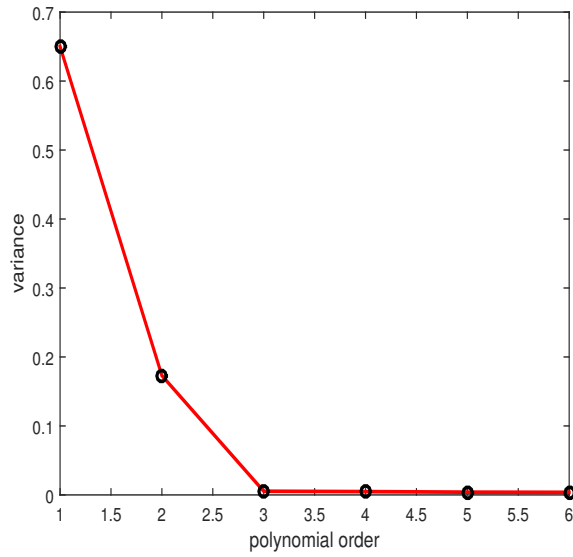
This is accomplished by first expressing the system in matrix form, then solving for the unknown vector  $(p_{00}, p_{10}, p_{01}, p_{20}, p_{02}, p_{11})$  by means of Gauss elimination [47]. The resulting values represent the polynomial coefficients for equation 3.2 above. The here mentioned methods works independently from the chosen degree of the polynomial in both  $x$  and  $y$  direction, but what is the optimum polynomial order to use for regression? Many times the shape of the surface it's so complex that is not possible to compute a good polynomial order at first sight, thus is convenient to use a more accurate method that will avoid to loose informations with a too low polynomial order and will not cause high computational cost with a too high one. For this reason, given the following definition of the variance

$$\left\{ \begin{array}{l} \sigma = \frac{Sr(m,n)}{n-m-k+1} \\ Sr(m,n) = \sum R_i^2 \\ n = \text{number of data} \\ m|k = \text{order of polynomial} \end{array} \right. \quad (3.4)$$

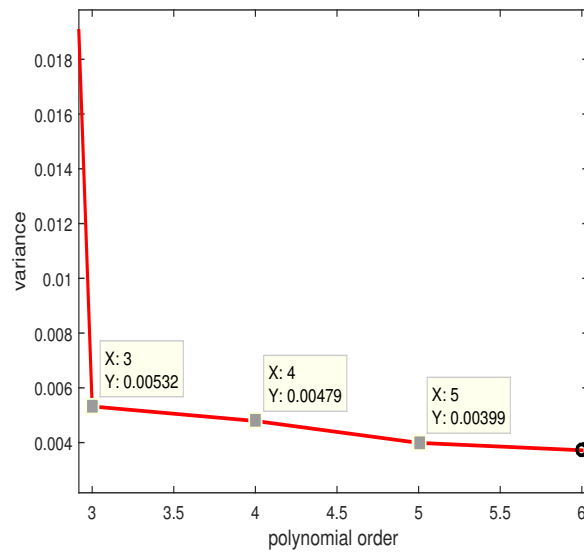
it is possible to choose the degree when  $\sigma$  is a minimum or when there is no significant decrease in its value as the degree of polynomial is increased. in figure 3.4 there is an example of a curve polynomial fitting, in which it's possible to say that a third degree polynomial is accurate enough for the problem since using a fourth order polynomial will drastically increase the computational cost with no significant precision on the polynomial fit (figure 3.4b) due to small decrease of  $\sigma$  minor than a threshold  $\epsilon$  arbitrarily stated.

### 3.3.2 Analytical description of the frame

As mentioned previously in this chapter, the basic idea where this work started from is the principle of having rectangular elements to behave like a mesh grid



(a) Overall trend



(b) Detail on convergence

Figure 3.4: Variance decreasing with polynomial order

necessary to place the control points that will warp the physical surface to meet the required shape. For this reason, the "mesh grid" will be considered the **frame**

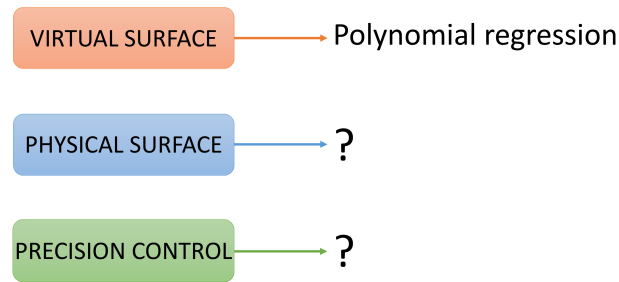


Figure 3.5: Components for the mathematical problem: virtual surface

for the positioning of the control points. At this design phase an analytical form

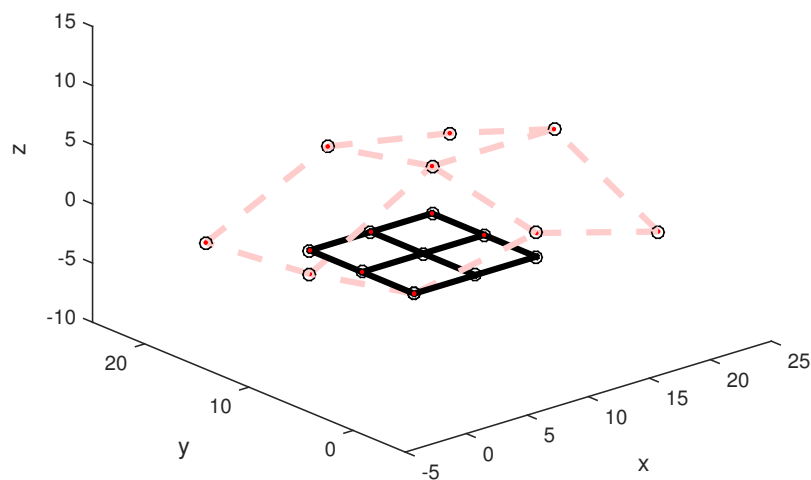


Figure 3.6: Basic concept of shapeshifting patch and control points

for the virtual surface has been found, and the next step is about finding an equation to reach a formal description of the Cartesian positioning with regards to a fixed coordinates system. This model has to take into account the main features shown in figure 3.6 and figure 3.7, namely:

- control points have to be on the same isolines (referring figure 3.7  $x_1 = x_4; x_2 = x_3; y_1 = y_2; y_3 = y_4$ )



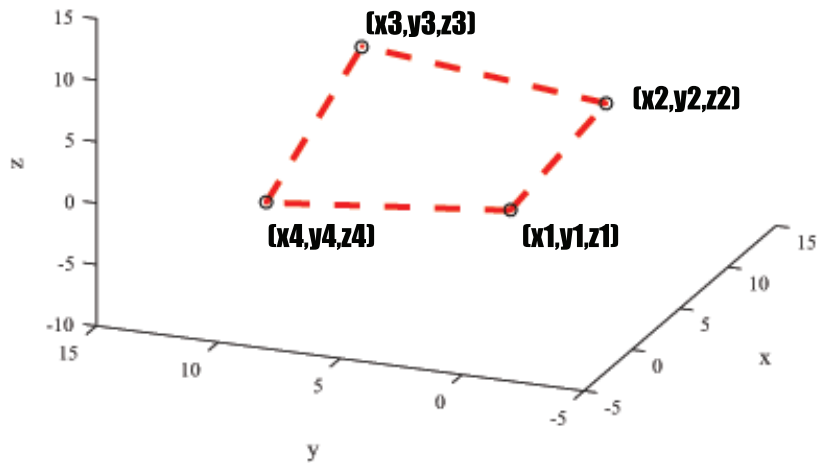


Figure 3.7: Single frame elements and control points coordinates

- control points coordinates have to be in ascending order (e.g referring fig 3.7  $x_1 < x_2$  and  $y_1 < y_4$ )
- system can expand with no apparent limits (e.g. referring fig 3.6 control point 3 can freely move to initial position  $[10,10,0]$  to any final position like  $[20,15,3]$ )

Following what has already been stated, a single patch element seems to behave like a *bilinear function*, where the control points define the extreme nodes of the function itself.

**Definition 3.1.** A function of two variables is bilinear if it is linear with respect to each of its variables.

The analytical form of a bilinear function is therefore (referring fig 3.7):

$$\left\{ \begin{array}{l} f(x,y) = a_0 + a_1x + a_2y + a_3xy \\ x_1 < x < x_2 \\ y_1 < y < y_4 \\ x_1 = x_4 \\ x_2 = x_3 \\ y_1 = y_2 \\ y_3 = y_4 \end{array} \right. \quad (3.5)$$

In which the vector  $\bar{a} = [a_0 a_1 a_2 a_3]$  is unknown. In this way it's possible to build a set of bilinear problems equal to the number of rectangular elements used to approximate the virtual surface (e.g. in figure 3.6 the four elements bring to a set of four bilinear equation with four unknown vectors and thus sixteen variables to find). To solve those problems it's so necessary to have  $4n$  points laying on the surface, where  $n$  is the number of rectangular elements. Assuming to take four points  $Q_{11}; Q_{12}; Q_{21}; Q_{22}$  belonging to the surface for whom:

$$\left\{ \begin{array}{l} f(Q_{11}) = f(x_1, y_1) \\ f(Q_{12}) = f(x_1, y_2) \\ f(Q_{21}) = f(x_2, y_1) \\ f(Q_{22}) = f(x_2, y_2) \end{array} \right. \quad (3.6)$$

and taking into account the constraint equations already stated in the problem 3.5

$$\left\{ \begin{array}{l} x_1 < x < x_2 \\ y_1 < y < y_3 \\ x_1 = x_4 \\ x_2 = x_3 \\ y_1 = y_2 \\ y_3 = y_4 \end{array} \right. \quad (3.7)$$

it's possible to write the the solution to the problem 3.5 in a matrix form:

$$\begin{bmatrix} 1 & x_1 & y_1 & x_1y_1 \\ 1 & x_1 & y_2 & x_1y_2 \\ 1 & x_2 & y_1 & x_2y_1 \\ 1 & x_2 & y_2 & x_2y_2 \end{bmatrix} \begin{pmatrix} a_0 \\ a_1 \\ a_2 \\ a_3 \end{pmatrix} = \begin{pmatrix} f(Q_{11}) \\ f(Q_{12}) \\ f(Q_{21}) \\ f(Q_{22}) \end{pmatrix} \quad (3.8)$$

inverting the matrix and putting in evidence the unknown  $\bar{a}$  vector

$$\begin{pmatrix} a_0 \\ a_1 \\ a_2 \\ a_3 \end{pmatrix} = \begin{bmatrix} 1 & x_1 & y_1 & x_1y_1 \\ 1 & x_1 & y_2 & x_1y_2 \\ 1 & x_2 & y_1 & x_2y_1 \\ 1 & x_2 & y_2 & x_2y_2 \end{bmatrix}^{-1} \begin{pmatrix} f(Q_{11}) \\ f(Q_{12}) \\ f(Q_{21}) \\ f(Q_{22}) \end{pmatrix} \quad (3.9)$$

it is finally defined a solution to the problem. It's obvious that for a problem involving huge sets of variables (real industrial applications can imply even thousand of variables) leads to an explosion of the computational cost due to inverting of the matrix. There are many solutions proposal in literature to achieve this goal with a numerical approach:

- pivoting LU decomposition
- QR decomposition
- Rank factorization
- Cholesky decomposition

it's proven that for large sets of variables the most effective algorithm is implemented in the Cholesky decomposition [20]. Under the hypothesis of Hermitian and positive-definite matrix Cholesky algorithm makes a decomposition into the product of a lower triangular matrix and its conjugate transpose, and, if applicable, it shows results in computational time roughly twice as efficient as the other methods.

### 3.4 Surface-control points interaction

Before proceeding with a concept of the physical surface, it's needful un discuss how to use the previous control points placement to control the surface itself and how this set of points will affect the approximation of the virtual surface. In a shape evaluation [37], users usually slide their hand on the surface mock-up making a first estimation of the curvature radius, and therefore there is enough evidence that prove the importance of keeping the continuity of the physical surface in the class of function  $C^k(\mathbb{R})$  with  $k = 2$  at least (i.e. the class of function with real variable belonging to the set of function differentiable an continue at least two times). On the analytical part this condition is verified due to nature of the polynomial formulation, since the polynomial belong to the class of smooth functions continue and differentiable infinite times in a point ( $C^\infty(\mathbb{R})$ ), but the bilinear formulation for the frame doesn't guarantee the continuity and differentiability two times in a point a thus it's not suitable as a choice for the physical surface behavior. For this reason it's useful to pass from a *point-based* control to a *strip-based* control, raising the precision of the approximation. To achieve this goal, it has been introduced a technique usually implemented in the geometrical modelling.

#### 3.4.1 NURBS curve ans strip control

Taking inspiration from the previous studies [10] on the geodesic strip control, it has been introduced a model whom takes as input the control points placement explained before to predict the warping of the strip, in a bending manner abandoning the twisting mode, and finally use that strip deformation to force the displacement of the physical surface. The technique used to predict the strip warping is a concept introduced in the geometrical modelling, that is the notion of *NURBS curve*. NURBS curves, acronym of non-uniform rational basis spline is a mathematical model commonly used in computer graphics for generating and representing curves and surfaces [38]. A NURBS curve is defined by its order, a set of weighted control points, and a knot vector. NURBS curves and surfaces are generalizations of both B-splines and Bézier curves and surfaces, the primary difference being the weighting of the control points, which makes NURBS curves rational (non-rational B-splines are a special case of rational B-splines). NURBS curves and surfaces are useful for a number of reasons:

- They are invariant under affine transformations:[5] operations like rotations and translations can be applied to NURBS curves and surfaces by applying them to their control points.
- They provide the flexibility to design a large variety of shapes.

- They reduce the memory consumption when storing shapes (compared to simpler methods).
- They can be evaluated reasonably quickly by numerically stable and accurate algorithms (e.g. de Casteljau algorithm [29])
- $C^2(\mathbb{R})$  continuity is always guaranteed

The B-spline basis functions used in the construction of NURBS curves are usually denoted as  $N_{i,n}(u)$  (to understand the construction of those basis functions please refer to [34]) and it's almost always triangular over the domain. a NURBS curve takes the following form

$$C(x) = \frac{\sum_{i=1}^k N_{i,n} w_i}{\sum_{j=1}^k N_{j,n} w_j} \mathbf{P}_i \quad (3.10)$$

In this,  $k$  is the number of control points  $\mathbf{P}_i$  and  $w_i$  are the corresponding weights. The denominator is a normalizing factor that evaluates to one if all weights are one. This can be seen from the partition of unity property of the basis functions. It is customary to write this as

$$C(x) = \sum_{i=1}^k R_{i,n}(x) \mathbf{P}_i \quad (3.11)$$

in which the functions

$$R_{i,n}(x) = \frac{N_{i,n}(x) w_i}{\sum_{j=1}^k N_{j,n}(x) w_j} \quad (3.12)$$

are known as the rational basis functions. Therefore knowing a set of control points  $\mathbf{P}_i$  and a taking an arbitrary vector  $w_i$  of weights, that influences the proximity of the control points to the curve, it's uniquely defined a NURBS curve, physically represented by the strip.

### 3.4.2 Accuracy of the approximation: degrees of freedom

The Cartesian placement of the control points implies three degrees of freedom (3 d.o.f.) for each nodes of the rectangular elements explained in the frame mathematical modelling, and due to the physical nature of the problem, each nodes will require a sort of a slider bushing under the surface. Kinematically talking, as shown in figure 3.8a, a bushing would react with a vertical force and torque to locally keep horizontal the strip, and this means that the control points placement

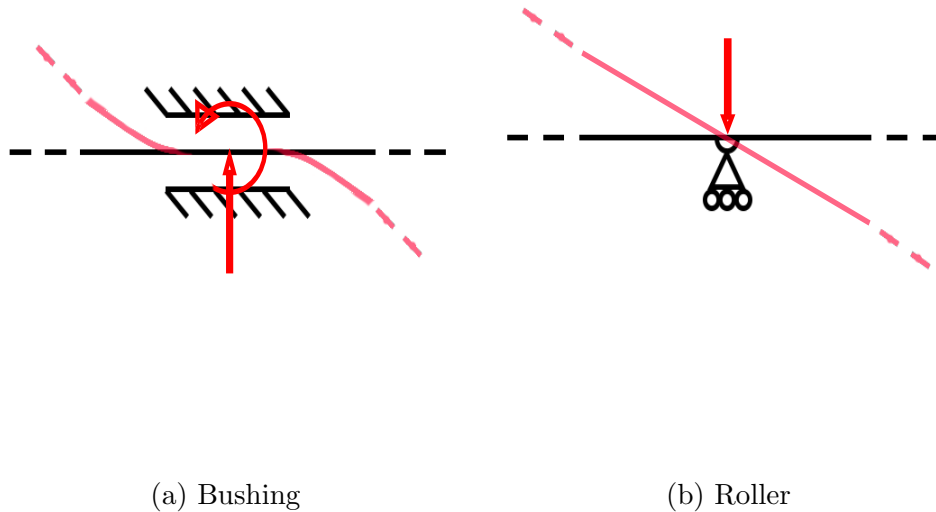


Figure 3.8: Control points kinematic constraints and local deformed shape

explained before is suitable only if the control point overlap with a local minimum or maximum because it verifies the condition of an horizontal trend, that is  $\frac{\partial(C(x))}{\partial(x)} = 0$ , being  $C(x)$  the NURBS expression previously stated. If the local curvature near the bushing is not horizontal, which it means the control point is not in a minimum or maximum, there will be a lack of accuracy of the representation. To add more precision to that approximation it's therefore convenient to have one more d.o.f freeing the rotation about the bushing, and kinematically this configuration is represented by a roller. Since problem is not one-dimensional for each control point there will be globally five degrees of freedom as shown in figure 3.9.

### 3.5 Surface displacement prediction

Recapping what has been discussed at this point of the analysis:

- An analytical form for the virtual surface by a polynomial interpolation has been stated
- The control points placement has been settled by a bilinear function used to describe the frame behaviour
- This set of control points it's used to characterize the displacement of the isolines that will control the physical surface

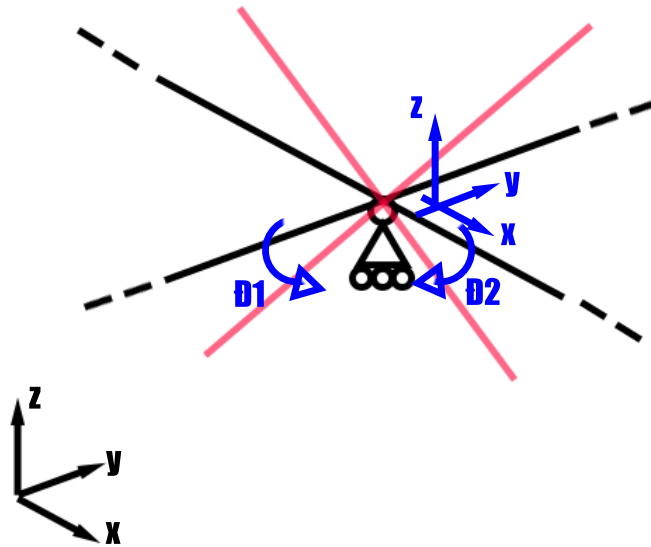


Figure 3.9: final control point configuration (in blue the 5 d.o.f.)

and what is really missing to complete a satisfactory description of the problem is a behaviour prediction of the physical surface on every point of the domain when it will be deformed by the control strips. To accomplish this a mathematical model of the surface must be introduced which has to take into account the following features:

- large displacements of the deformed shapes
- availability of high curvature radii at the same time
- material with low strain energy to keep low the actuators force

### 3.5.1 Kirchhoff theory of plates

Having based the previous study on an analytical form it's suitable to continue on this path. In literature we can find lot of theories to find a relation between stresses and strain for plates and membranes, and for sure the Kirchhoff theory on plates and shells [9] it's nowadays the most referred. This theory is based on the following hypothesis:

- No membranal forces applied
- Material has to be considered as linear, isotropic and elastic
- Middle plane of the plates must not warp

- Normal sections to the middle plane must stay straight after deformation
- Small displacement has to be taken into account

To understand the problem settlement please refer to [9]. The theory final form has the appearance of a *biarmonic* function:

$$\frac{\partial^4 w}{\partial x^4} + 2 \frac{\partial^4 w}{\partial x^2 \partial y^2} + \frac{\partial^4 w}{\partial y^4} = \frac{p}{D} \quad (3.13)$$

where  $D$  is the bending stiffness of the plate and is defined as

$$D = \frac{E}{1 - \nu^2} \int_{-\frac{s}{2}}^{+\frac{s}{2}} z^2 dz = \frac{Es^3}{12(1 - \nu^2)} \quad (3.14)$$

The solution to equation 3.13 can be find as a combination of biarmonic solutions that satisfy a set of constraints function. Although this theory define a rigorous analytical form, the hypothesis on which it's based on are not suitable from their roots for this work, due to large displacement of the physical surface. To overcome this issue there is the necessity to abandon an analytical formulation resorting to a finite element method that can take into account a formulation for a large displacement non linearity.

### 3.5.2 Finite element method approach

A generic form of the finite element method problem can be written as

$$[\bar{K}] \{\bar{D}\} = \{\bar{R}\} \quad (3.15)$$

where  $[\bar{K}]$  is the stiffness matrix which size and composition depends on the mesh element kind,  $\{\bar{D}\}$  is the vector of nodal displacements or the unknown set of variables, and  $\{\bar{R}\}$  is the vector of nodal loads. Being a problem in matrix form the solution is directly evaluated as

$$\{\bar{D}\} = [\bar{K}]^{-1} \{\bar{R}\} \quad (3.16)$$



In a finite element problem is possible to find three kinds of non-linearity affecting the relation between the relation between nodal displacements and nodal loads

- Non-linearity due to **material** where the property of the material (and therefore the formulation of the stiffness matrix) is a function of the stress state (i.e. plasticity, hyperelasticity)
- Non-linearity due to **contact** where the zone of application of the loads change with the loads itself (i.e. tyre-terrain contact)
- **Geometric** non-linearity due to large displacement affecting the point of application of the forces that may change in time (i.e. a forklift truck in its max elongation)

Those kind of problems are therefore non-linear because the stiffness matrix and the load vector becomes dependent from the displacement vector. The problem stated in equation 3.15 hence takes the following form

$$[\bar{K}(\bar{D})] \{\bar{D}\} = \{\bar{R}(\bar{D})\} \quad (3.17)$$

and the solution cannot be directly evaluated inverting the matrix as in equation 3.16. Referring to the physical surface problem it's necessary to take into account the geometric non-linearity introduced by large displacements. The solution it's evaluated using an iterative process starting from the undeformed configuration and stopping the iteration when the increment of displacements due to an increment of external loads it's minor than an arbitrary threshold. knowing the initial load  $\{R^{int}\}_1$  and the stiffness matrix  $[K_t]_1$  is directly evaluated the initial displacements vector  $\{D\}_1$ , then the external load is incremented, becoming  $\{R^{ext}\}$ , and the iterative process takes place

$$\{\Delta D\}_{i+1} = [K_t]_i^{-1}(\{R^{ext}\} \{-R_i^{int}\}) \quad (3.18)$$

$$\{D\}_{i+1} = \{D\}_i + \{\Delta D\}_{i+1} \quad (3.19)$$

Then it's directly constructed the new stiffness matrix  $[K_t]_{i+1}$  and the new load vector  $\{R^{int}\}_{i+1}$ . This process continue until a satisfactory condition is met:

$$\{\Delta D\}_{i+1} < \varepsilon \quad (3.20)$$

with  $\varepsilon$  arbitrary chosen. To finally state the complete finite element problem there is the need of another one component, that is the material specifications for the physical surface. To choose the right material for this purpose it's useful to use the Ashby's diagrams for material selection. The idea is to have a material that will

- minimize overall weight of the physical surface
- have a low strain energy and stiffness lower than a prescribed value
- have to possibility to warp in both perpendicular directions without reaching cusp shapes (i.e. to deform like a paraboloid)

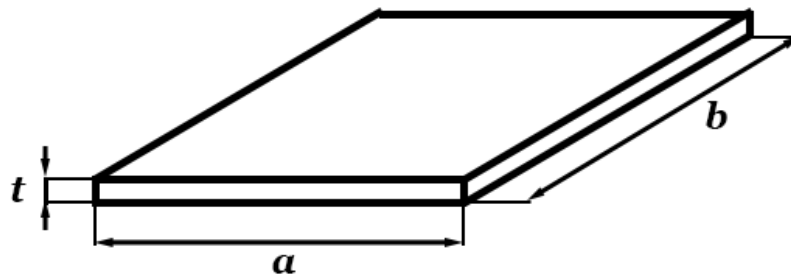


Figure 3.10: Physical surface measures

Referring to picture 3.10 are then defined the objective function that minimize the mass and the constraint function on the plate bending stiffness (from the equation of kirchhoff theory expressed in equation 3.14)

$$m = \rho abt = \rho At \quad (3.21)$$

$$D = \frac{Et^3}{12(1-\nu^2)} \leq D^* \quad (3.22)$$

Inverting equation 3.22

$$t = \left( \frac{12(1-\nu^2)}{E} D^* \right)^{\frac{1}{3}} \quad (3.23)$$

and substituting in equation 3.21

$$m = \rho A \left( \frac{12(1 - \nu^2)}{E} \right)^{\frac{1}{3}} = A(12(1 - \nu^2))^{\frac{1}{3}} \left( \frac{\rho}{E^{\frac{1}{3}}} \right) = A(12(1 - \nu^2))^{\frac{1}{3}} M \quad (3.24)$$

with

$$M = \frac{\rho}{E^{\frac{1}{3}}} \quad (3.25)$$

performance index for the further material selection stage. Since Ashby's diagrams are usually in a logarithmic scale, we pass the performance index in a logarithmic form as well

$$E = \frac{\rho^3}{M^3} \quad (3.26)$$

$$\log(E) = 3\log(\rho) - 3\log(M) \quad (3.27)$$

which represent a curve with slope equal to 3 on the plane density-Young's module. Mapping then classes of material on an Ashby's diagram it's possible to find which materials minimize the function 3.21.

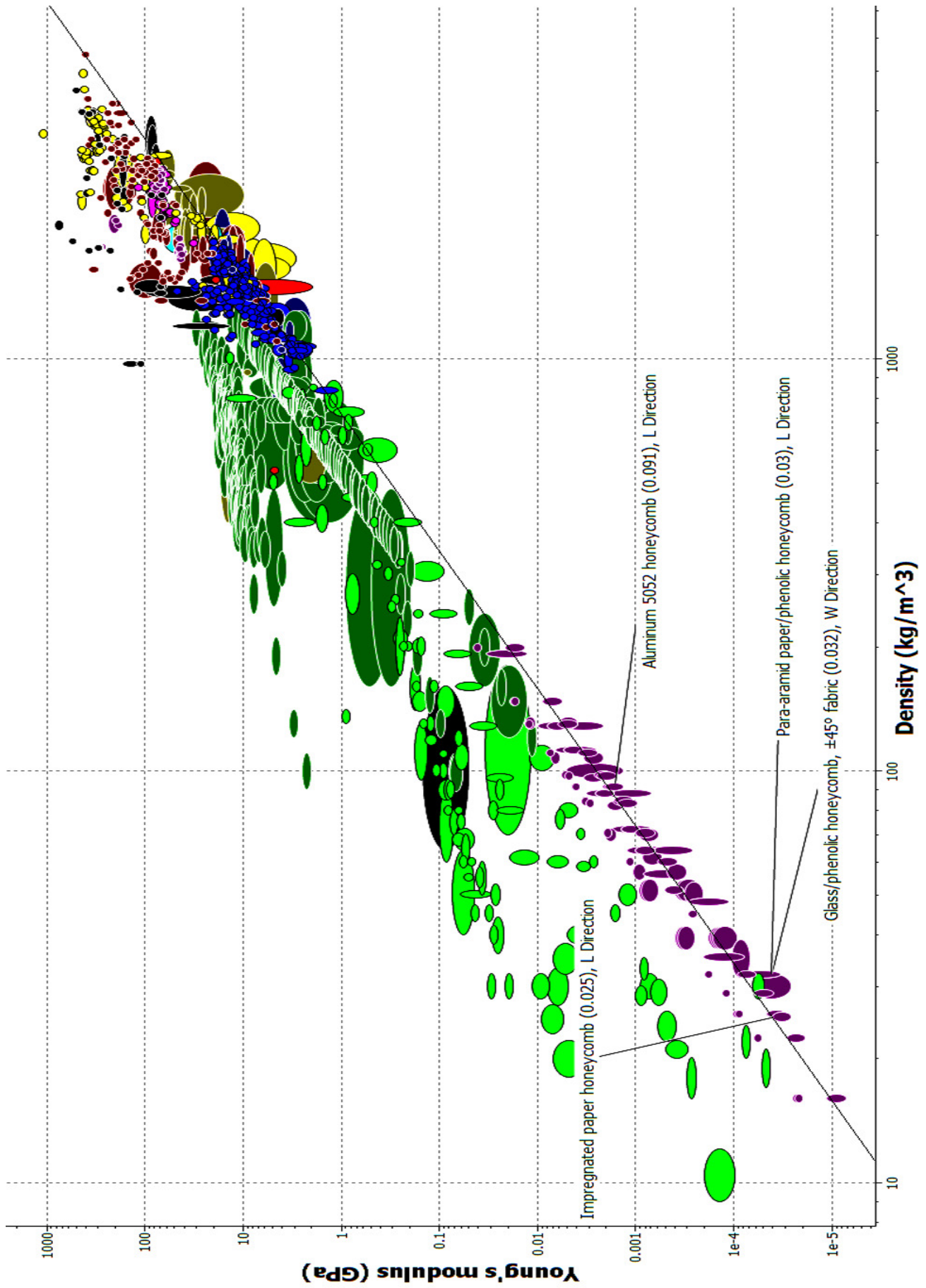


Figure 3.11: Ashby's diagram

Honeycomb properties						
Honeycomb material	Stabilized compression		Plate shear			
	Strenght [MPa]	Modulus [MPa]	Strenght [MPa]	Modulus [MPa]	Strenght [MPa]	Modulus [MPa]
			L direction	L direction	W direction	W direction
Aramidic paper	7.70	400	2.60	85	1.50	50
Aluminum alloy	3.31	393	1.45	90	0.90	45
Glass/Phenolic	0.86	90	0.62	41	0.31	21
Impregnated paper	0.60	38	0.50	16	0.25	11

Table 3.1: Honeycomb properties

As it's possible to see from figure 3.11 there is a common properties on different class of material, that is the honeycomb structure for core applications [15], which it's suitable for the stated problem but it also accomplishes the third main issue of this problem, that is the possibility to warp like a paraboloid.

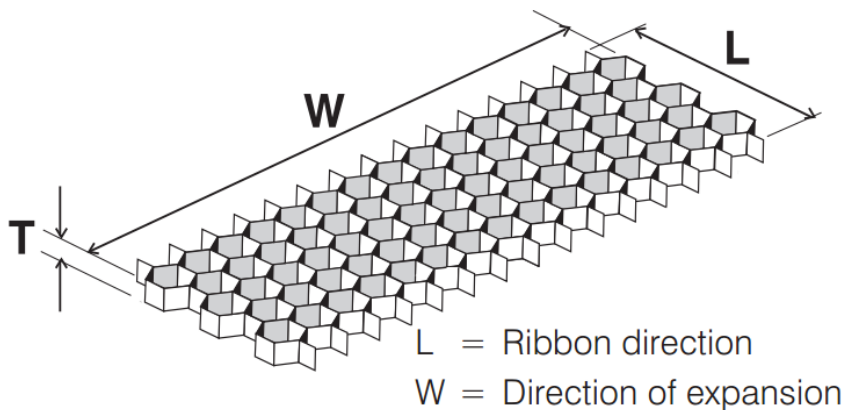


Figure 3.12: Honeycomb principal directions

In table 3.1 it's evident the honeycomb principal feature, that is the very poor mechanical properties in plane. For all this reasons a honeycomb sheet will be used as the physical surface and to remove the issue of discontinuity due to each elementary cell shape (i.e. hollow hexagon), this will be covered with a soft and elastic fabric that won't change the mechanical properties of the sheet but will give the right sense of continuity to the users touch while sliding their hand upon the shape. Another class of materials that lies on the selection curve and that could be an oddity for mechanical design is the class of auxetic materials, which features a negative Poisson's ratio. This class of materials requires a specific and

deepened analysis for a correct usage, for this reason a more accurate investigation has to be done in further dissertations.

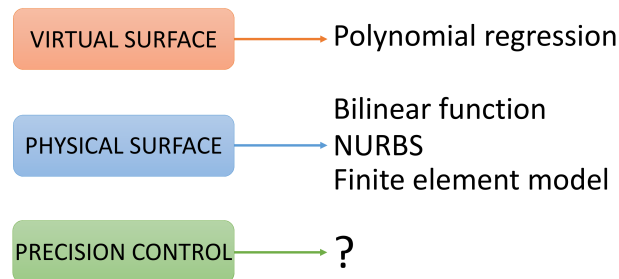


Figure 3.13: Components for the mathematical problem: physical surface

## 3.6 Final algorithm construction

The output of the process is defined by a set of five variables for each node, and to achieve this is necessary to put all the previous definitions together to construct an error function which will be minimized to obtain the highest possible accuracy from the physical surface approximating the virtual one.

### 3.6.1 Definition of an error function

Outcoming from the finite element analysis we have a set of nodal displacements spaced by a finite quantity defined by the mesh elements dimension. With the aid of a numerical method is possible then to asses the surface derivative  $e$  to compare it with the analytical function of the virtual surface previously stated. Before settling the error function, we recall the method to numerically estimate a derivative of whatever order.

**Definition 3.2.** Let  $f$  be a function defined on a set  $A \subseteq \mathbb{R}^2$ . The partial

derivatives of  $f$  at an interior point  $(a, b) \in A$  are given by

$$\begin{aligned} \left. \frac{\partial f(x,y)}{\partial x} \right|_{(a,b)} &= \lim_{h \rightarrow 0} \frac{f(a+h, b) - f(a, b)}{h} \\ \left. \frac{\partial f(x,y)}{\partial y} \right|_{(a,b)} &= \lim_{h \rightarrow 0} \frac{f(a, b+h) - f(a, b)}{h} \end{aligned} \quad (3.28)$$

in equation 3.28 assuming  $h$  as the smallest length defined by the mesh elements length it's possible to use the numerical approximation of the finite differences for the first order partial derivatives

$$\begin{aligned} \left. \frac{\partial f(x,y)}{\partial x} \right|_{(a,b)} &\approx \frac{f(a+h, b) - f(a, b)}{h} = D_1 \\ \left. \frac{\partial f(x,y)}{\partial y} \right|_{(a,b)} &\approx \frac{f(a, b+h) - f(a, b)}{h} = D_2 \end{aligned} \quad (3.29)$$

and following the same path we define the second order partial derivatives

$$\begin{aligned} \left. \frac{\partial^2 f(x,y)}{\partial x^2} \right|_{(a,b)} &\approx \frac{-f(a-h, b) + 2f(a, b) - f(a+h, b)}{h^2} = D_{11} \\ \left. \frac{\partial^2 f(x,y)}{\partial y^2} \right|_{(a,b)} &\approx \frac{-f(a, b-h) + 2f(a, b) - f(a, b+h)}{h^2} = D_{22} \end{aligned} \quad (3.30)$$

and the mixed partial derivative

$$\begin{aligned} \left. \frac{\partial^2 f(x,y)}{\partial x \partial y} \right|_{(a,b)} &\approx \frac{f_{1,1} - f_{1,-1} - f_{-1,1} + f_{-1,-1}}{4h^2} = D_{12} \\ f_{1,1} &= f(a+h, b+h) \\ f_{1,-1} &= f(a+h, b-h) \\ f_{-1,1} &= f(a-h, b+h) \\ f_{-1,-1} &= f(a-h, b-h) \end{aligned} \quad (3.31)$$

It's possible then to define the error on every single estimation:

$$\begin{aligned}
 \bar{e}_1 &= \left[ \frac{\partial f(x,y)}{\partial x} \Big|_{(x_i,y_i)} \right] - \bar{D}_1 \\
 \bar{e}_2 &= \left[ \frac{\partial f(x,y)}{\partial y} \Big|_{(x_i,y_i)} \right] - \bar{D}_2 \\
 \bar{e}_{11} &= \left[ \frac{\partial f(x,y)}{\partial x^2} \Big|_{(x_i,y_i)} \right] - \bar{D}_{11} \\
 \bar{e}_{22} &= \left[ \frac{\partial f(x,y)}{\partial y^2} \Big|_{(x_i,y_i)} \right] - \bar{D}_{22} \\
 \bar{e}_{12} &= \left[ \frac{\partial f(x,y)}{\partial x \partial y} \Big|_{(x_i,y_i)} \right] - \bar{D}_{12}
 \end{aligned} \tag{3.32}$$

and finally the error function

$$\begin{aligned}
 \bar{e} &= a_1 \bar{e}_1 + a_2 \bar{e}_2 + a_{11} \bar{e}_{11} + a_{22} \bar{e}_{22} + a_{12} \bar{e}_{12} \\
 \|err\| &:= \sqrt{\sum_{i=1}^n e_i}; \quad n = [1, 2, \dots, length(\bar{e})]
 \end{aligned} \tag{3.33}$$

where  $\|err\|$  is the euclidean norm of the error vector. Opportunely setting the values of  $[a_1 a_2 a_{11} a_{22} a_{12}]$  it's possible to give more importance to one term instead of another one, in this work the following values has been taken:

$$\begin{aligned}
 a_1 &= 0.125 \\
 a_2 &= 0.125 \\
 a_{11} &= 0.25 \\
 a_{22} &= 0.25 \\
 a_{12} &= 0.25
 \end{aligned} \tag{3.34}$$

in order to better weigh the second derivatives instead of the first ones, according to the studies about shape perception explained in the previous chapter.



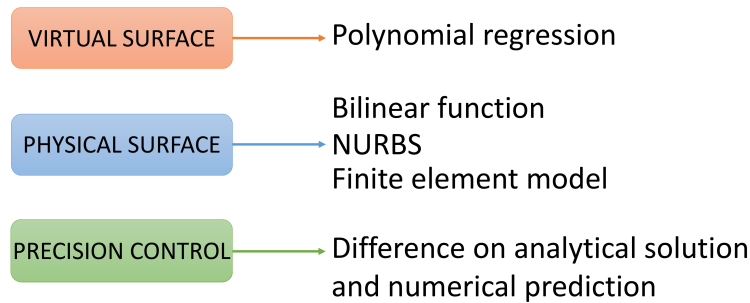


Figure 3.14: Components for the mathematical problem: error function

### 3.6.2 Functioning principle

Defined all the elements needed to state the algorithm it's necessary to build a sequence where this sub-algorithms will be called and used to minimize the error function 3.33. Referring to figure 3.15 after the polynomial fitting we obtain an analytical form of the virtual surface, as stated in section 3.3.1 with whom it's possible to search for points of minimum, maximum or saddles which will be used as constraints for the minimization problem. Firstly a random set of variable is generated taking into account the derivative constraints, and using the NURBS formulation discussed in section 3.4.1 the input for finite element analysis is written imposing displacements at certain nodes according to the strip warping predicted by the NURBS form. With the output of FEM analysis the error function is estimated with the equation 3.33 and if the difference of the euclidean norm of the error between two subsequent steps is minor than a small arbitrary threshold the algorithm stops and gives as output the last used set of variables, otherwise the initial solution is perturbed and changed exploring all the domain, trying to reach a global minimum for the error function. This final sets of variable will be then sent to the device which will translate the objective position from Cartesian coordinates to input signal for the actuators beginning the deformation of the physical surface. How this device is made and how it works will be discussed next.

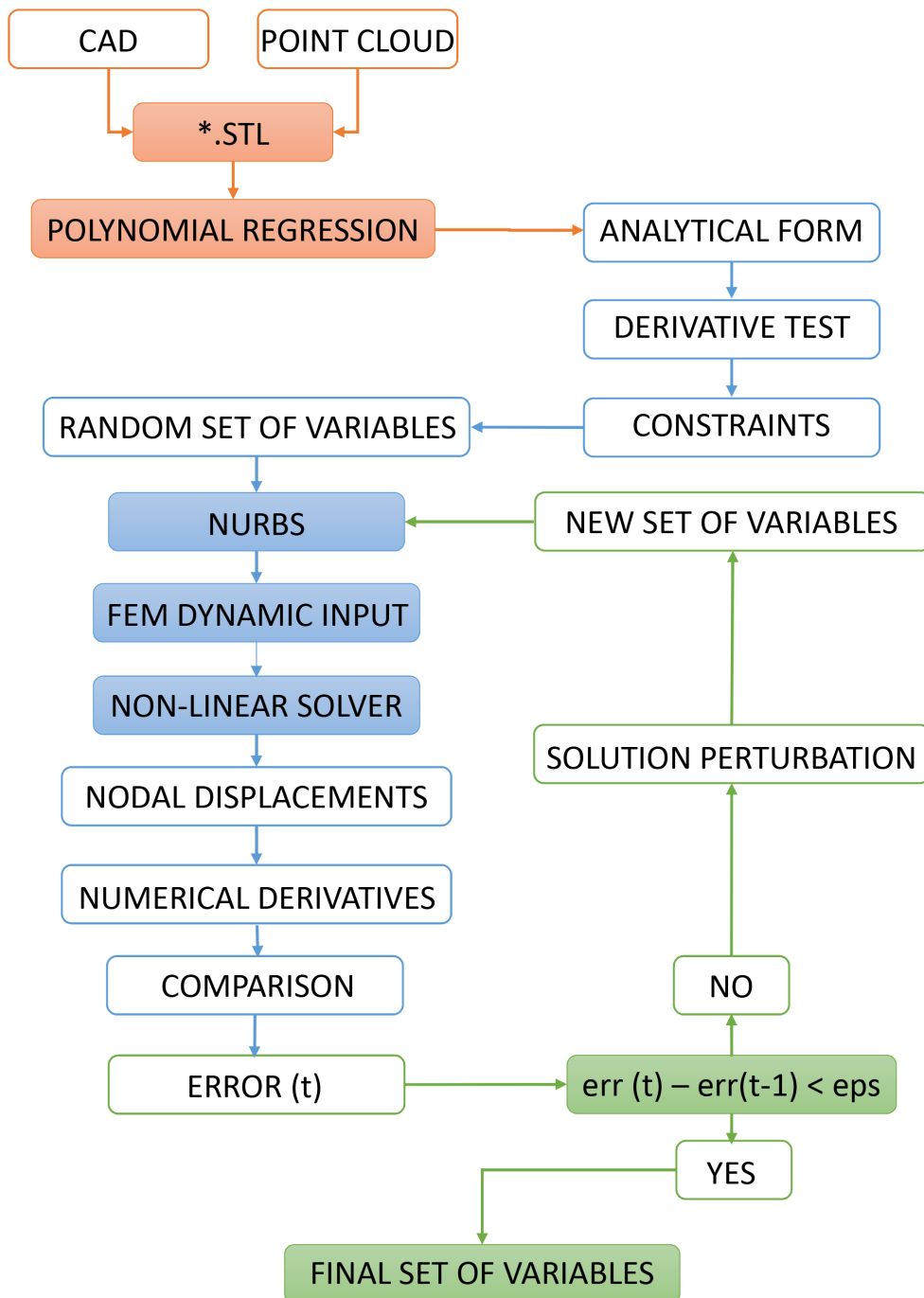


Figure 3.15: Algorithm

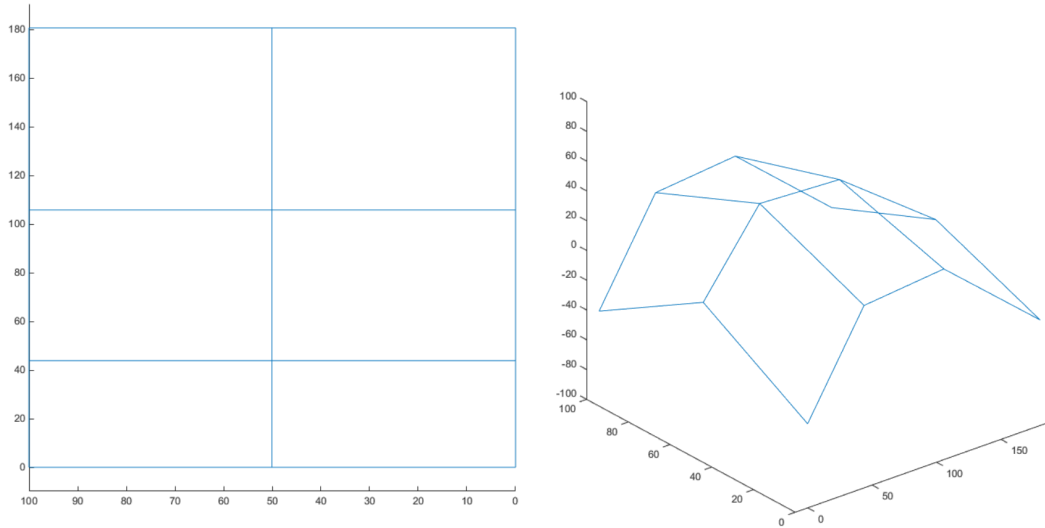


Figure 3.16: Bilinear function for the frame

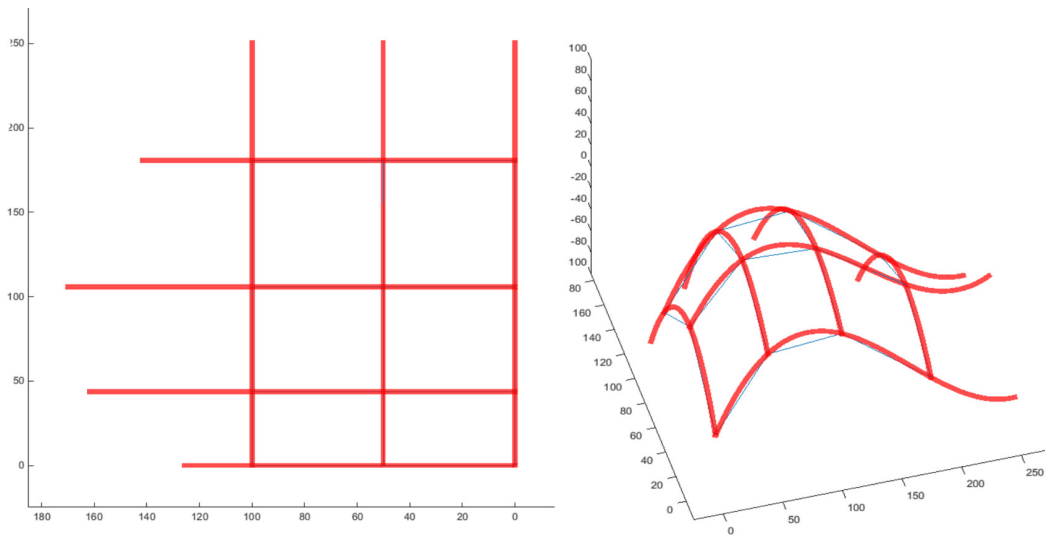


Figure 3.17: NURBS approximation

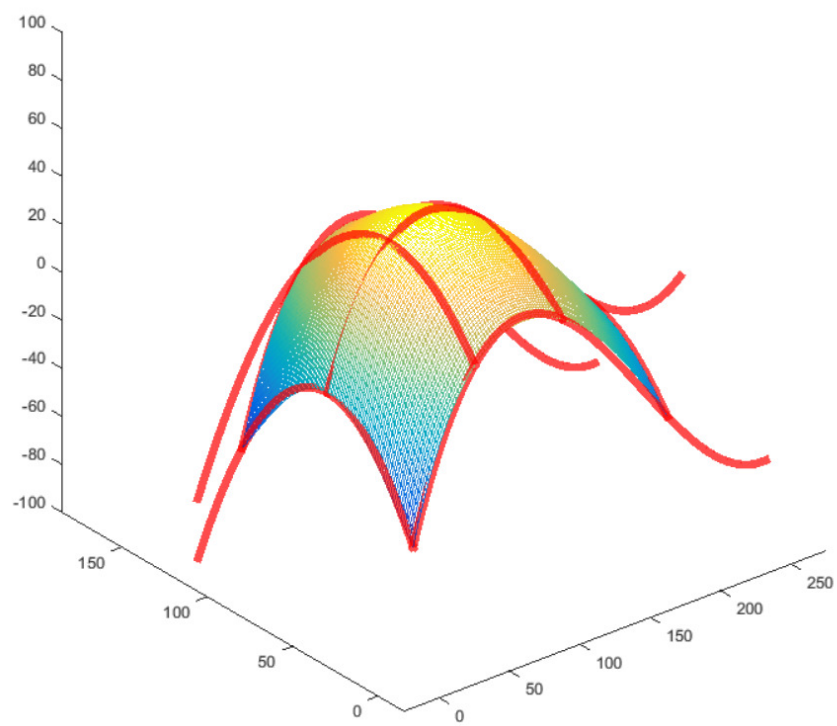


Figure 3.18: Honeycomb displacement prediction

# 4

## Physical Interface Design

This chapter shows a possible solution to design the tactile device. Starting from the outputs format established in the previous chapter will be given the instruments to achieve a good mechanical design paying attention on the resolution of the actuators and transmission systems in order to guarantee the right stiffness of the frame and minimize the backlash between mechanical components. In the first section will be selected the method to actuate every single degree of freedom. After that is proposed a possible sizing strategy to accomplish main features of the tactile interface. In the last section will be discussed a feasible approach to correctly control the mechanical system.

### 4.1 Initial considerations

Before starting to model the device itself, it is necessary to define the level of detail of the model and the developing approach. Recalling the main features of the interface:

- Modularity is the most important feature, therefore mechanical design can't

depend on the number of nodes used as control points

- Each node has to actuate five degrees of freedom
- Maximum surface area representable is defined by the external frame dimension
- Each module has to be as small as possible to increase device resolution

Those are the features that is required to deal with, and the final concept must be compared with them to check whether the design is attainable or not.

#### 4.1.1 Reducing d.o.f.

Given that each node has to actuate 5 d.o.f. it's immediate to understand the complexity of the mechanical problem, both the concentration of a lot actuator in a small place, both the huge number of overall actuators the system has to control (i.e. for a system with 40 nodes would need 200 actuators), and this is not feasible. For these reasons there is the necessity of decreasing the number of degrees of freedom without lowering the accuracy of the mathematical model explained in the previous chapter. Due to the formulation of the problem stated in section 3.3.2, every single frame node share the same planar x and y coordinates with other nodes as also graphically shown in figure 3.7 and 3.18, and thus is suitable to consider a unique a degree of freedom that will govern the x or y position of an entire isoline, indeed of all the control nodes laying on that isoline.

In figure 4.1 are shown the degrees of freedom for a 3-by-2 patch, using 60 degrees of freedom for only 12 control points (slope control d.o.f. are not shown). Using the explained technique it's possible to considerably reduce the overall degrees of freedom (figure 4.2 the 24 degrees of freedom imputable to slope control stay the same, but the 36 d.o.f. due to frame positioning become 19 and, considering  $x_1$  and  $y_1$  as the origin, even 17, thus globally 41 d.o.f., that is about 33% of initial actuators saved. In this way the total number of degrees of freedom that still remain in the proximity of the nodes become three (i.e. the  $z$  vertical displacement and  $\theta_x$  ;  $\theta_y$  the rotation of the strips about the node) instead of five, the other two d.o.f. can be moved on the side and placed in order to actuate the entire spline on which nodes share the same coordinate (e.g.  $[z_5 z_6 z_7 z_8]$  share the same coordinate  $x_2$ ). The struggle of decentralizing the degrees of freedom will consist in finding a way to actuate more nodes on the same side without being affected of the number of d.o.f. that will be placed on it.

#### 4.1.2 Overview on actuating system

An actuator is a type of motor that is responsible for moving or controlling a mechanism or system. It is operated by a source of energy, typically electric

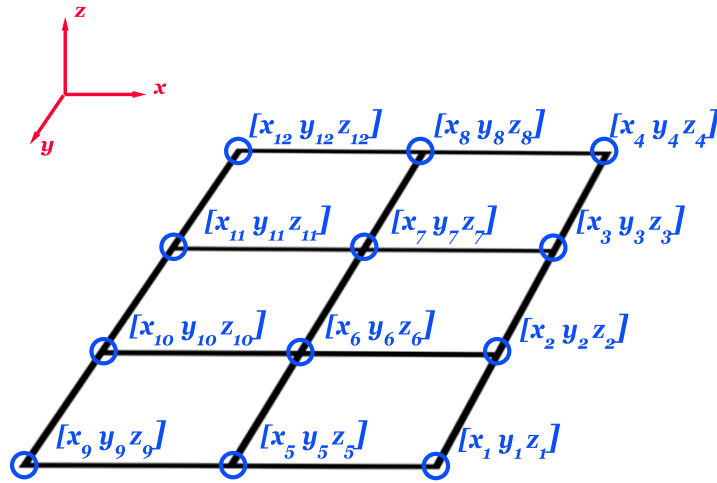


Figure 4.1: Frame positioning d.o.f.

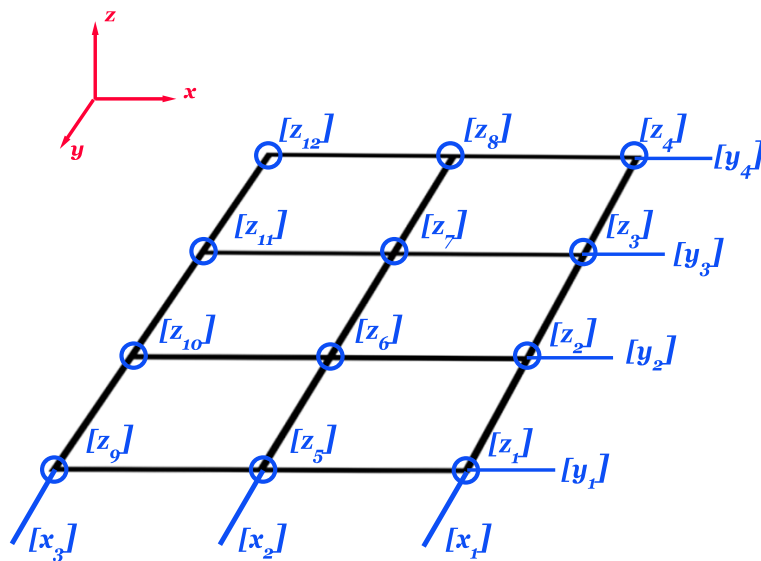


Figure 4.2: Reduced d.o.f. number

current, hydraulic fluid pressure, or pneumatic pressure, and converts that energy into motion. Before starting an overview on mechanical actuating systems,

it's necessary to make a first big distinction. Actuating system are divide into *cartesian* and *relative*.

- **Cartesian actuating system** use a fixed reference system and every degree of freedom refers to it with a proper equation of motion (cf figure 4.3). This solution removes the possibility of representing implicit surface shape (e.g. a cylinder) but guarantee the maximum stiffness to the frame and minimize the overall actuating forces
- in **Relative actuating system** every node is not referred to a space-fixed reference system but a space-relative reference system placed in the preceding node. For this reason, usually it's used a spherical reference system instead of a Cartesian one (cf figure 4.4). This solution is the most flexible in term of representable shapes but to ensure a proper stiffness, since every actuator depends on the previous one, the first actuator of the chain has to provide a huge blocking torque or force, and furthermore to avoid mechanical backlash.

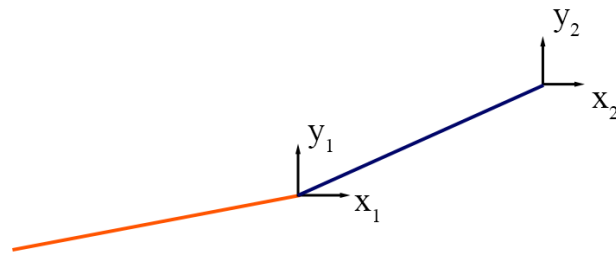


Figure 4.3: Degrees of freedom for a cartesian actuating system

furthermore the mechanical system can be:

- **Directly actuated** placing the actuator directly in the degree of freedom that will be actuated. This choice increase the dimension of the overall solution but reduce the possibility of non-located control problem, first cause of instability in the mechanical system
- **Remotely actuated** using an actuator that is placed far away from the degree of freedom and using a proper transmission system, introducing an auxiliary fictitious degree of freedom. On the other hand this solution leads to instability, actuator jittering but substantially reduce the size of the mechanical system.



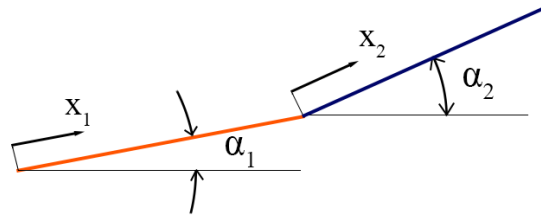


Figure 4.4: Degrees of freedom for a relative actuating system

Taking into account what explained right now, in this dissertation has been chosen a space-fixed Cartesian actuating method, directly placing the actuators wherever it would have been necessary to have them. Following discussion thus regards only the choice of the proper actuator and transmission methods to ensure the features previously explained. Referring to figure 4.2, in this works has been uncoupled the overall degrees of freedom in three main groups:

- $x$  and  $y$  planar d.o.f.
- $z$  vertical d.o.f.
- $\theta_1$  and  $\theta_2$  slopes d.o.f

and therefore is possible to inspect them separately.

## 4.2 Device structure and kinematic analysis

Before proceeding with the model sizing is necessary to give a background of kinematic analysis to understand how the device will behave. In figure 4.5 is shown a first concept of a quadrilateral element, and to characterize the movement of a single module we need to separate the 3D equations of motions in an equivalent form of combined planar equations.

Given the kinematic chain in figure 4.6, is possible to write down the vectorial equation that describe the position in space of the control point:

$$\bar{a} + \bar{b} + \bar{c} = \bar{d} \quad (4.1)$$

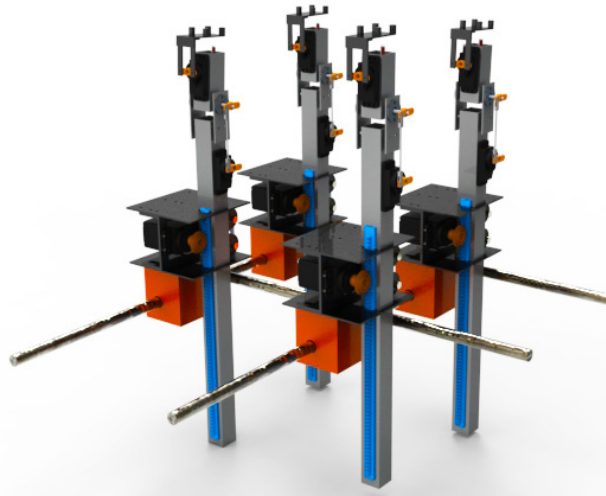


Figure 4.5: Concept of a quadrilateral element

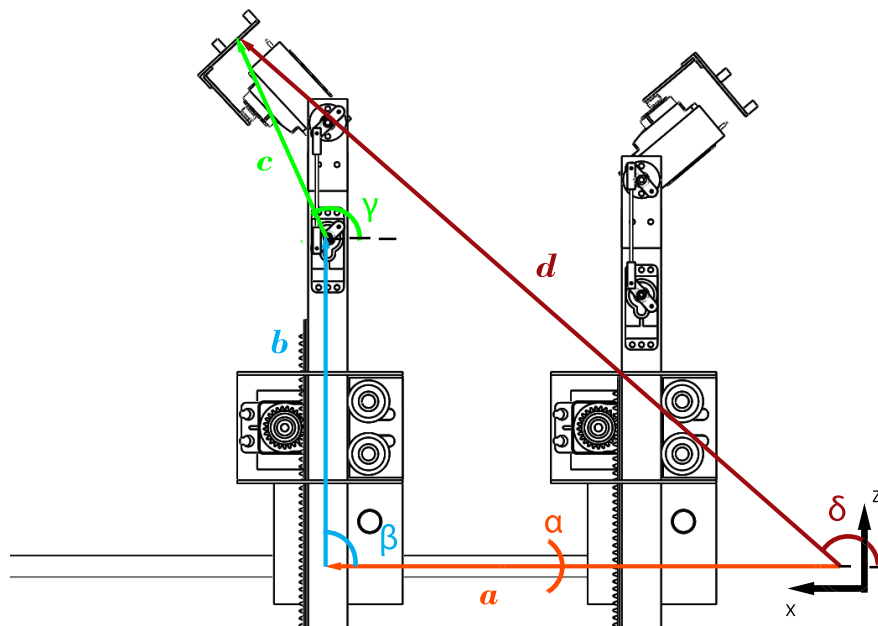


Figure 4.6: Kinematic chain in x-z plane

splitting it in a scalar form

$$\begin{cases} a \cos \alpha + b \cos \beta + c \cos \gamma = d \cos \delta \\ a \sin \alpha + b \sin \beta + c \sin \gamma = d \sin \delta \end{cases} \quad (4.2)$$

Kinematic chain properties		
variable	type	state
a	variable	unknown
b	variable	unknown
c	constant	known
d	variable	known
$\alpha$	constant	known
$\beta$	constant	known
$\gamma$	variable	known
$\delta$	variable	known

Table 4.1: Kinematic chain properties

In equation 4.2 the only unknowns are  $a$  and  $b$  that aren't the  $x$  and  $z$  coordinate of the control point but the position of the module that let the slope control module to reach the control point with the desired curvature. Some terms of this equations are even constant and known, like  $\alpha = 0^\circ$  and  $\beta = 0^\circ$ , all of its properties are reported in table 4.1. The equations of planar motion indeed becomes:

$$\begin{cases} a = d \cos \delta - c \cos \gamma \\ b = d \sin \delta - c \sin \gamma \end{cases} \quad (4.3)$$

The same reasoning can be done on the kinematic chain in  $y$ - $z$  plane, as shown in figure 4.7 Therefore it's easy to understand that to completely define the problem it is necessary to have an initial and a final position for  $x, y$  and  $z$  coordinates, and to control the system we need to pass the final position to the servomotor that make the control with its internal closed loop.

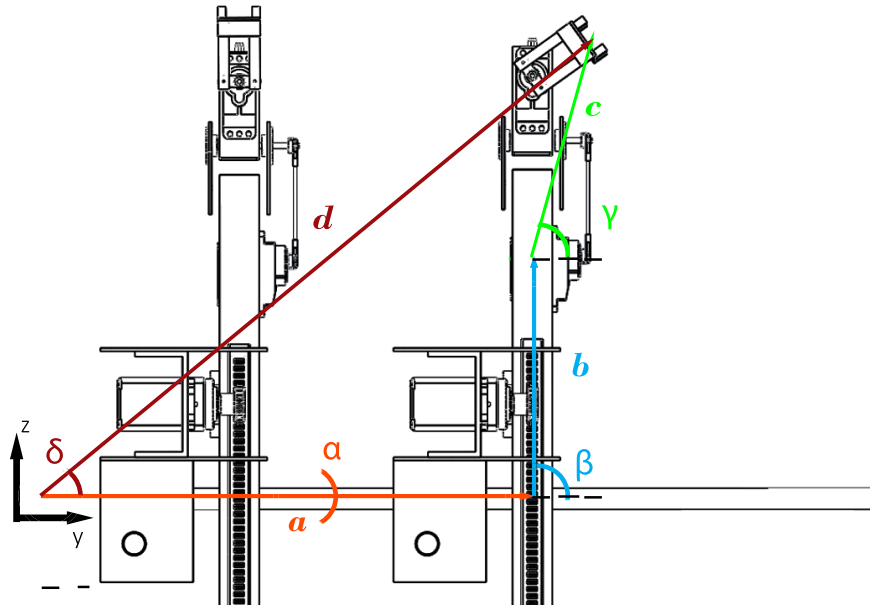


Figure 4.7: Kinematic chain in y-z plane

### 4.2.1 Servomotor control

A servomotor [31] is a dc motor designed specifically to be used in a control system. A pair of potentiometers acts as an error-measuring device. They convert the input and output positions into proportional electric signals. The command input signal determines the angular position  $r$  of the wiper arm of the input potentiometer. The angular position  $r$  is the reference input to the system, and the electric potential of the arm is proportional to the angular position of the arm. The output shaft position determines the angular position  $c$  of the wiper arm of the output potentiometer. The difference between the input angular position  $r$  and the output angular position  $c$  is the error signal  $e$ , or

$$e = r - c \quad (4.4)$$

The potential difference  $e_r - e_c = e_v$  is the error voltage, where  $e_r$  is proportional to  $r$  and  $e_c$  is proportional to  $c$ ; that is,  $e_r = K_0 r$  and  $e_c = K_0 c$  where  $K_0$  is a proportionality constant. The error voltage that appears at the potentiometer terminals is amplified by the amplifier whose gain constant is  $K_1$ . The output voltage of this amplifier is applied to the armature circuit of the dc motor. A fixed voltage is applied to the field winding. If an error exists, the motor develops a torque to rotate the output load in such a way as to reduce the error to zero.

For constant field current, the torque developed by the motor is

$$T = K_2 i_a \quad (4.5)$$

where  $K_2$  is the motor torque constant and  $i_a$  is the armature current. When the armature is rotating, a voltage proportional to the product of the flux and angular velocity is induced in the armature. For a constant flux, the induced voltage  $e_b$  is directly proportional to the angular velocity or

$$e_b = K_3 \frac{d\theta}{dt} \quad (4.6)$$

where  $e_b$  is the back emf,  $K_3$  is the back emf constant of the motor, and  $\theta$  is the angular displacement of the motor shaft. Therefore having as an input the final position of the servo, the mechanical system will evolve till the final position is reached and maintained, and the servo will keep this position even if an external load is applied, providing a torque reaction.

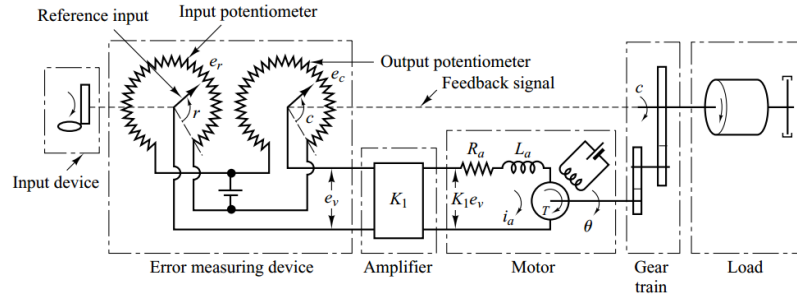
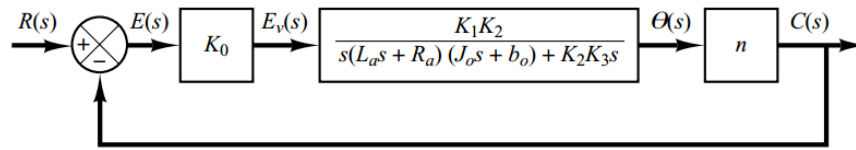


Figure 4.8: Schematic diagram of servo system [31]

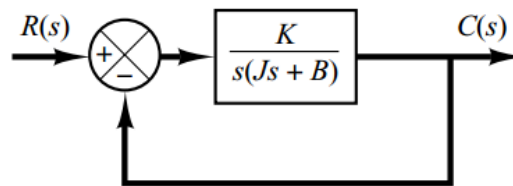
### 4.2.2 x y and z actuating system

The basic idea behind the actuating of  $x$  and  $y$  planar d.o.f. is to move the isolines in perpendicular direction in order to position a control point in its  $x$  and  $y$  coordinate as shown in figure 4.10

The same idea is used in the working principle of 3D printers and CNC milling machines, even with different kind of actuation. Before making a decision is necessary to evaluate the several possibilities to linearly move the isolines.



(a) Complete block diagram



(b) Simplified block diagram

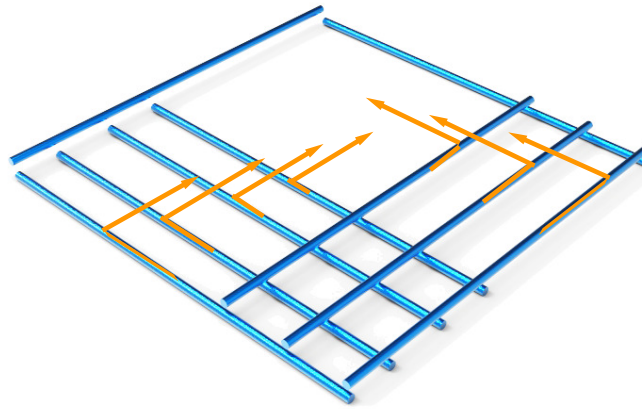
Figure 4.9: Block diagram of servo system [31]

One of the most used, accurate and precise solution for linear motion is **ball screws**. They use a nut that slides upon a lead screw whenever the lead screw is rotating (cf figure 4.11, to a rotation of  $\alpha$  is related an advancement of  $x$ ), and the motion is supported by ball spheres that flow through the nut. Their main advantages are:

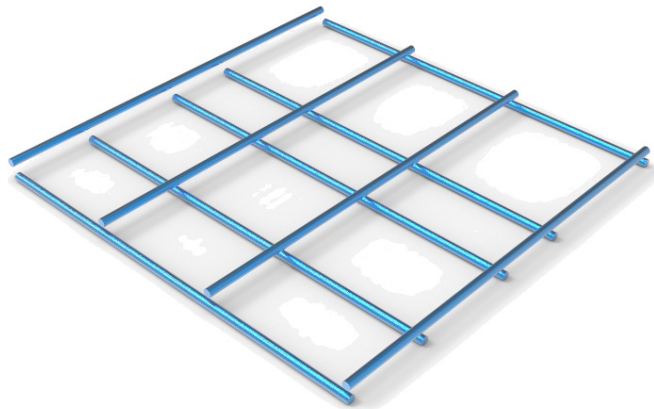
- Highest precision among linear actuating system
- Possibility of long range of actuation. Actually there is no influence of the total length of the screw
- High stiffness and low backlash
- Lowest friction
- Handle both compression and tensile loads

main disadvantage are:

- Very expensive, due to the surface treatment of the lead screw and its manufacturing precision
- Possibility of actuating only one nut per screw



(a) Isolines initial position



(b) Isolines final position

Figure 4.10: X-Y positioning

As it's possible to see from figure 4.10, assuming a side blue line as a lead screw, on every screw will be placed many isolines and not only one. Since the ball screws can actuate only one nut at time, even if their mechanical properties are certainly suitable, this cannot be the right choice, due to the modularity constraint stated before. Other popular choices for linear motion are *hydraulic actuators*, *piezoelectric actuators* and *geared brushless motors coupled with timing*

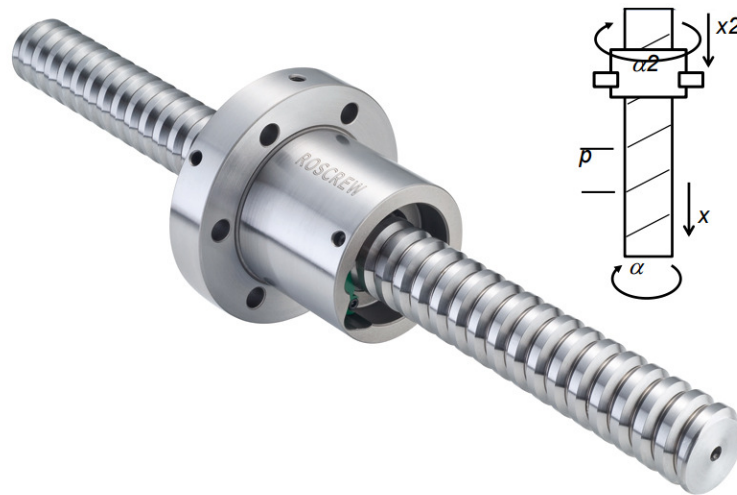


Figure 4.11: Ball screw scheme

*belts*, but all of that possibilities are affected by the same ball-screws issue, that is the necessity of a single system dedicated to every isoline movement, increasing the total amount of space required, losing therefore the modularity effect.

To overcome this issue can be adopted a *rack-pinion coupling* as suggested by Mansutti [25]. Assuming every isoline is a shaft with two opposite gears shrink-fitted on it, is possible to consider the external frame as four squared racks (as shown on figure 4.12) on which the pinions can slide. The intersection of two orthogonal shafts will be the housing of two roller bearings that sustain the module needed to actuate the  $z, \theta_1, \theta_2$  degrees of freedom. Main advantages of this solution are:

- No dependence on number of isolines actuated
- Cheapness
- Compactness and robustness
- Easiest way to convert rotation motion into linear motion
- Simple maintenance

On the other hand main disadvantages are:

- Backlash
- Racks and pinions can only work with certain levels of friction. Too high the friction and the mechanism will be subject to wear more than usual and will require more force to operate



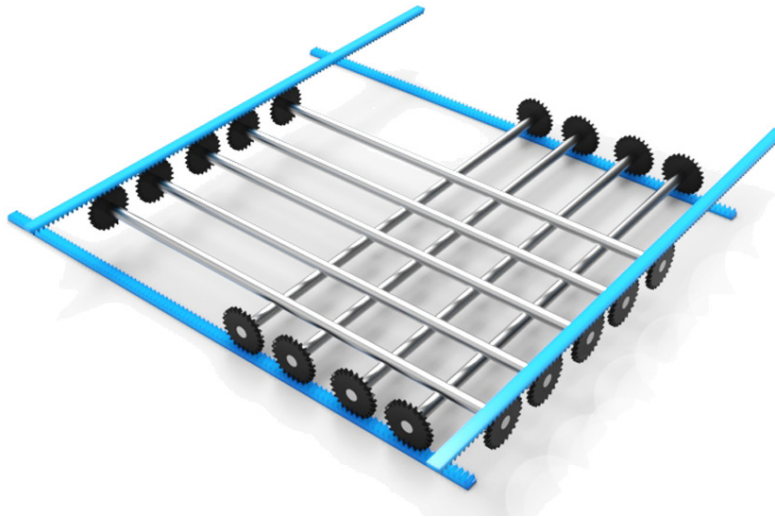


Figure 4.12: Concept of x-y actuating system

- Possibility of jamming

With a proper sizing strategy would be possible to limit those disadvantages. It will be discussed in the next section. As explained, to let this transmission method work there is the necessity of making the shaft rotate. To accomplish this there are two principal ways

- Directly coupling the motor with the transmission shaft (figure 4.13)
- Pushing back the motor and transmitting the motion through a spur gear (figure 4.14)

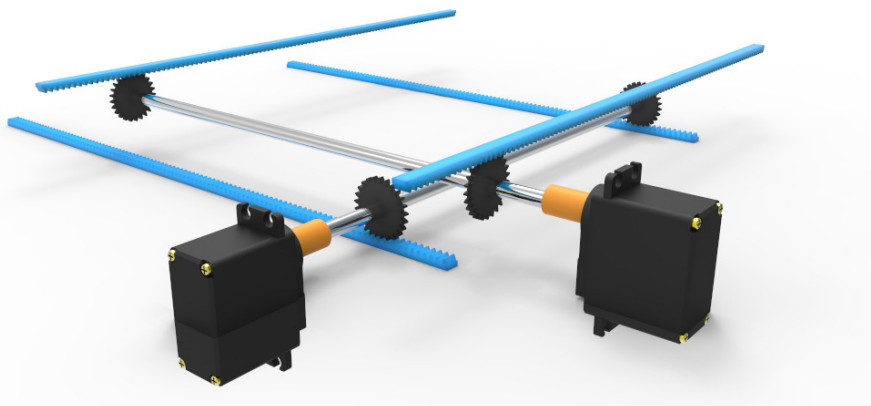


Figure 4.13: Direct motor coupling

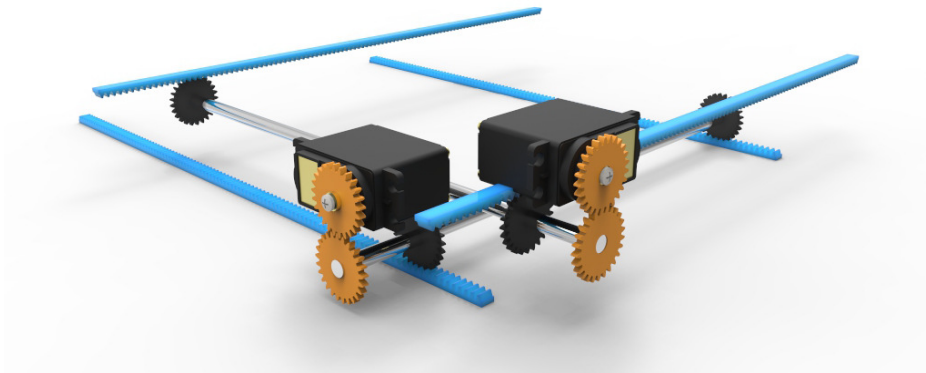


Figure 4.14: Spur geared transmission

Since in the final concept of the tactile display will be a huge amount of side motors, in order to keep low the overall cost, with the second method it's possible to achieve the same torque level with a smaller motor. For this reason the spur gear transmission will be considered the suitable one in this work.

With the explained method is possible to identify the  $x$  and  $y$  coordinates of a control point and it remains  $z$   $\theta_1$  and  $\theta_2$  degrees of freedom. While the two slope d.o.f. movement will be explained next, for what concerns the  $z$  position is acceptable to use the same considerations made before to choose the right actuating system, that is the same as the  $x$  and  $y$  degrees of freedom. The  $z$  position will be featured by a module, placed over the nut, which can push up and down a block for the slope control with a rack-pinion system.

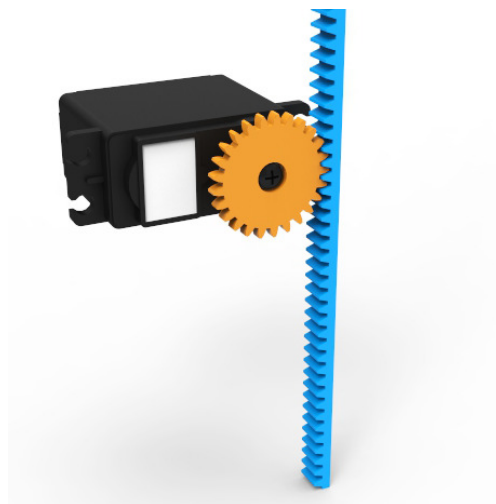


Figure 4.15: Vertical movement of the module

### 4.2.3 $\theta_1$ and $\theta_2$ actuating system

Defined a position for the control point in its Cartesian coordinates, it remains only to define a local curvature in both  $x$  and  $y$  direction. The enlightenment for this solution has been provided by previous study on geodesic strip [25], where similar solution were used to actuate bending and twisting degrees of freedom. The idea behind that is to have two housing for likewise servomotors, one upon another and to use their rotation to locally have uncoupled rotations of the control strips.

Starting from the vertical pin explained previously a servomotor is placed on the side of the rack housing, and using a four-bar linkage transmission system with two cranks of equal length to have the rocker arm always vertical. On the other

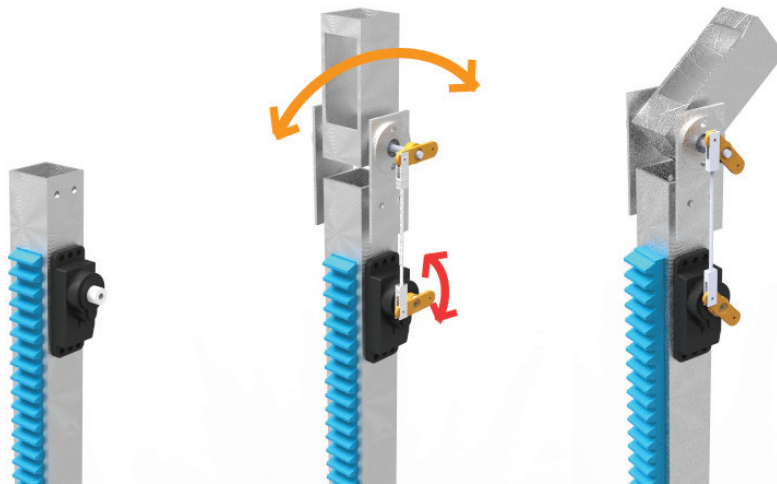


Figure 4.16: Slope control: housing for  $\theta_1$

side of the linkage is placed a second housing rigidly bonded to a transmission shaft that permit a  $180^\circ$  rotation of the housing (cf figure 4.16). In the second housing is placed the second servomotor on which is directly attached a bracket (cf figure 4.17) that can also rotate at least  $180^\circ$ , depending on the servomotor features (usually servomotors allow about  $270^\circ$  of rotation).

## 4.3 Components sizing

In this section will be discussed a possible strategy to design main components of the actuating system stated previously. Some of the following data has been reasonably supposed starting from commercial datasheets freely available on companies catalogues.

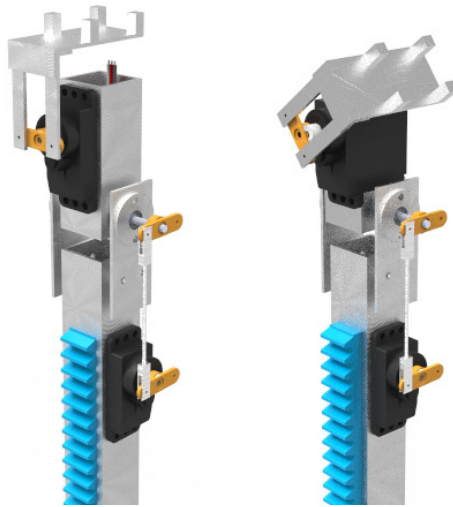


Figure 4.17: Slope control: housing for  $\theta_2$

### 4.3.1 Rack-pinion system for vertical degree of freedom

To correctly design the rack pinion coupling is possible to approximate the rack with a second spur horizontal teeth gear with primitive radius much bigger than the first one, as shown in figure 4.18. The design approach recalls the standard

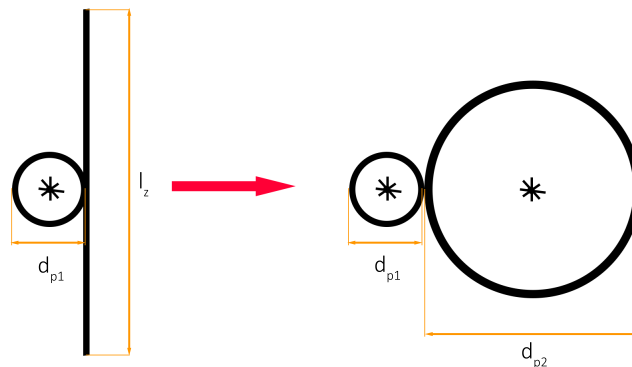


Figure 4.18: Approximation for the  $z$  rack-pinion coupling

method used for 3D printers, that is assuming the displacement and a standard time in which the gear must push the rack to the desired position. Assuming  $l_z = 200mm$  the overall length of the rack,  $\Delta t = 5s$  the time necessary to travel along the entire rack and  $d_{p1} = 20mm$  the primitive diameter of the servomotor

gear, it is possible to calculate the contact speed

$$v_c = \frac{l_z}{\Delta t} = 40 \frac{mm}{s} \quad (4.7)$$

and the gear angular speed

$$\omega_z = \frac{v_c}{d_{p1}} = 4 \text{rad s}^{-1} = 38.2 \text{rpm} \quad (4.8)$$

From previous studies [25] has been stated that the users during the shape evaluation usually perform a force  $F_z$  not bigger than 3 kg and then about 30 N. Then the servomotor has to provide a torque necessary to oppose this force:

$$T_z \geq F_z d_{p1} = 300 \text{N mm} \quad (4.9)$$

Assuming the rack as a gear of circumference equal to  $l_z$  we can evaluate its diameter  $d_{p2}$

$$d_{p2} = \frac{l_z}{\pi} = 63.66 \text{mm} \quad (4.10)$$

An important parameter for gears design is the module  $m$ , it relates the primitive diameter with the number of teeth  $n_t$  necessary to correctly transmit the motion between two gears. It is defined as following

$$m = \frac{d_p}{n_t} \quad (4.11)$$

For small gears and torques under 1000 N mm the commonly used module is  $m = 0.8$ . Number of teeth are therefore known for both rack and pinion:

$$n_{t1} = \frac{d_{p1}}{m} = 12.5 \simeq 13 \quad (4.12)$$

$$n_{t2} = \frac{d_{p2}}{m} = 79.59 \simeq 80 \quad (4.13)$$

With the same method is possible then to correctly size both  $x$  and  $y$  gears.

### 4.3.2 Four bar linkage design

$\theta_1$  degree of freedom, as explained, is necessary to control the slope of the strip, and to save space has been decided to put the servo motor far away from the joint a to use a four bar linkage to send the motion from the servomotor to the second motor housing. Using two cranks of equal length is possible to send the motion with no transmission ratio [30] and therefore there is no dependence of the cranks geometry on this solution. However the rocker has to be designed to rigidly transmit the motion with no deflection, and the main cause of possible deflections is the buckling that is a mathematical instability, leading to a failure mode. Buckling is characterized by a failure of a structural member subjected to high compressive stress, where the compressive stress at the point of failure is less than the ultimate compressive stress that the material is capable of withstanding. Mathematical analysis of buckling often makes use of an "artificial" axial load eccentricity that introduces a secondary bending moment that is not a part of the primary applied forces being studied. As an applied load is increased on a member, such as a column, it will ultimately become large enough to cause the member to become unstable and is said to have buckled. Further load will cause significant and somewhat unpredictable deformations, possibly leading to complete loss of the member's load-carrying capacity [19]. Due to the complexity of the problem is difficult to predict the deflection caused by the buckling, but a simple formulation has been provided by Euler. The normal maximum force can be evaluated as

$$F_n = \frac{F_{cr}}{\eta_s} = \frac{\pi^2 E I_{min}}{\eta_s L_0^2} \quad (4.14)$$

where  $E$  is the Young's module of the rocker,  $I_{min}$  is the minimum inertia of the section, that for a circular section is

$$I_{min} = \frac{\pi}{4} r^4 \quad (4.15)$$


$\eta_s$  is a safety factor instead and is defined as following

$$\eta_s = \frac{\pi^2 E}{\lambda^2 \sigma_y} \quad (4.16)$$

where  $\sigma_y$  is the yield stress and  $\lambda$  is the slenderness factor

$$\lambda = \frac{L_0}{\rho_{min}} \quad (4.17)$$

and  $\rho_{min}$  is the minimum radius of inertia equal to  $\sqrt{\frac{I_{min}}{A}}$  Taking the same servo-



Specifications	
Motor Type	Coreless
Bearing Type	Bushing
Speed	0.17 / 0.14 sec at 60°
Torque	1.1 / 1.3 kg.cm (4.8v/6v)
Size	22.60 x 11.40 x 23.90 mm
Pulse cycle	20 ms
Pulse width	900-2100 $\mu$ s
Weight	18.00g

Figure 4.19: Tilting servomotor characteristics

motor model from the previous study on geodesic strip we know the main features about the torque at the starting point, and using the Euler formulation for compressive instability we can obtain the minimum radius of the circle that avoid the buckling under compressive load caused by the servo ( $r_{rocker} = 1.7\text{mm}$ ).

### 4.3.3 Z servomotor bracket design

From the beginning of this dissertation stiffness has always been considered one of the most important parameter for the tactile device, but it has been never discussed from a mathematical point of view. The module used to actuate the  $z$  degree of freedom has been defined as a nut with double perpendicular linear bearings, with a servomotor on the top pushing a rack to actuate the slope control module; furthermore it is the only element which can oppose the force applied by the user hand during shape evaluation, therefore the bracket can be designed in order to minimize the vertical deflection and to guarantee the proper stiffness of the tactile device. From the model established in section 4.2.2, rack is still free to move and so it is the servomotor since there are some directions not fixed (cf figure 4.20). To solve this problem has been introduced two subsystems (cf

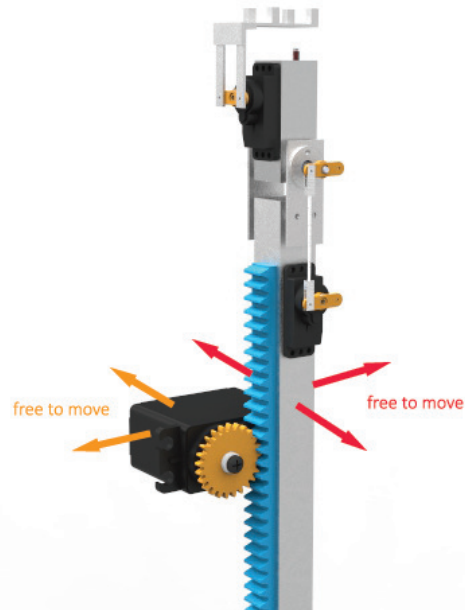


Figure 4.20: Module initial concept

figure 4.21):

- A slab IPE beam needed to hinge the servomotor and to create rail for the rack
- Two bearings needed to transform the rail into a sleeve and to give a kinematic stability to it

The IPE beam will be placed over the nut and will give the essential stiffness to the system. To use a standard *H-section*, the web and flanges thickness has been chosen equal to 2 mm

$$t_{flange} = t_{web} = 2\text{mm} \quad (4.18)$$

and the flange and web lengths has been chosen to fit the size of the system

$$\begin{aligned} l_{flange} &= 63\text{mm} \\ l_{web} &= 40\text{mm} \\ l_{IPE} &= 63\text{mm} \end{aligned} \quad (4.19)$$

To compute the section stiffness, a finite element model has been implemented to evaluate the real displacements in view of the load applied by the user ( $F_z = 30\text{N}$ )



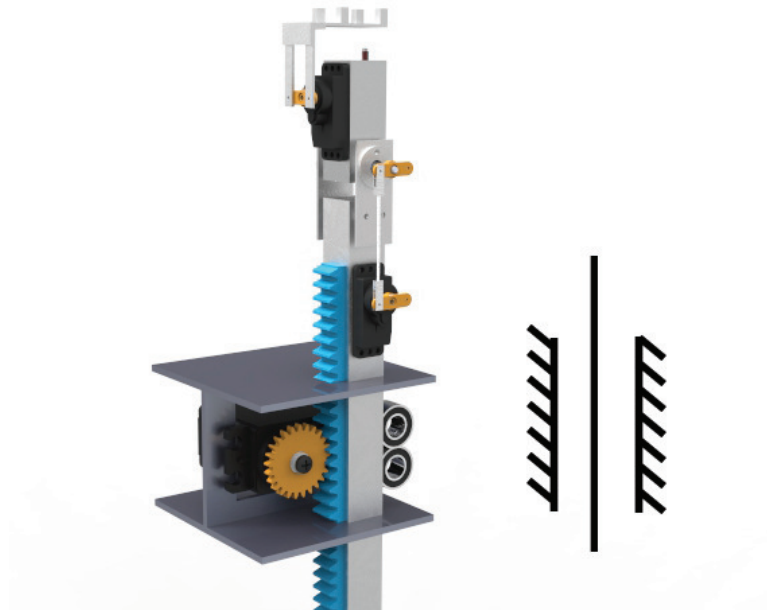


Figure 4.21: Module with bracket

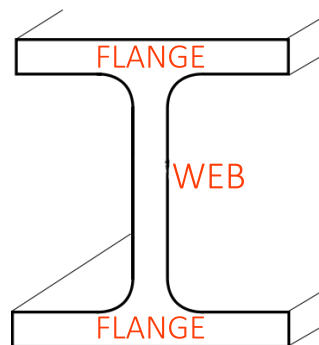


Figure 4.22: IPE beam nomenclature

and then evaluate the stiffness as

$$S = \frac{f_z}{\delta} \quad (4.20)$$

where  $\delta$  is the maximum displacement of the section. As it is possible to see from fem analysis results shown in figure 4.24, the maximum displacement is  $\delta = 0.01079\text{mm}$  on the external part of the upper flange, congruent with what theory says (i.e. it is the farthest point from the centre of inertia). Assessing the

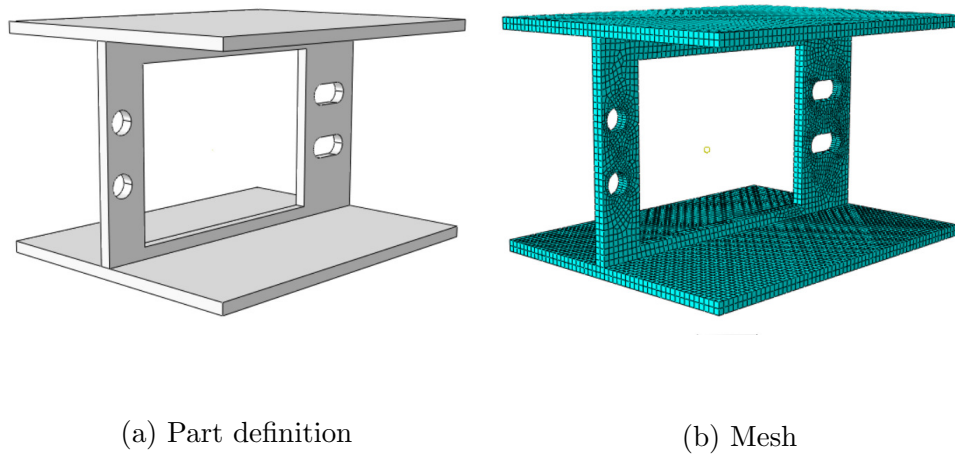
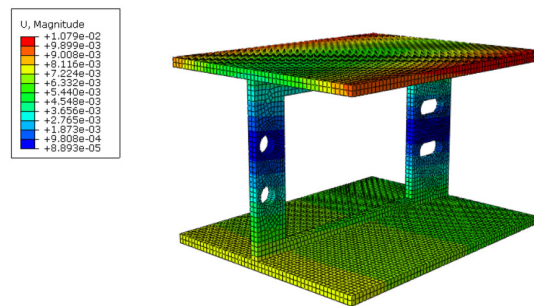
Figure 4.23: FEM analysis on IPE *H-section* beam

Figure 4.24: IPE displacements

stiffness:

$$\begin{aligned}
 \delta &= 0.01079\text{mm} = 1.079 * 10^{-5}\text{m} \\
 F_z &= 30\text{N} \\
 S &= \frac{F_z}{\delta} = 2.78 * 10^6\text{N m}^{-1}
 \end{aligned}
 \tag{4.21}$$

that is reasonable both in term of displacements both in term of stiffness.

## 4.4 Final model

In initial part of this chapter has been provided five main features on which it's possible to check the feasibility of the device:

- Five degrees of freedom for each control point
- Modularity

- High stiffness
- Small dimension of the single module
- Maximum area defined only by the external frame dimension

In figure 4.25 is shown 3-by-2 final concept of the tactile device. As required the modularity has been implemented with the isolines strategy: from a commercial point of view the user can establish the external frame dimension which represent the maximum surface area, and choose whatever number of isolines (and modules) to have under the honeycomb patch achieving a required level of accuracy. For each node has been implemented five fictitious degrees of freedom, placing the  $x$  and  $y$  motors aside. Stiffness has been discussed with the main component that could ensures it and the numerical results seems to meet the requirements. Furthermore, each module has an overall dimension of 63x63 mm which identify even the minimum distance between consecutive control points. It is therefore possible to assert that the proposed model for the tactile device meet the project requirements.

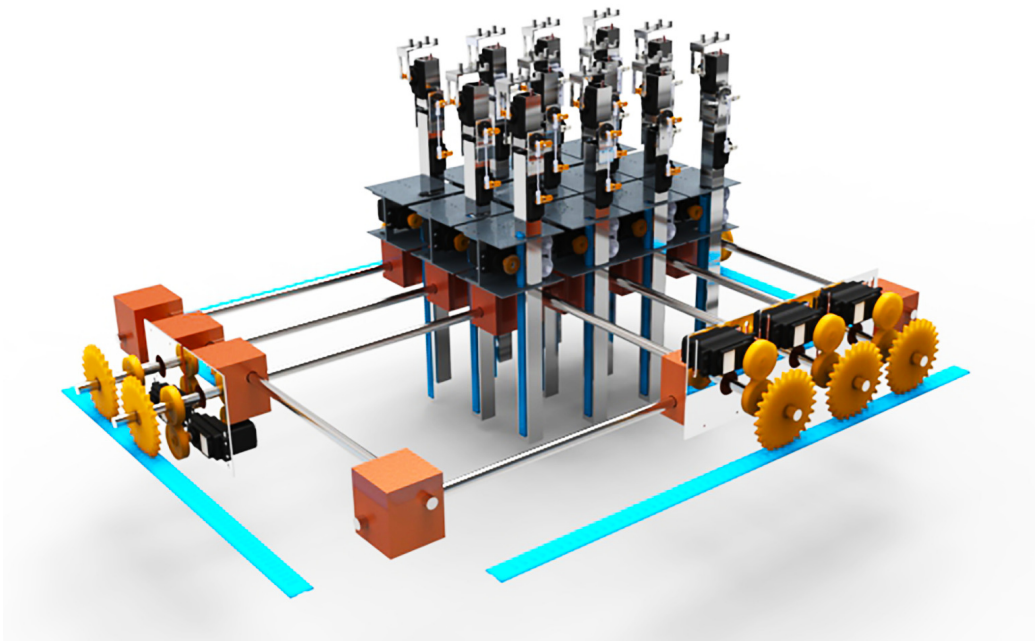


Figure 4.25: Final concept of the tactile device



# 5

## Model Validation

At this dissertation stage, a feasible model has been provided. In this chapter is presented some attempts to validate the previously explained model. In the first section is shown a numerical test led upon a real industrial component; after this will be illustrated the physical prototype used to test the construction of the tactile device and to compare it with some simplified shapes commonly used in product design.

### **5.1 Numerical test**

In order to verify the mathematical model and to test if this could be applied in a real industrial context it's necessary to compare it with a real industrial product design and examine whether it could bring to satisfying results in terms of the error function stated in section 3.6.1.

Many of the typical industrial product which require an important amount on resources spent in prototyping can be taken from the automotive industry. One of the most significant product is the car bonnet on which companies employ

for hours talented clay sculptor. Starting from this idea, a simplified shape of a



Figure 5.1: Car bonnet

bonnet has been designed in a CAD software, just like an industrial designer would do (figure 5.2), acquiring a geometric mesh. This mesh has been submitted in the

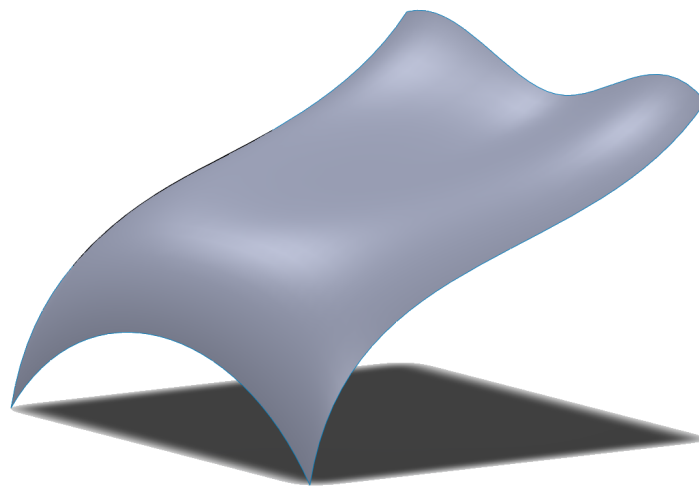


Figure 5.2: Simplified shape of a generic car bonnet

explained algorithm, which has been developed under the MATLAB numerical calculus environment (most significant part of the code is reported in appendix B). In this application we made the hypothesis of using a tactile device made by ten-by-ten elements to have a more accurate approximation, as shown in figure 5.3. The results outcoming from the algorithm are shown below

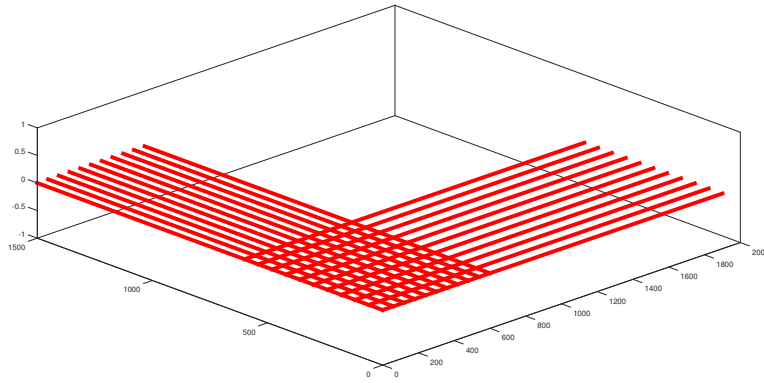


Figure 5.3: Initial undeformed configuration

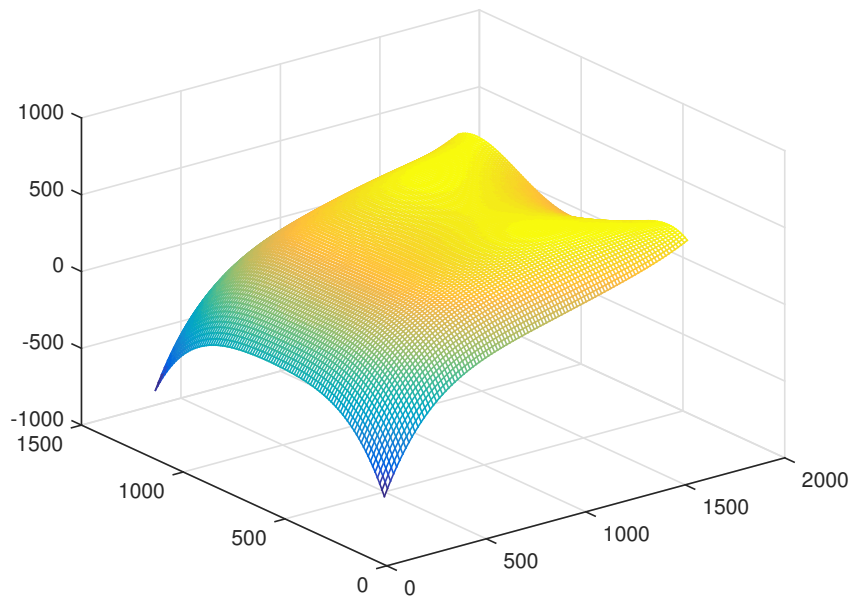


Figure 5.4: Polynomial surface interpolation

### 5.1.1 Results discussion

figures from 5.8 to 5.13 shows the error map evaluated at each mesh element individually for each components of the error function 3.33. As it was easy to expect, the algorithm penalize the first derivative in favour of the second ones, because in this thesis has been provided more important weights to them (cf. equation 3.34). Bigger error percentage occurs where the control strips,

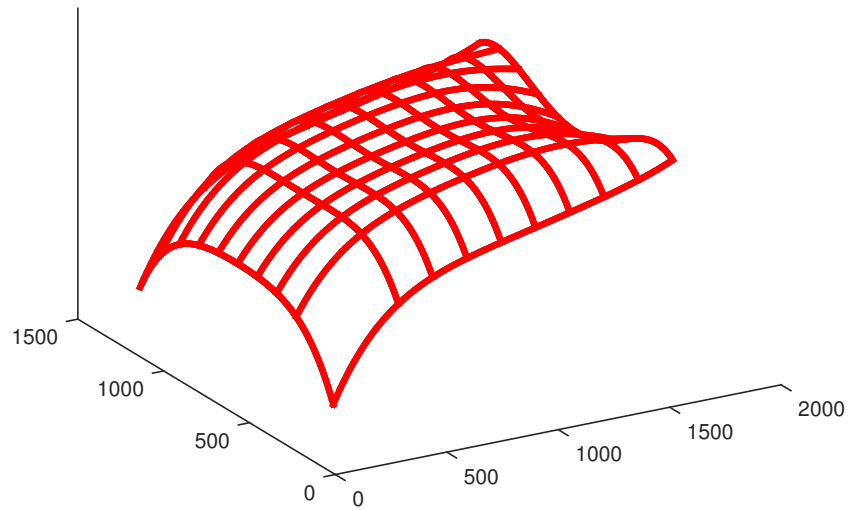


Figure 5.5: Control strips approximation

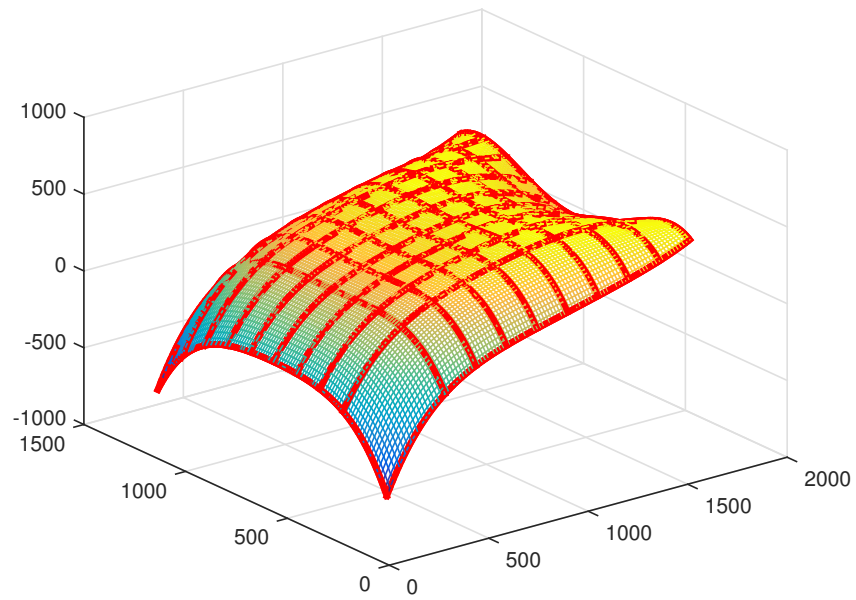


Figure 5.6: Comparison between control strips and virtual surface



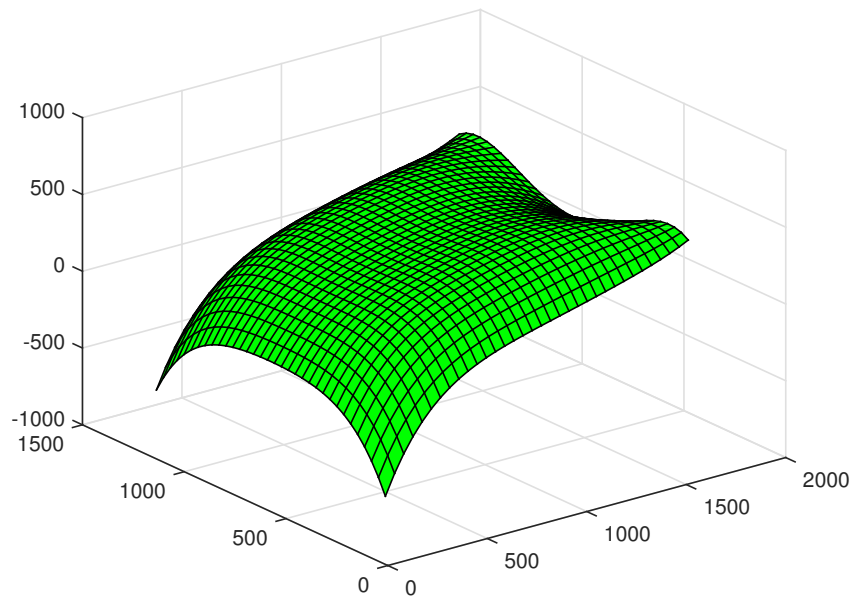


Figure 5.7: Finite element surface displacement prediction

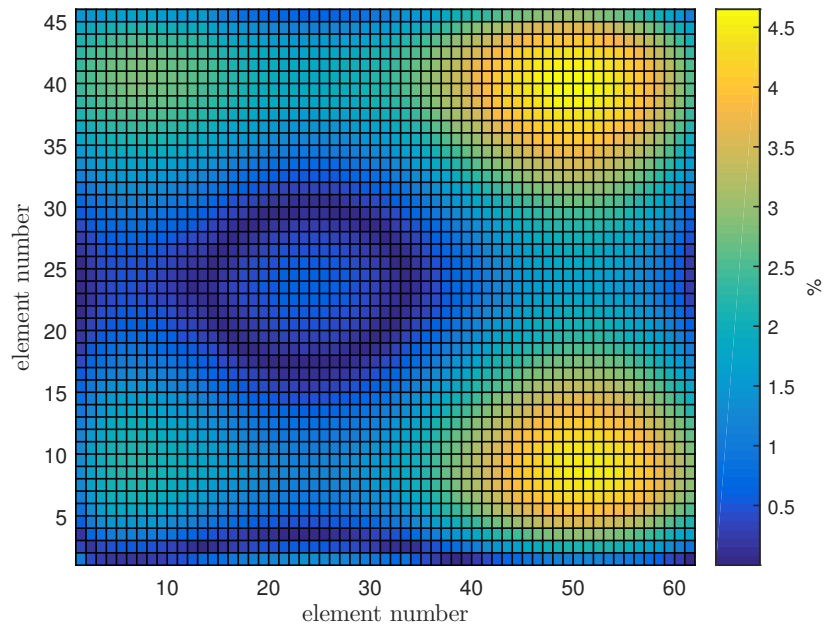


Figure 5.8: Error function: gap on nodal vertical displacement

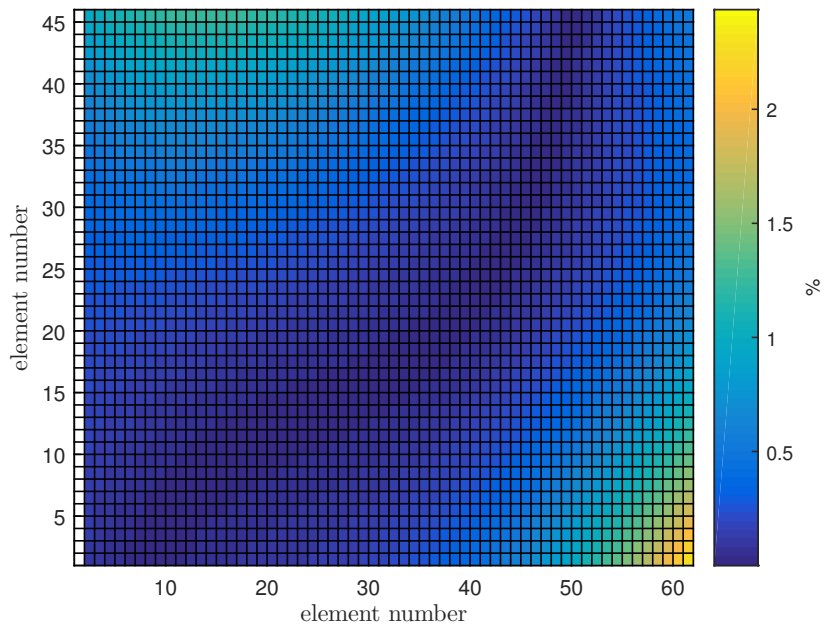


Figure 5.9: Error function: gap on first derivative in  $x$  direction

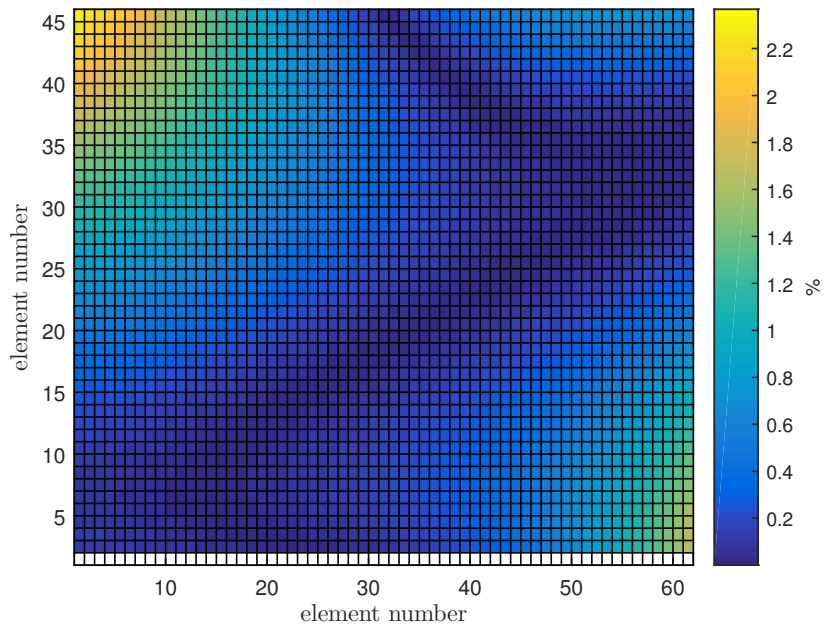
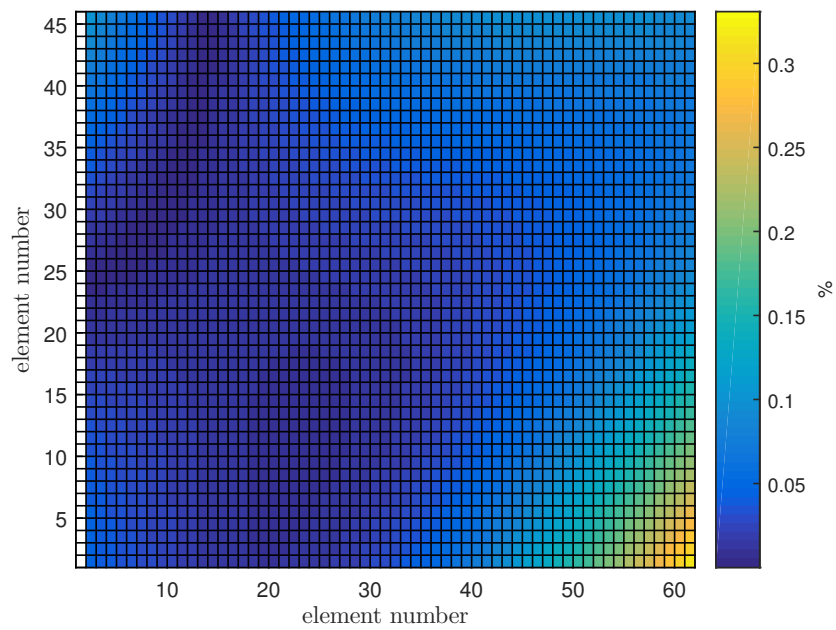
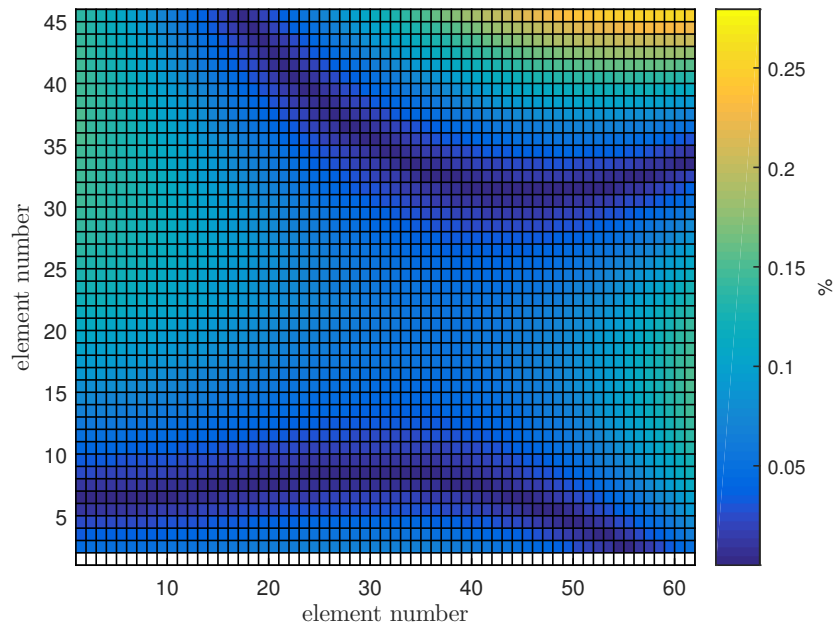


Figure 5.10: Error function: gap on first derivative in  $y$  direction

Figure 5.11: Error function: gap on second derivative in  $x$  directionFigure 5.12: Error function: gap on second derivative in  $y$  direction

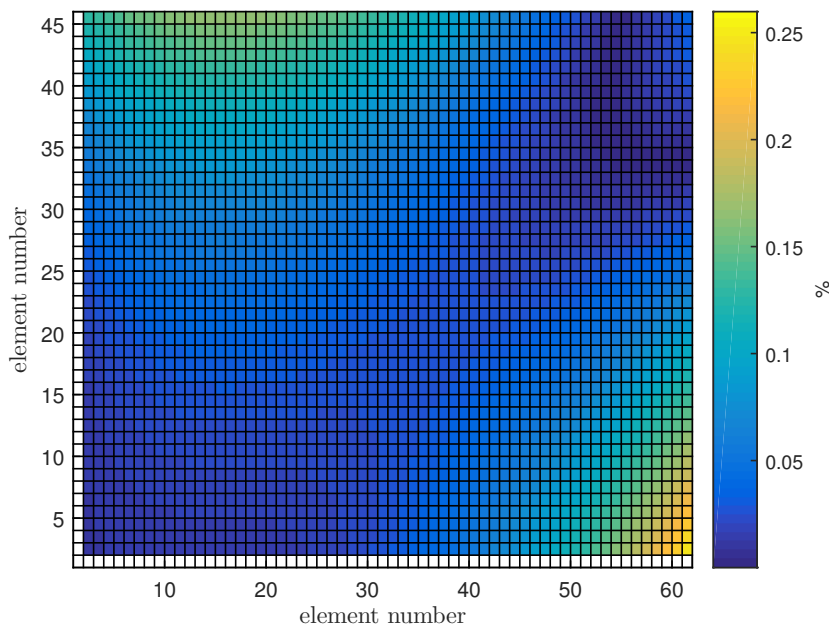


Figure 5.13: Error function: gap on mixed second derivative

and therefore the patch surface, are more distant to the control points, actually where the displacements and the curvature are only predicted and interpolated. Furthermore, from a computational point of view, the overall time required to complete all the subalgorithm has to be considered satisfying with only 97 seconds of research for a global minimum.

Referring to what previously explained on user experience during a shape evaluation, probably they would not notice the difference between the physical surface and the real one due to the small overall error percentage (always minor than 4%), but this point of view can be only verified with a test involving user opinions.

## 5.2 Prototyping

Before considering the project as reliable and ready to be implemented in a real industrial situation, it is important to check the construction and the trust of the results that this device can provide. To test the real performance of the designed device and to evaluate the tactile device construction it has been developed a prototype made up of 3-by-2 quadrilateral elements and thus twelve identical modules. The base is made of an anodised aluminium frame, which hosts the nuts and the servomotors in charge of moving isolines on the side and the runner.

By means of a rack and pinion transmission system made of hardened plastic, the servomotor is able to translate the single isoline along the longitudinal degree of freedom, and the vertical servomotor housing will push up and down the control point. Even if the mathematical model has been developed with the constraints of five degrees of freedom for each node, a prototype with only three degrees of freedom has to be considered more efficient to check the experimental results in a first try to build the device. For this reason the  $\theta_1$   $\theta_2$  degrees of freedom will be implemented in a further, more accurate, prototype. Building this prototype we hence consider admissible the limits of avoiding a curvature control as explained in section 3.4.2. Generally talking, a prototype is an original and functioning model of something from which other forms are copied or developed, and that fulfil the function stated in the task clarification phase, even if it is not made by the materials and forms expected in the original project design. Chasing this idea, the prototype has been constructed with the following properties:

- The steel *IPE H-section slab beam* has been substituted with two aluminium plates jointed by an anodised aluminium C-section beam (cf figure 5.16)
- Gears and racks has been maintained with the same module and number of teeth, but hardened plastic has been used instead of steel (cf figure)
- Nuts has been obtained from a block of hardened polycarbonate and ad hoc designed and machined with a desktop CNC machine, to perfectly fit and give the proper preload to the linear bearings (cf figure 5.14a and 5.15)
- Seventeen servomotors has been wired to a control board for servomotors capable of taking the input from the MATLAB algorithm and convert it to a PWM signal (i.e. pulsed squared waves) useful to assign the correct direction and speed of rotation to the servomotors shaft
- To avoid placement issues, every hole needed to joint brackets and components has been changed into a slot, overtaking then tolerances problems that could bring to interference (cf figure 5.19)
- Control strips has been made of polypropylene following the previous studies on geodesic strip

Furthermore, having the approximation of only 3 d.o.f. and some imprecisions outcoming from a hand construction, we considered not necessary to place the honeycomb patch over the control strips, even because it requires a more accurate analysis on what kind of honeycomb it's necessary to use and a more precise design of mechanical linking between honeycomb patch and control strips, that could be taken on further dissertations. As explained next, the experimental test will be based only on control strips evaluation.



(a) Polycarbonate milling

(b) Brackets

(c) Plates

Figure 5.14: Components CNC machining

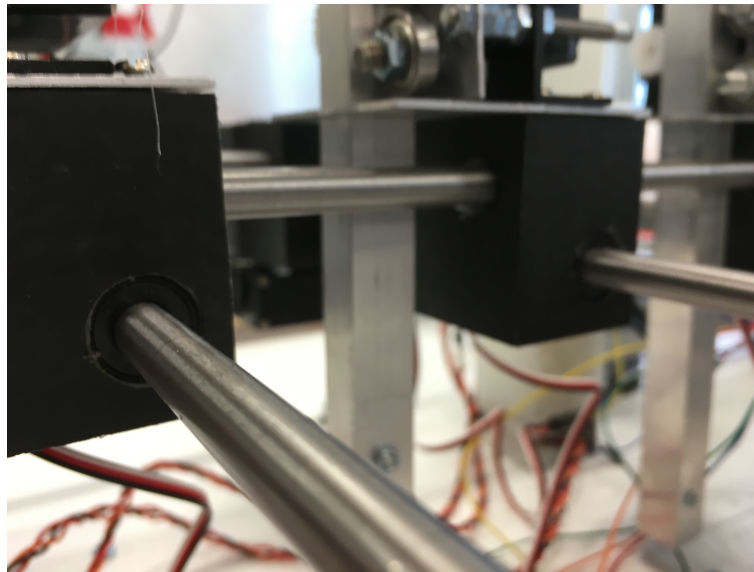


Figure 5.15: Linear bearing housing within the nuts

By assembling all the described elements, it has been possible to obtain the final prototype of the entire module (cf figure 5.17); after that the twelve modules has been assembled in order to obtain the tactile station. To allow the modules to work together a common frame is needed. To obtain this structure the four linear rails are mounted on four side pillars that are leaned against the ground. Each pillar is made by a polycarbonate block and an aluminum C-shape block. The designed configuration (figure 5.19) allows to adjust both the  $x$  and  $y$  position

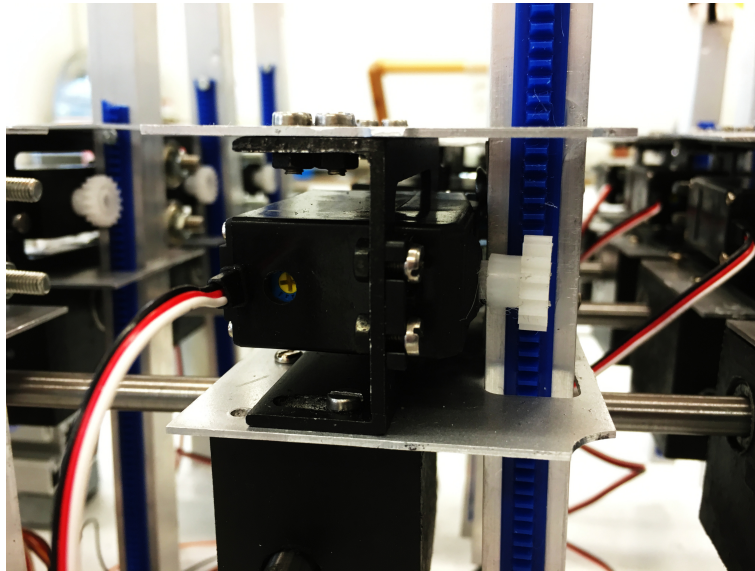


Figure 5.16: Simplified H-section IPE beam

of the racks. This regulation is needed both to allow mounting the isolines on the rail and to ensure the correct contact between the racks and the translational pinions. The energy supply and the control board are placed behind the prototype (cf figure 5.21). It has been chosen to use the same board for the geodesic strip prototype [25] in order to let the possibility of using them together (i.e. make a comparison between the two methods of representing virtual surfaces). Lastly has been developed a manual control board (figure 5.22) for servomotors movement in order to let the user to make final correction on control points position and save the last configuration needed to refresh the CAD model, changing the function of the tactile device from a output device only, to an input-output system.

### 5.2.1 Control board

To control the servomotors, the device has been equipped with the Servo controller SSC-32 produced by Lynxmotion. It is a small pre-assembled servo controller with some important features. It has high resolution ( $1\ \mu\text{s}$ ) for accurate positioning, and extremely smooth moves. The range is from  $500\ \mu\text{s}$  to  $2500\ \mu\text{s}$  for a range of about  $180^\circ$ . The SSC-32 allows the user to connect and control simultaneously 32 different servomotors. Therefore, with this board, it is possible to manage both the geodesic strip prototype, both the patch based one. By means of the serial connection, it is possible to send to the controller the RC PWM signal from the PC. The RC PWM (*pulse width modulation*) is a position communication protocol based on a signal that is a periodic pulse with a width



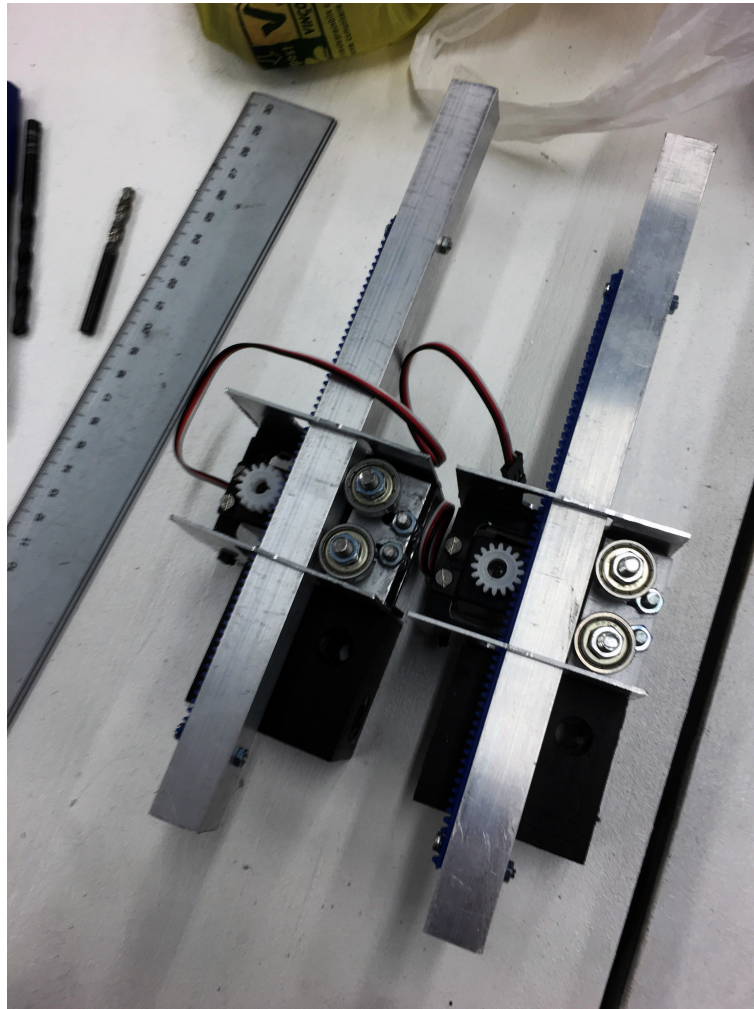


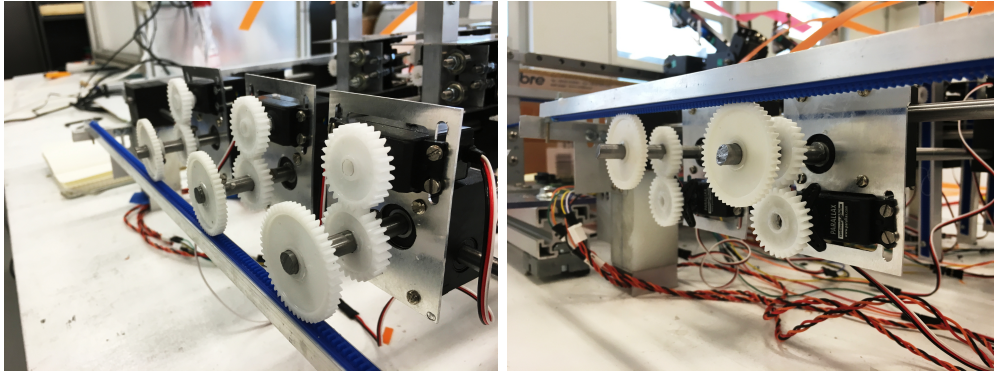
Figure 5.17: Assembly of a module

between  $500\ \mu\text{s}$  and  $2500\ \mu\text{s}$ . The operation principle behind this position protocol is that  $1500\ \mu\text{s}$  commands the servo to go to the centre position. A  $500\ \mu\text{s}$  pulse commands the motor to attempt reaching its leftmost position and  $2500\ \mu\text{s}$  its rightmost position (figure 5.24). Any pulse measuring in between these values is decoded as a position in between leftmost and rightmost. Therefore, the resolution of the servo rotation is equal to  $1\ \mu\text{s} = 0.09^\circ$ .

### 5.3 Experimental test

In order to complete the device analysis, several test has been done with simple forms recurrently used to design industrial product shape. Since we made the





(a) Left side

(b) Right side

Figure 5.18: Rack-pinion transmission system

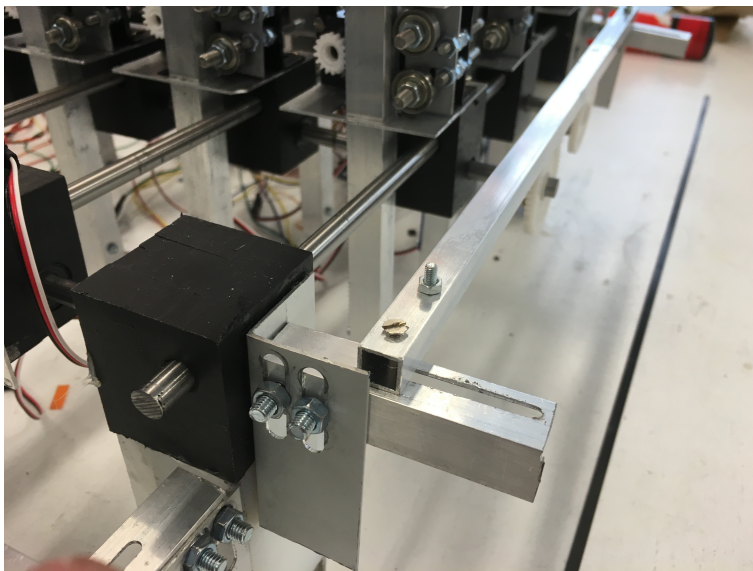


Figure 5.19: Regulation system

choice of not using the honeycomb patch on this prototype, it's not possible to evaluate directly the surface displacements between virtual and physical surface, but it's possible to do this with the control strips. After the algorithm calculation and the the control board signal conversion into a servomotor position, we can check the differences from what the algorithm foresees and the polypropylene strips deflection; to achieve this it is necessary to use a measurement method that can easily detect the position in space of the control strip. One of the method that is convenient to use, due to the ease and wide availability of instruments

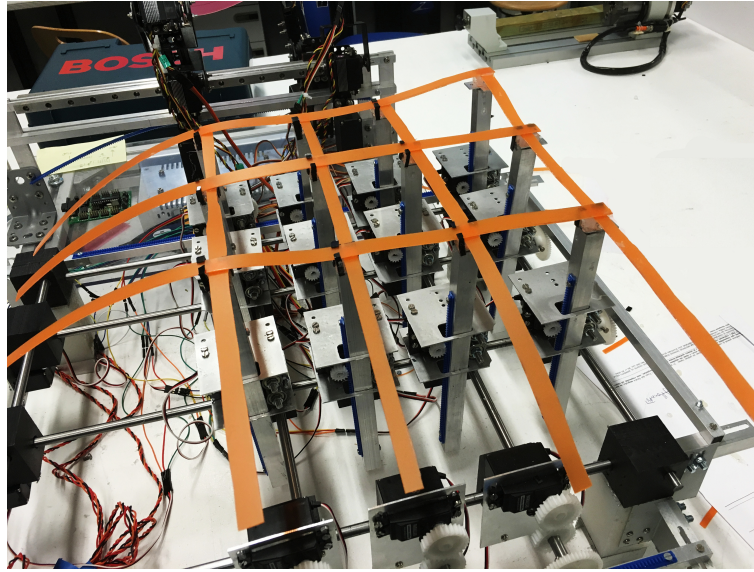


Figure 5.20: Final prototype

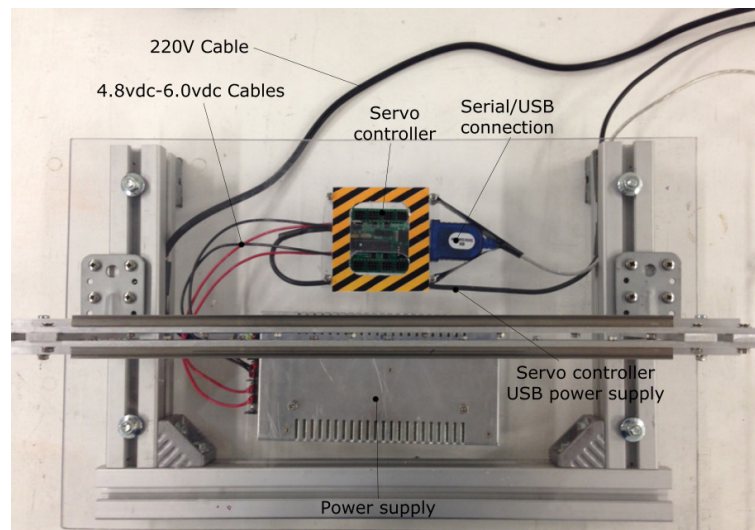


Figure 5.21: Control board and power supply housing

and software usage, is the photogrammetry.

### 5.3.1 Photogrammetry

Photogrammetry is the art and science of using overlapping photographs to reconstruct three dimensional scenes or objects. It consists of

- Choosing a proper camera with fix lenses pair to achieve always the same

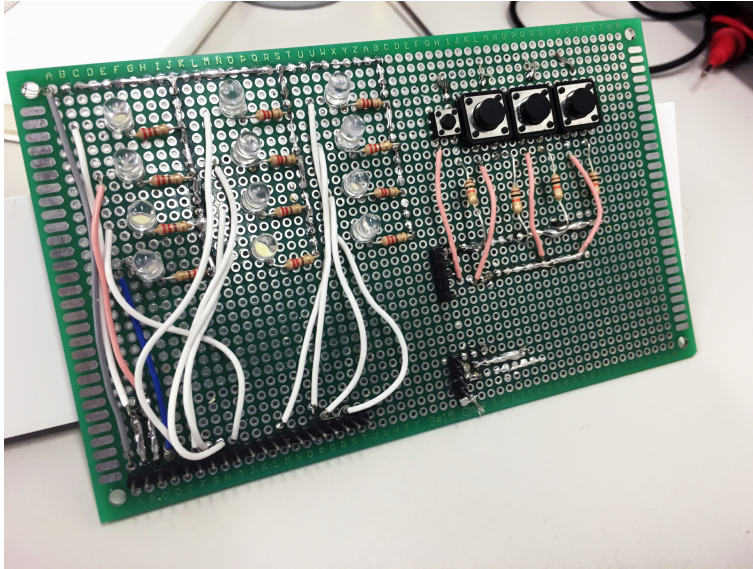


Figure 5.22: Manual movement board

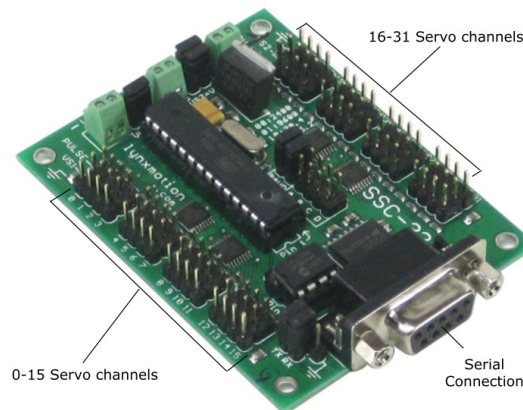


Figure 5.23: Lynxmotion controller

focal length

- Setting a scene with markers known in size and distances between them to have a proper reference in the scene itself
- Making a redundant set of photography to facilitate the overlapping phase
- Post processing phase to clean and repair the geometry outcoming from the software

It is a simple method to acquire a 3D complex object without involving expensive instruments. One of the biggest issues in this technique is the low accuracy of

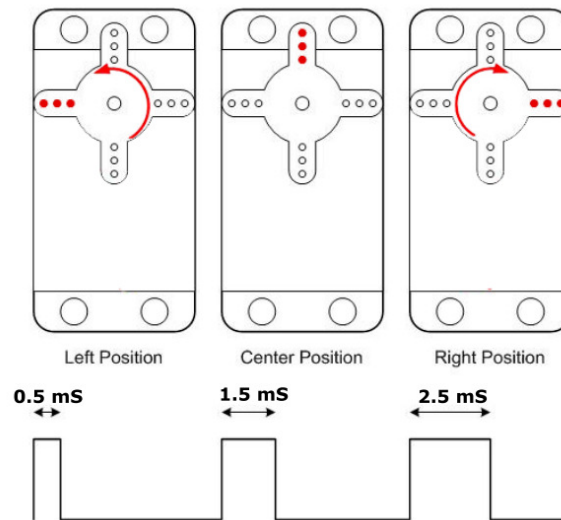


Figure 5.24: PWM signal relations

the outcoming model, strictly related to the quality of camera lenses and pixel ground sampling. From literature it's easy to find an equation leading the error

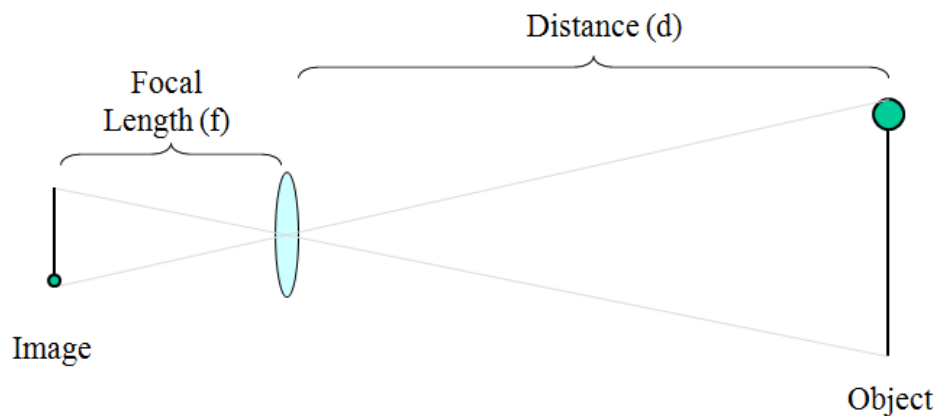


Figure 5.25: Main parameters in camera acquisition

sampling on photogrammetry and hence the accuracy; referring to figure 5.25

$$GSD = \frac{d}{f} l_{pixel} \quad (5.1)$$

where  $GSD$  is the ground sample distance, that is the accuracy of the photogram-



metry process,  $d$  is the distance between the lens pair and the object,  $f$  the focal length and  $l_{pixel}$  is the real pixel dimension. To have an exhaustive background explanation on photogrammetry please refer to [3] and [11].

### 5.3.2 Accuracy of the experimental setup

The camera used to accomplish the experimental test is a commercial reflex (i.e. uses a mirror and prism system, hence *reflex*) camera, paired with a 100 mm fix lens, whom features these main characteristics:

- Image sensor: 36 mm x 24 mm
- Maximum resolution: 5616 pixels x 3744 pixels

Therefore, making the hypotheses of using the camera to shot photographs from a distance of about 800 mm, it's immediate to calculate the other parameters:

$$l_{pixel} = \frac{36 \text{ mm}}{5616} = 0.00641 \text{ mm} \quad (5.2)$$

Hence we expect to have an accuracy of

$$GSD = \frac{800 \text{ mm}}{100 \text{ mm}} 0.00641 \text{ mm} = 0.05128 \text{ mm} \quad (5.3)$$

that is accurate enough for this application.

### 5.3.3 Evaluation protocol

In order to correctly proceed with the test, a protocol for completing analysis of the approximation has been defined. This protocol has been applied to guarantee their repeatability and to avoid the influence of the human interaction on the results. This procedure comprised the following stages:

- **Invention** of a new surface on a commercial CAD software
- **Exportation** of the \*.STL file
- **Algorithm** minimization of the modified error function
- **Movement** of the servomotors until steady-state is reached

- **Shooting** a set of 100 photographs at different height to perfectly catch the strips deflection
- **Construction** of the dense point cloud
- **Construction** of the mesh based on de Casteljau algorithm
- Quick and non destructive **cleaning** of the mesh
- **Acquisition** of the median line of each single strip
- Numerical **comparison** between virtual surface and and control strips

## 5.4 Example test

Four different tests has been done to check the tactile device properties. Since the obtained amount of data are too long to report, in this section will be reported only one example test and its results. For the other tests, please refer to appendix A.

### 5.4.1 Saddle shape

A saddle surface is a smooth surface containing one or more saddle points (figure 5.26). In mathematics, a saddle point is a point in the domain of a function that is a stationary point but not a local extremum. The name derives from the fact that the prototypical example in two dimensions is a surface that curves up in one direction, and curves down in a different direction, resembling a saddle. This shape is widely used both in architecture and product design, for this reason is one of the most substantial basic form on which we can evaluate the tactile device.

In figure 5.27 is shown the shape designed in a CAD software, as we can see it is a simplified version of a typical saddle shape in which has been introduced more stationary points near the border side, and the algorithm gave back the control strips deflection visible in figure 5.28.

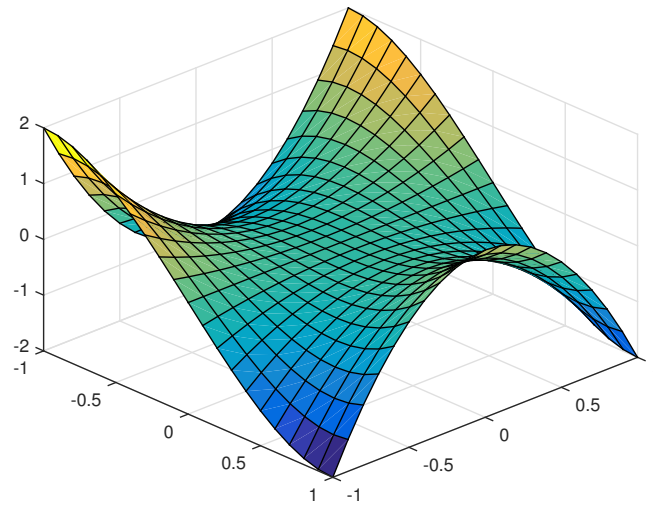


Figure 5.26: Monkey saddle surface:  $z = x^3 - 3xy^2$

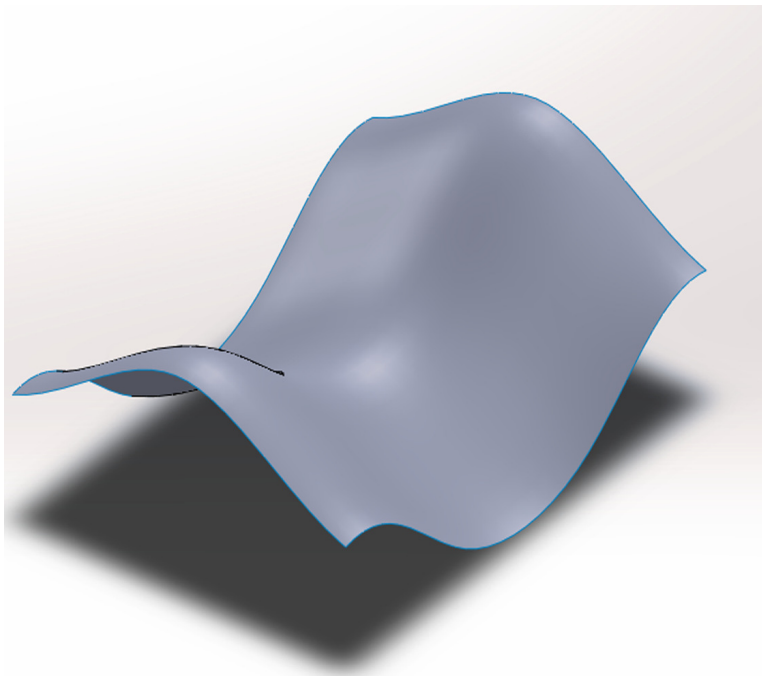


Figure 5.27: Saddle CAD geometry

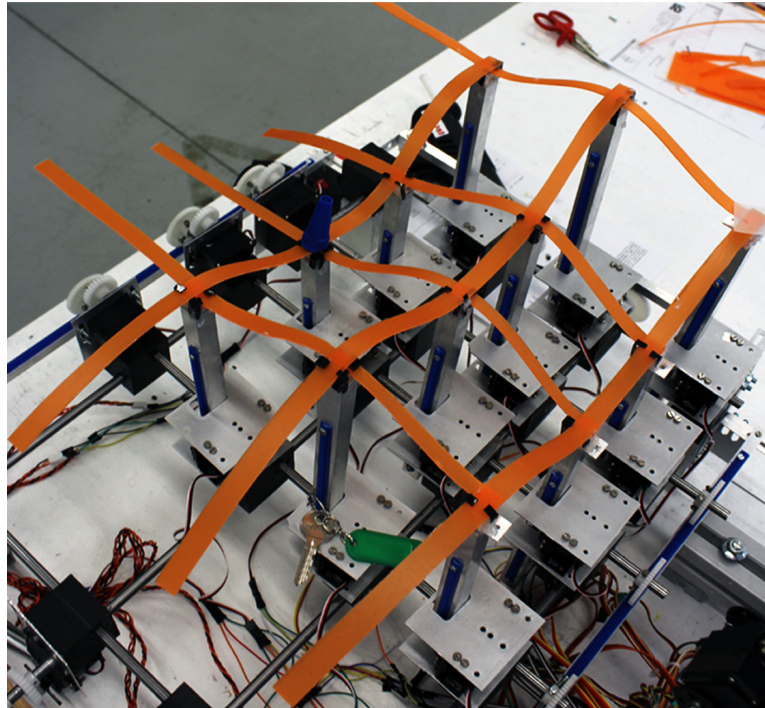


Figure 5.28: Tactile device positioning

Following the steps explained in previous section 5.3.3, the photogrammetry set-up has been arranged and has been taken a set of 100 photographs from different heights and perspectives, needed to complete the processes of camera parameters correction and bundle adjustment [24] [1] which give as an output the dense cloud from what de Casteljau's algorithm [8] starts to build the structured mesh and its texture informations (figure 5.29), that will be submitted to a cleaning process needed to reduce the number of redundant and inconsistent faces.



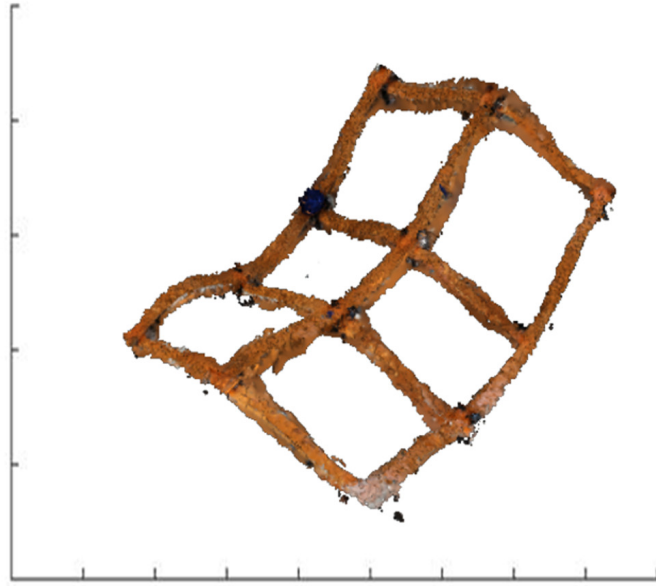


Figure 5.29: Acquired photogrammetry mesh

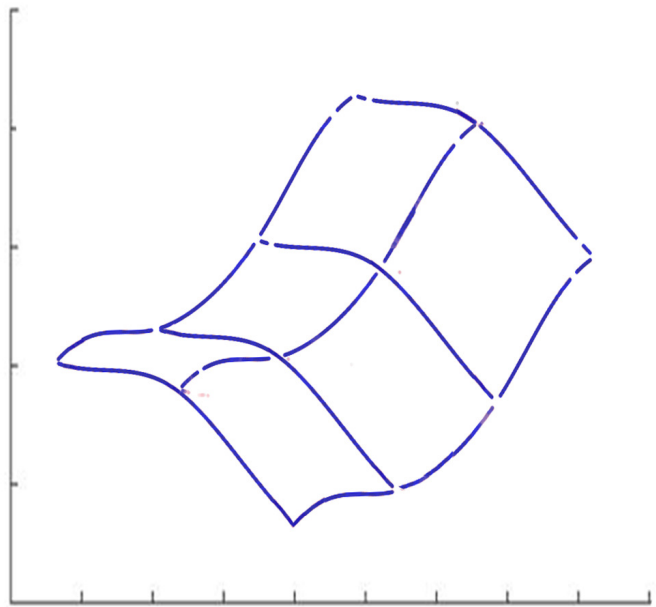


Figure 5.30: Median lines of control strips

Due to the huge number of inclusions in the obtained mesh, to extract the median line of each control strips it has been checked the Gaussian distribution of several sets of Cartesian coordinates belonging to consecutive mesh points, in order to keep out those inclusions considered as outliers of the distribution. In this way can be extracted the measured warping of control strips, reported in figure 5.30, and, repeating the previously explained numerical process, compare the curvature along the curvilinear abscissa between mathematical prediction and experimental model. Results are reported in figures from 5.31 to 5.37.

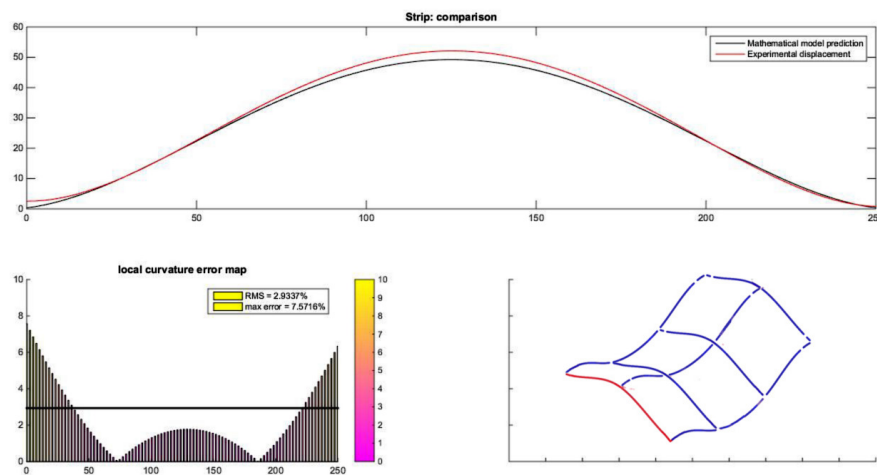


Figure 5.31: Experimental comparison on strip 1

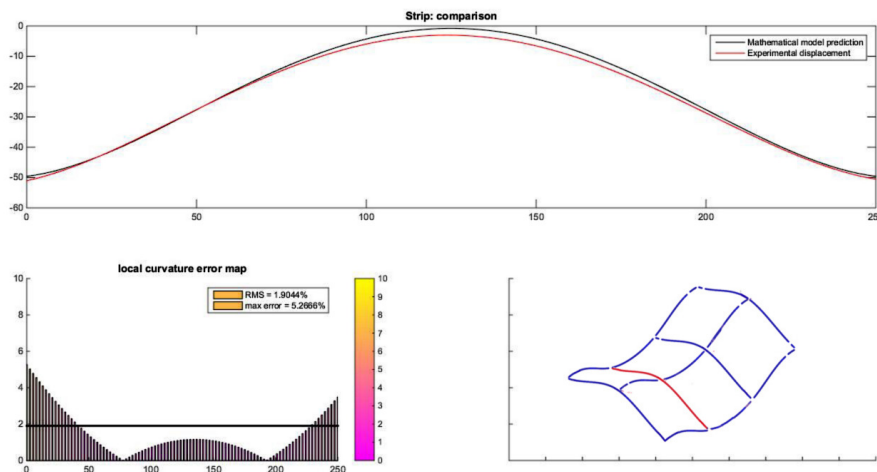


Figure 5.32: Experimental comparison on strip 2

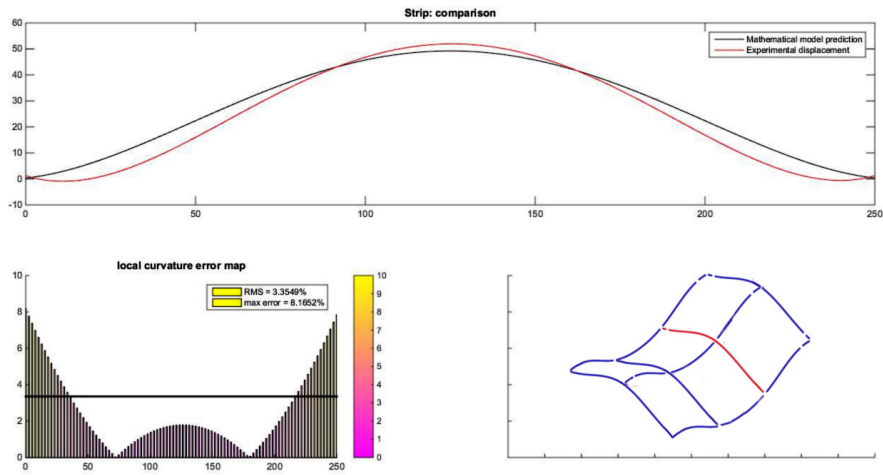


Figure 5.33: Experimental comparison on strip 3

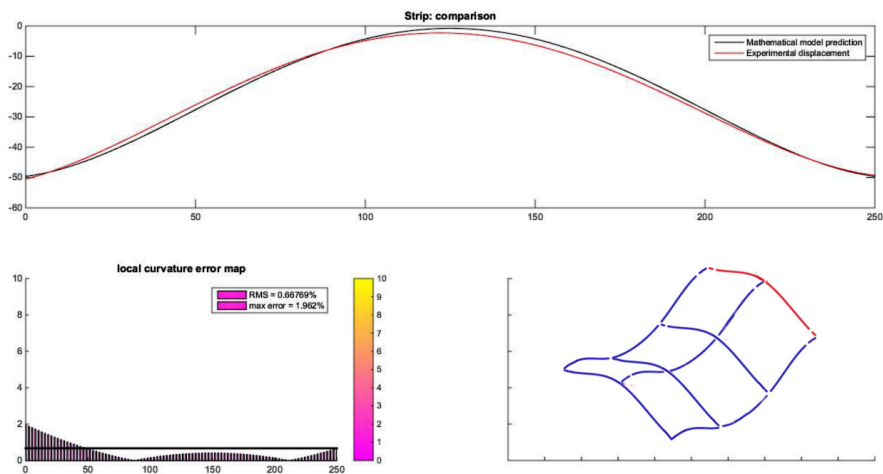


Figure 5.34: Experimental comparison on strip 4

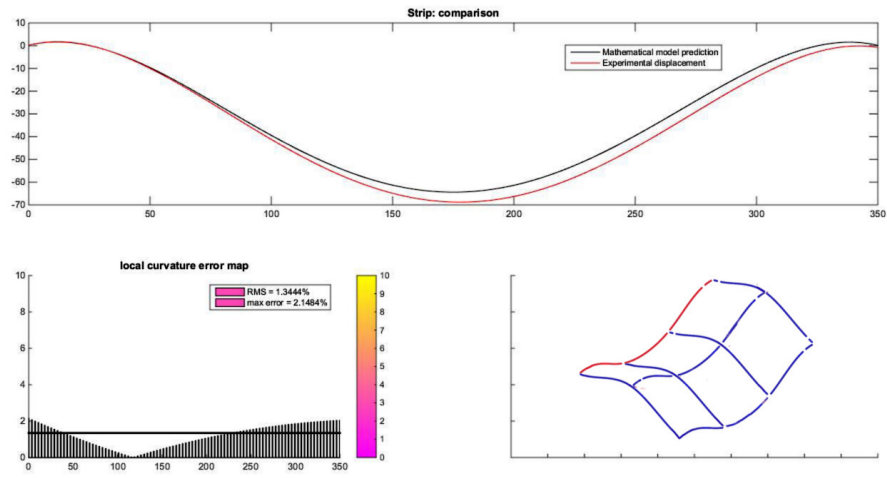


Figure 5.35: Experimental comparison on strip 5

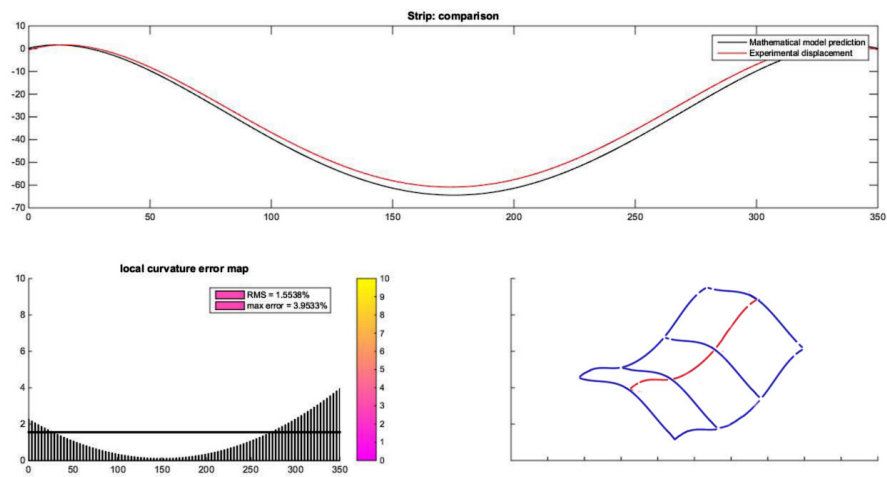


Figure 5.36: Experimental comparison on strip 6

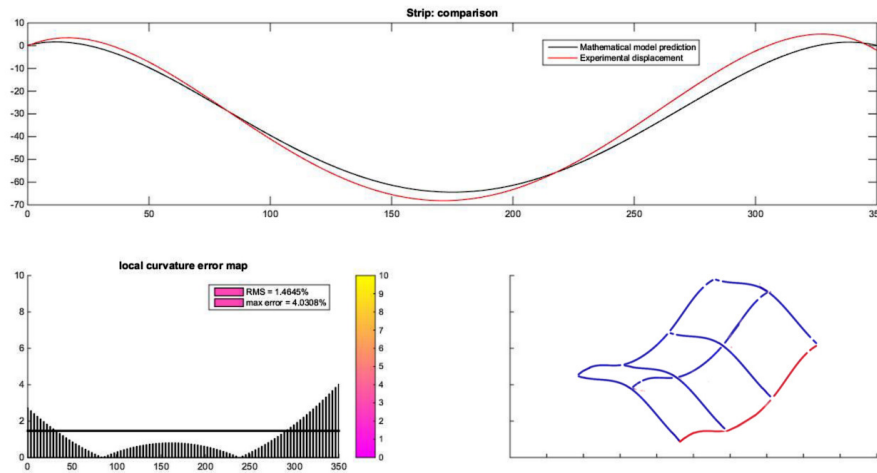


Figure 5.37: Experimental comparison on strip 7

### 5.4.2 Results discussion

As stated, figures from 5.31 to 5.37 shows the comparison between mathematical prediction of control strip displacements and measured ones, and so does figures reported in appendix A. Referring to them, we can say that the tactile device behave correctly related to the algorithm that impose its movements. From numerical test explained in section 5.1 we expected to achieve percentages of error roughly near to 5% and anyway lower than 10% (limit of non-perceivable errors from users) and the experimental tests confirmed those expectations. Furthermore, like previously discussed, the mere fact of not having two important degrees of freedom for the local curvature control (i.e.  $\theta_1$  and  $\theta_2$ ) bring the results to be highly conditioned in control points proximity, in fact error maps (e.g. in figure 5.33) show high values on curvature comparison. As it is legit to expect, results on test applied on shapes with smaller areas to represent appear to be minor, in terms of max nodal error, instead of shapes with bigger ones. What is peculiar to report is that on almost the whole set of test, local error map show the same trend behaviour, although with different values; this means that error map is still conditioned by some parameters, indeed it can be predicted with deepened analysis focused on it and therefore corrected adding a coefficient in the algorithm, increasing the approximation precision. Last consideration on experimental tests refers to the prototype itself. In figure 5.38 are shown for each test the gap between predicted values and measured ones of Cartesian coordinates of each control points in  $x$ ,  $y$  and  $z$  direction; The overall trend seems to confirm that the gap is totally fortuitous, not weighted neither biased, and always lower than 5 mm. Furthermore errors in  $x$  and  $y$  directions appears to

be always higher than in  $z$  direction, easily explained by the fact of having more components needed to transmit the motion in x-y plane and due to higher friction caused by rails. Therefore it is possible to label these kind of errors as mechanical ones, conditioned only by the mechanical interactions between prototype components and hence can be reduced with high quality materials. Last thing that is important to underline in such analyses is the time of execution. Generally the time that passes between the shape generation on CAD software and the design evaluation is in the order of weeks, on the contrary time required to obtain the shape from the algorithm submission was only four minutes, that could entail a considerable reduction in *time-to-market* and in number of mockups needed to achieve the ultimate product shape.

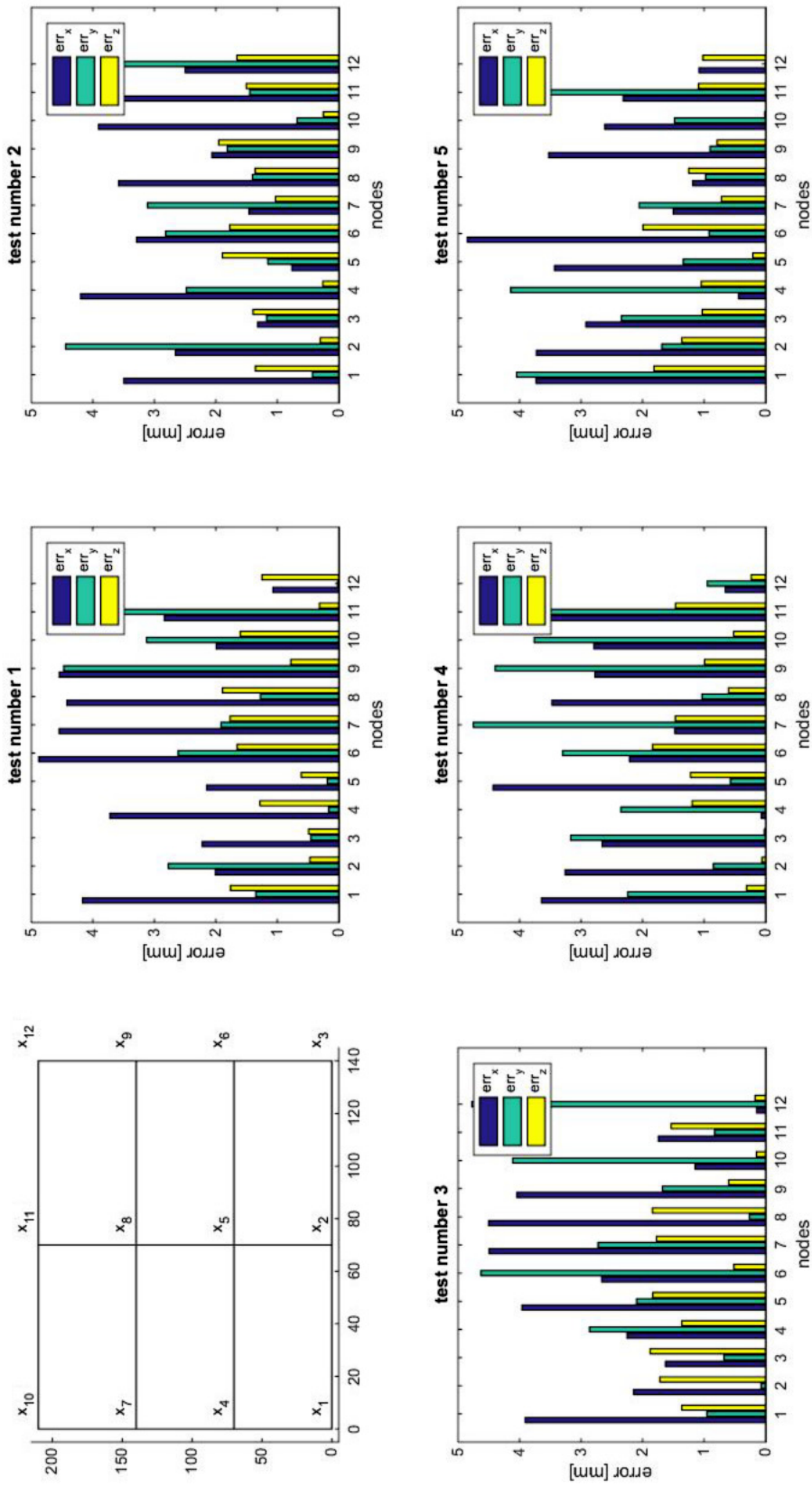


Figure 5.38: Control points placement: positioning error in  $x$ ,  $y$  and  $z$  direction





# 6

## Conclusions

The product quality, product costs and development time are the main factors that is leading companies to search for brand new project methods, in order to design *user-inspired* products necessary to fulfil customer requirements and to be competitive in a global market always more careful of user needs and wills. The biggest barrier to accomplish this situation is the necessity of a remarkable reduction in product development time, because deepened investigations proved that the greater part of it is spent in design evaluation and mockups fabrication. For such reason a development of a new instrument of shape evaluation available to industrial designer can drastically change the time-to-market.

The main purpose of this thesis was to check the feasibility of a surface tactile display developing an analytical model to strictly predict its behaviour in a future real industrial scenario, and to design a concept of this new device. Particularly it wants to demonstrate that the implementation of this brand new design method can actually improve the companies performances in terms of time required to achieve a definitive product shape: the classical approach of industrial product design needs an iterative process to meet all the *integrated project sub-teams* requirements and it may excessively weigh on the overall production costs. On

the other hand, thoughtlessly avoiding this iterative procedure cannot be the right decision to fulfil the customer needs.

The necessities of an industrial designer during conceptual design phase has been analysed considering available inputs and desired output. They can be summarized as following:

- Industrial designers are assisted by many *information technology* (IT) instruments that promote their creativity (i.e. CAD and free sketching shape sculpting softwares)
- Industrial designers require a non-invasive instrument capable of give them a quick feedback based on what they are drawing
- This instrument has to behave both like an output device representing the desired surface, and an input device able to directly change the inspected shape

The way chosen to overcome this work issues, taking into account the industrial designers needs, is based on a sort of shapeshifting surface for which has been formalized a mathematical method to predict its behaviour. Main steps of this methods are outlined as:

- Settlement of an analytical form for the virtual surface starting from an *STL file*, output of any commercial CAD software
- Device chassis mathematical expression needed to place the control points in a Cartesian space
- Raise of degrees of freedom by a control strip approach, ruled by *NURBS formulation*, to achieve better confidence in a surface approximation
- Definition of a finite element problem to properly predict the physical surface displacements
- Assessment of an error function gathering all the previous components in order to minimize it

After that, a possible configuration for the tactile device has been suggested to satisfy all the analytical model features, and to guarantee all the parameters needed to provide a clean user experience during shape evaluation. Every components for the Cartesian device has been designed to achieve the maximum performance. Each module forming the device have five degrees of freedom (5 d.o.f.), enough to give a correct representation of the inquired shape: three d.o.f. necessary to the Cartesian placement of the control nodes and two d.o.f. able to perform the local curvature control. This approach based on movement of the control points under the surface has never been used in any of the previous full

---

<b>Properties of the tactile device</b>		
	Prototype	Generic model
max A [mm]	600x500	NO limitations
Number of control points	12	4n
Min distance between control points [mm]	63	63
Min curvature radius [mm]	30	30
Modularity	YES	YES
Portability	YES	Depends on A
Relative implementation costs	Low	Low

---

Table 6.1: Tactile device properties

shape display, therefore this is a strong improvement with respect to the current *state of art* technologies and a first attempt to achieve a full tactile display with variable resolution, able to approximate a wide range of surface with various size and different accuracy depending on required level of detail. The development of a prototype based on twelve identical modules allowed me to analyse the solution and locate its limits related to the positional error introduced by the loss of stiffness whenever modules are too much distant from each other and the mechanical backlash of the gear transmission. Main features of this solution are reported in table 6.1

Tests on real industrial application and with commonly used shapes was used to validate this kind of approach. Results point out that the device meets all the stated requirements. It can be considered as the concrete future in industrial design and it probably will be settled in the everyday usage designers tools, as today we consider the IT technology. It allows a fast feedback in product management, encourage the *user-inspired* design strategy and promotes the *first-*

*time-right* projects. Moreover, further studies can actually improve this new tool usage to reach always more refined analytical model and enhanced device properties.

## 6.1 Future improvements

The future works aim to choose the right properties for the physical surface. In this dissertation we assumed to use the properties of a generic honeycomb material, but a deepened analysis is required to define the proper elementary cell dimensions and material, implementing a more accurate finite element analysis and testing the effects of different material on user experience. Furthermore is possible to study the effects of new materials for both the control strips and the physical surface, in particular:

- Auxetic materials, which behave like anisotropic materials with negative Poisson's coefficient in every direction [12] [2].
- Monocrystalline copper materials, that showed interesting properties related to the high shape memory and the same deformation behaviour as the hyperelastic materials with no yield [6] [7].

Another thing to focus on is the correct connection between the control strips and the physical surface. It has to be without mechanical interaction because the control strips must slide under the surface but they have to provide a sort of locking to grab the surface to the required position; for this reason we recommend to study an interaction based on electromagnets. One more point to develop is the possible implementation of this tactile device in different fields from the industrial one, like the biomedical training of surgeons, the educational aspect and the possible relationships with other rapid prototyping tools, like 3D printing.

# Appendices





## Experimental test results

### **A.1 Test 1**

Test on a small concave bent surface

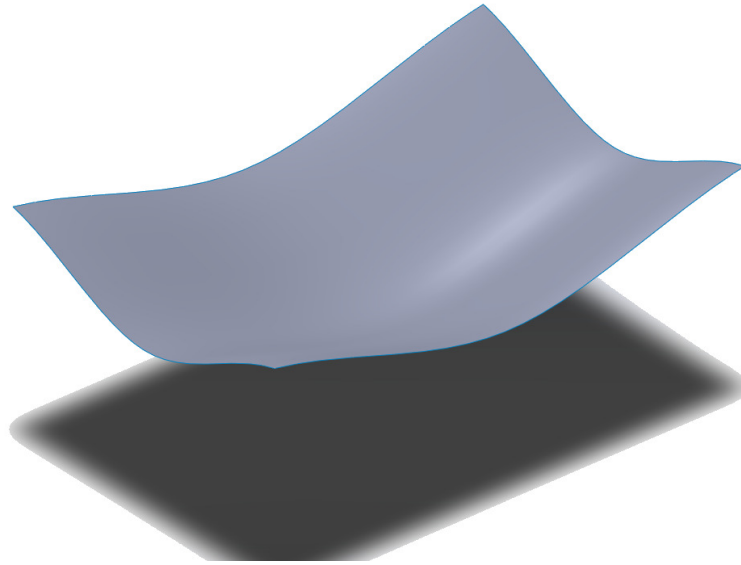


Figure A.1: Small concave surface

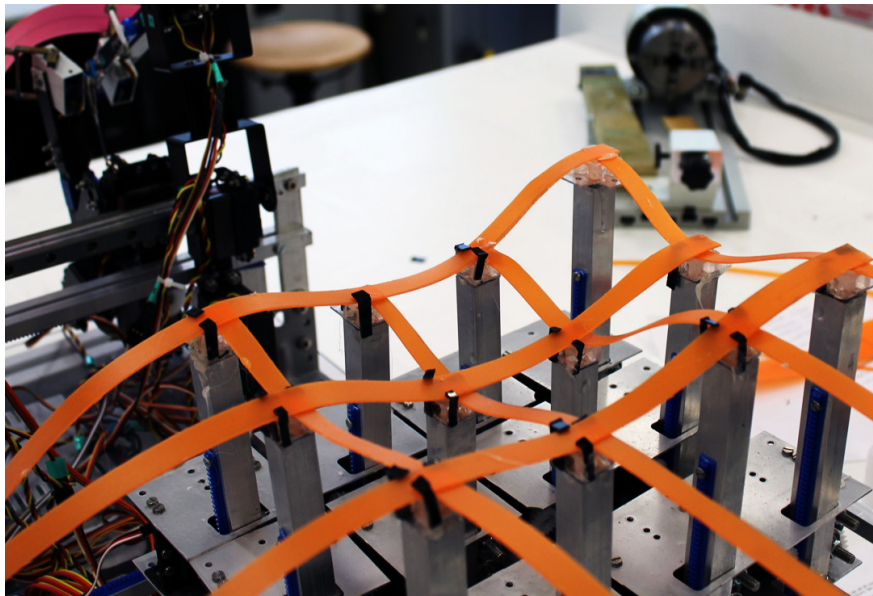
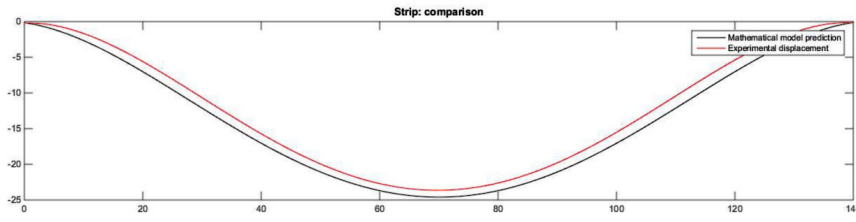
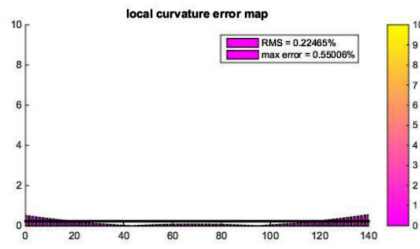


Figure A.2: Device arrangement



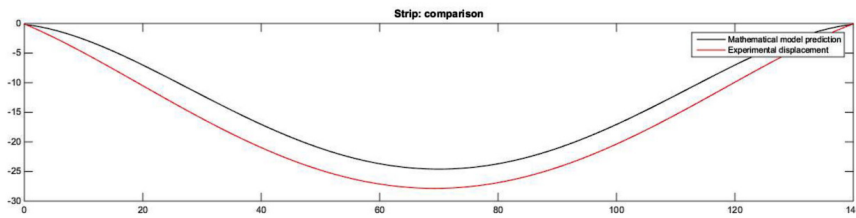


(a) Strip

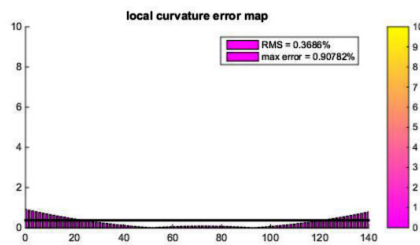


(b) Error map

Figure A.3: Test1: Experimental comparison on strip 1

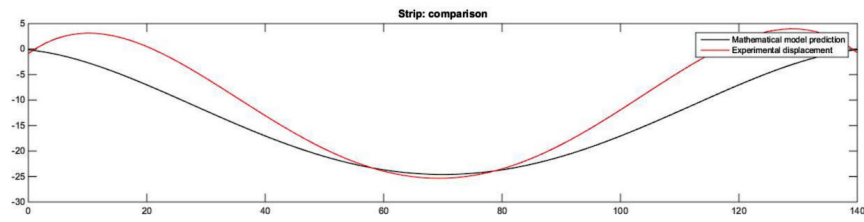


(a) Strip

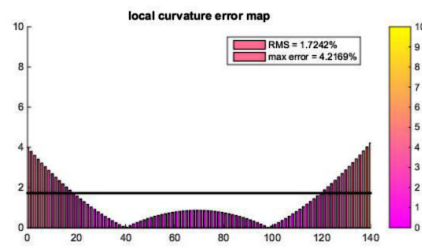


(b) Error map

Figure A.4: Test1: Experimental comparison on strip 2

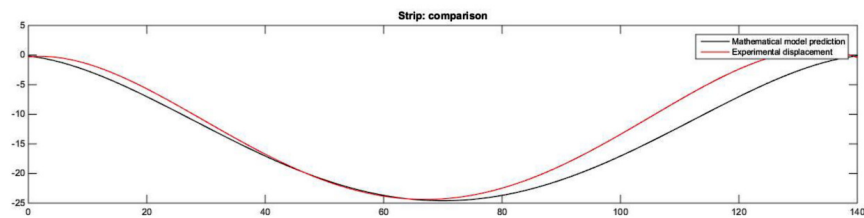


(a) Strip

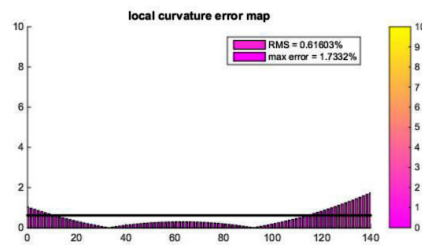


(b) Error map

Figure A.5: Test1: Experimental comparison on strip 3

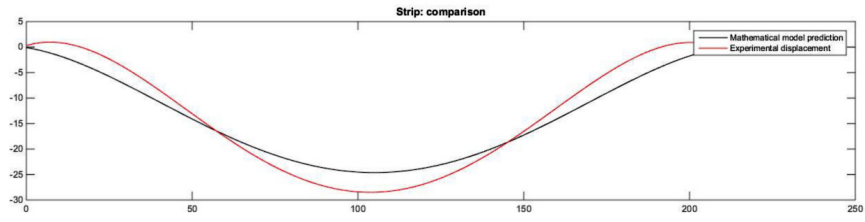


(a) Strip

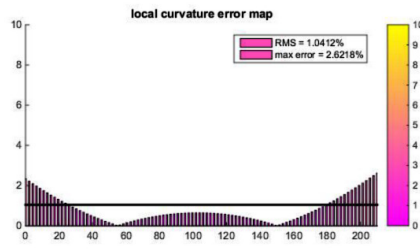


(b) Error map

Figure A.6: Test1: Experimental comparison on strip 4

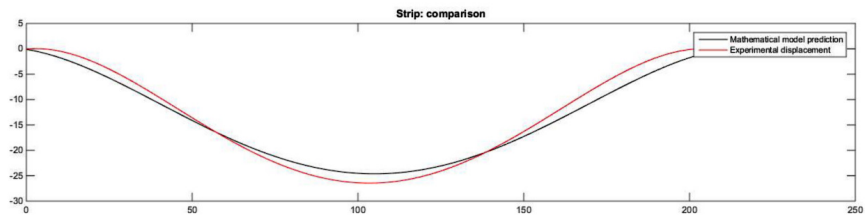


(a) Strip

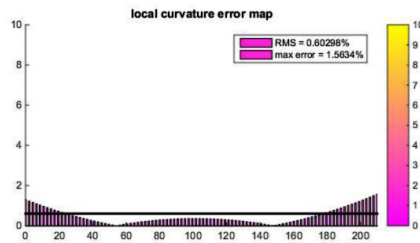


(b) Error map

Figure A.7: Test1: Experimental comparison on strip 5

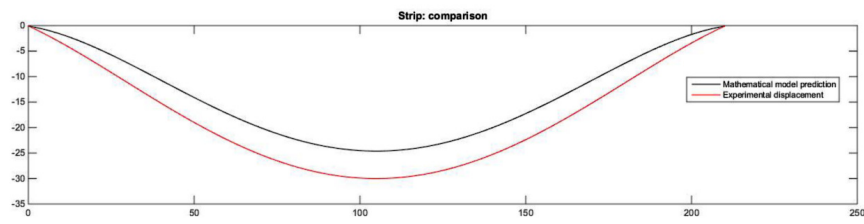


(a) Strip

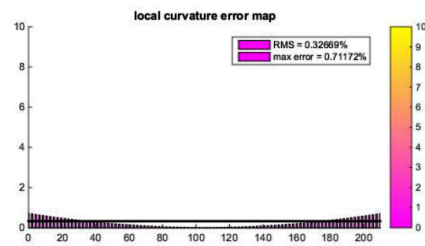


(b) Error map

Figure A.8: Test1: Experimental comparison on strip 6



(a) Strip



(b) Error map

Figure A.9: Test1: Experimental comparison on strip 7

## A.2 Test 2

Test on a small convex bent surface

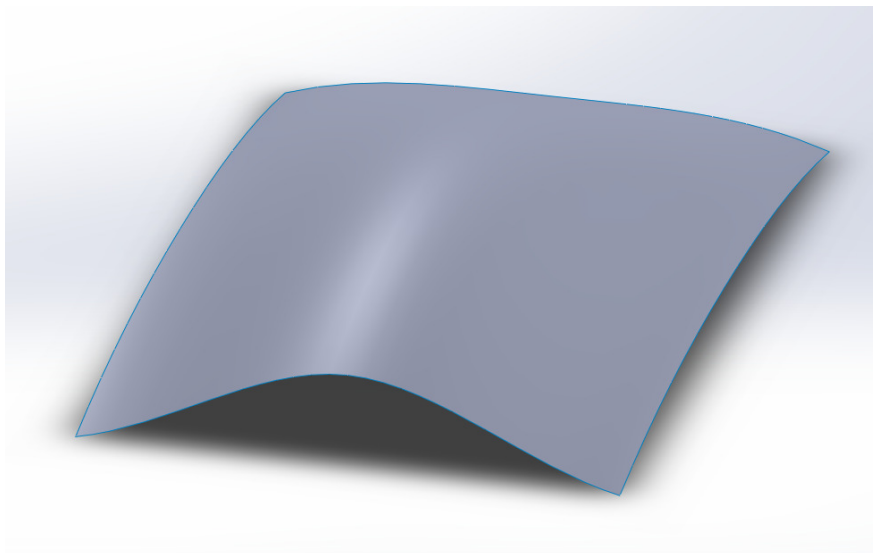


Figure A.10: Small convex surface

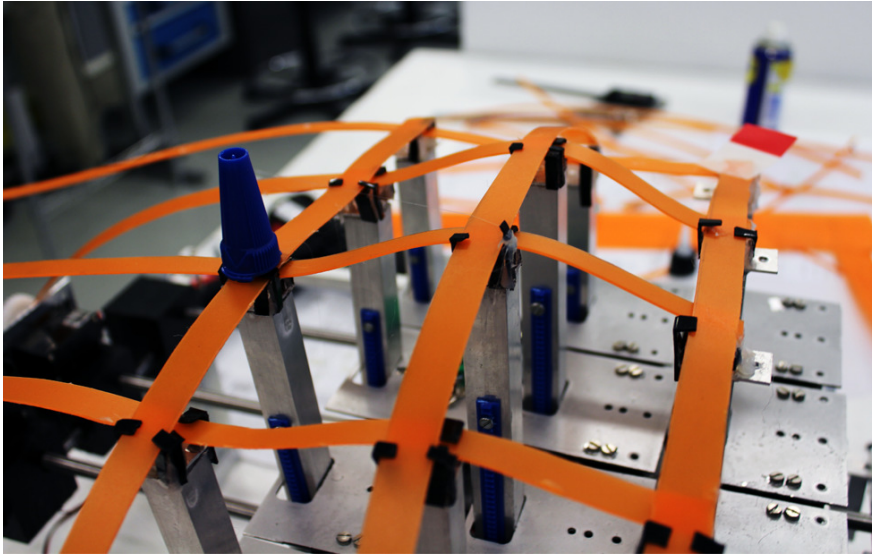
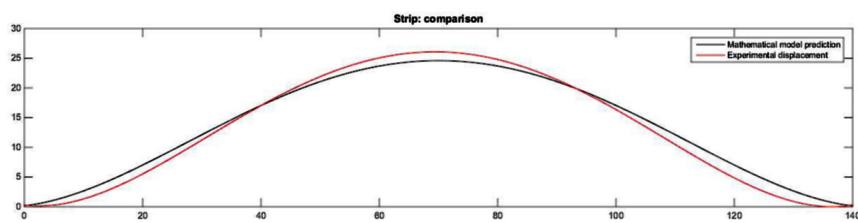
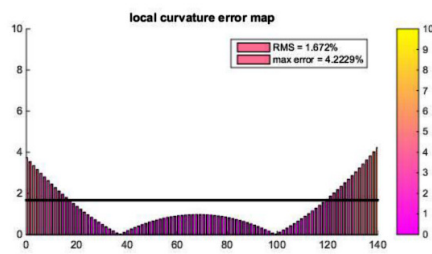


Figure A.11: Device arrangement

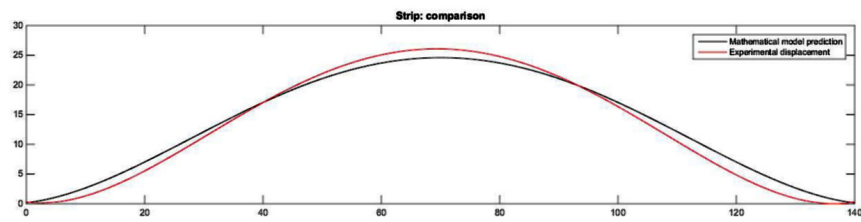


(a) Strip

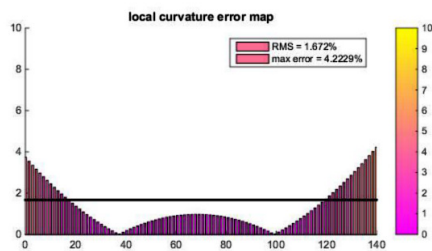


(b) Error map

Figure A.12: Test2: Experimental comparison on strip 1

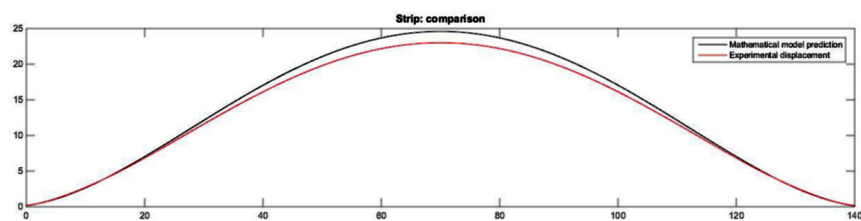


(a) Strip

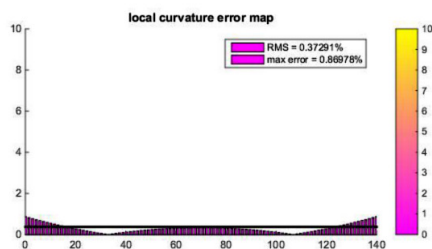


(b) Error map

Figure A.13: Test2: Experimental comparison on strip 2

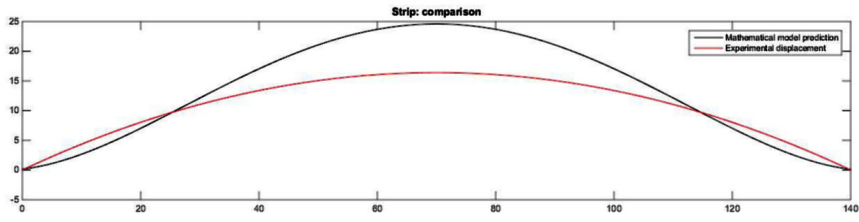


(a) Strip

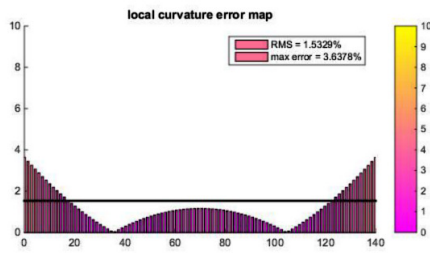


(b) Error map

Figure A.14: Test2: Experimental comparison on strip 3

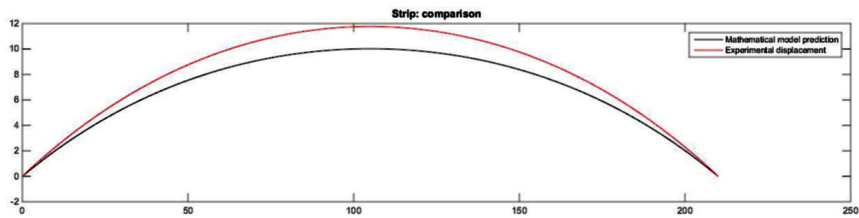


(a) Strip

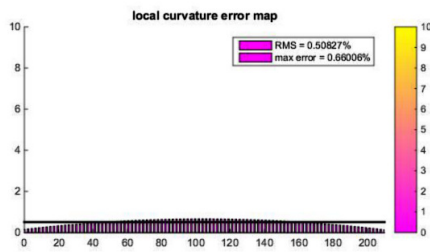


(b) Error map

Figure A.15: Test2: Experimental comparison on strip 4

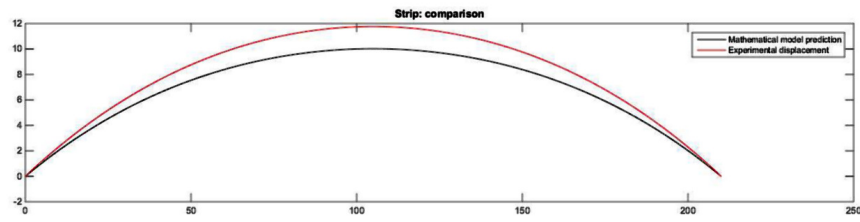


(a) Strip

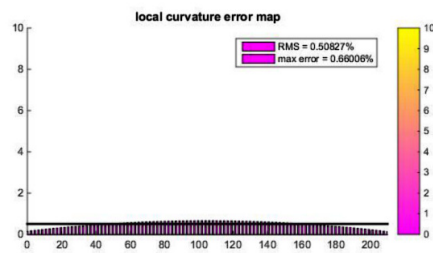


(b) Error map

Figure A.16: Test2: Experimental comparison on strip 5

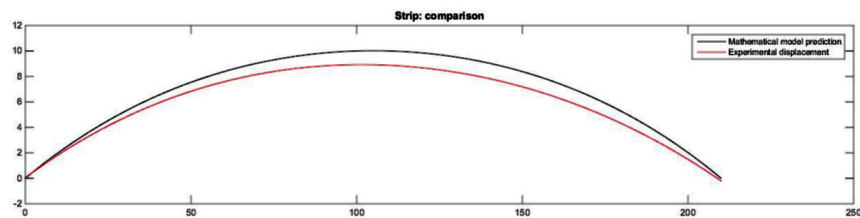


(a) Strip

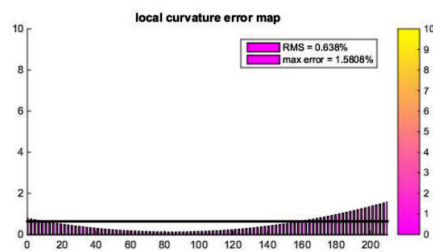


(b) Error map

Figure A.17: Test2: Experimental comparison on strip 6



(a) Strip



(b) Error map

Figure A.18: Test2: Experimental comparison on strip 7



## A.3 Test 3

Test on a wide concave bent surface

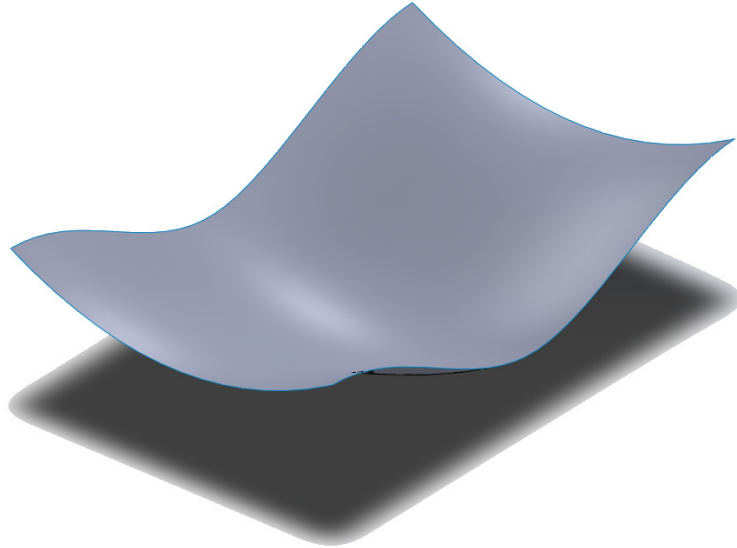


Figure A.19: Wide convex surface

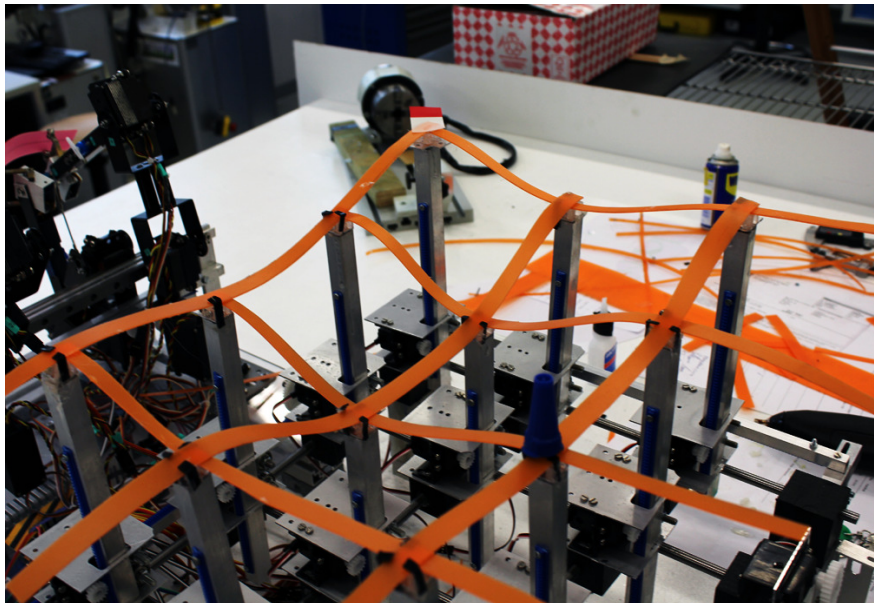
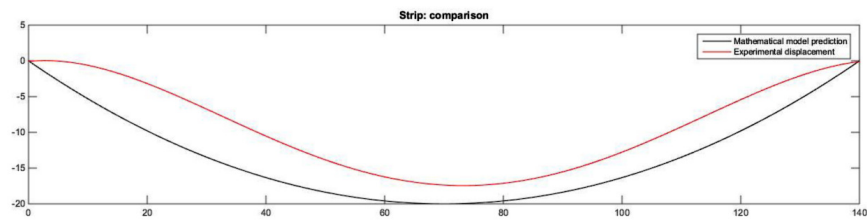
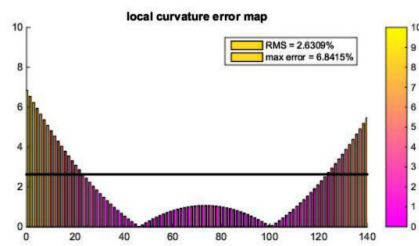


Figure A.20: Device arrangement

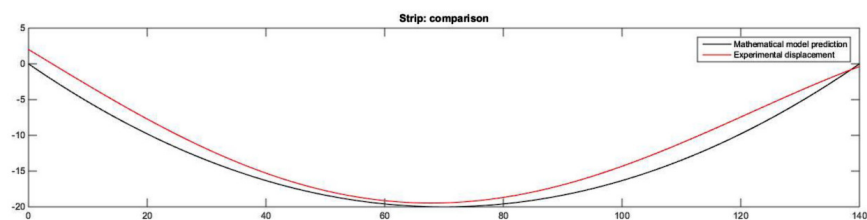


(a) Strip

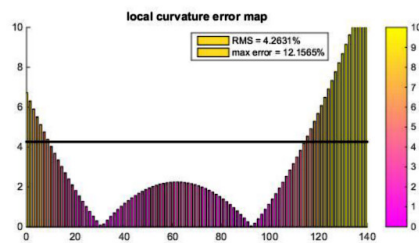


(b) Error map

Figure A.21: Test3: Experimental comparison on strip 1

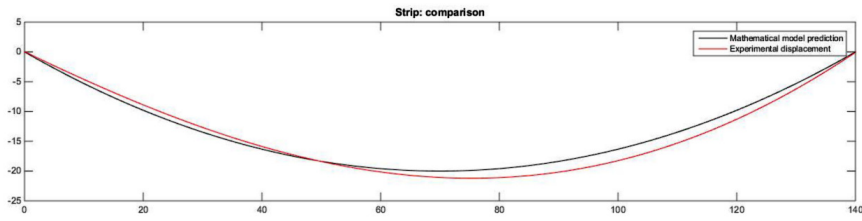


(a) Strip

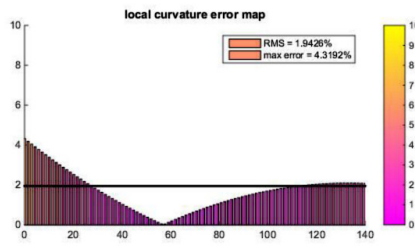


(b) Error map

Figure A.22: Test3: Experimental comparison on strip 2

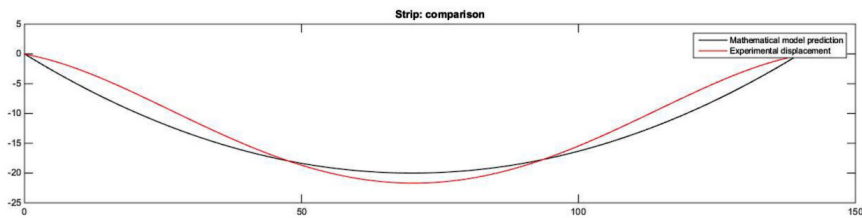


(a) Strip

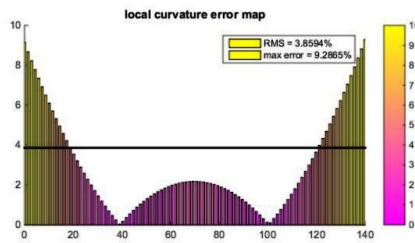


(b) Error map

Figure A.23: Test3: Experimental comparison on strip 3

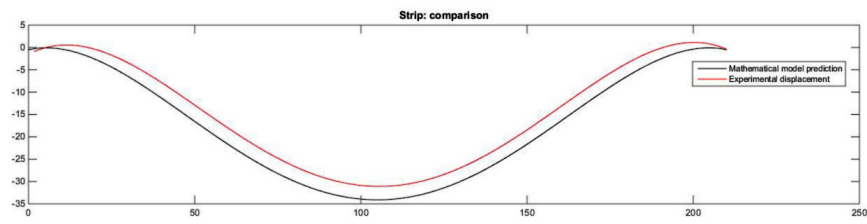


(a) Strip

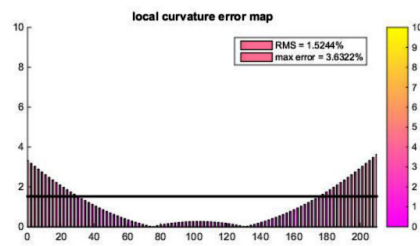


(b) Error map

Figure A.24: Test3: Experimental comparison on strip 4

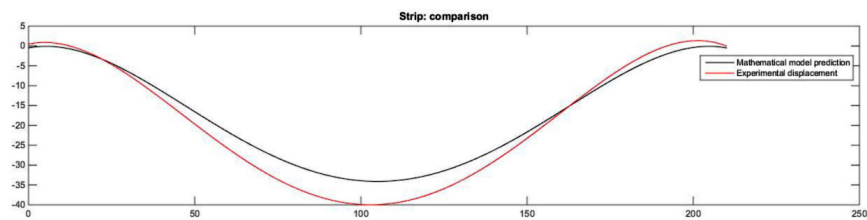


(a) Strip

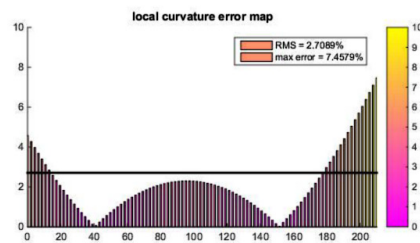


(b) Error map

Figure A.25: Test3: Experimental comparison on strip 5

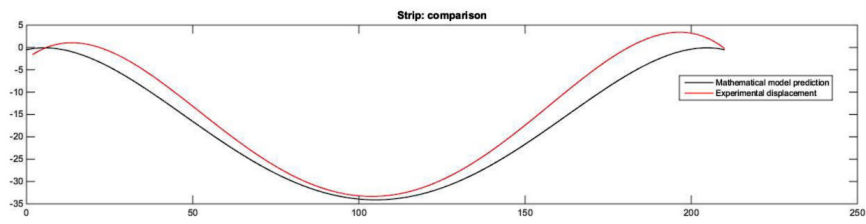


(a) Strip

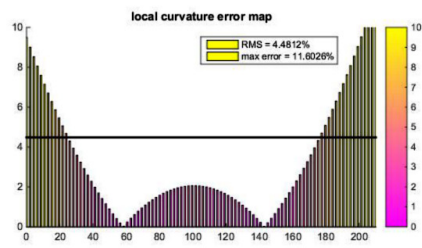


(b) Error map

Figure A.26: Test3: Experimental comparison on strip 6



(a) Strip



(b) Error map

Figure A.27: Test3: Experimental comparison on strip 7



# B

## Algorithm implementation

### STL data import and processing

```
function [x,y,z] = dataProcessing(x,y,z)
slend=500;
rem=randi([1 length(x)],length(x),1);
rem=randperm(length(x));
m=length(x)-slend;
rem=rem(1:m);
x(rem)=[];
y(rem)=[];
z(rem)=[];
mat1=[x y z];
mat1=unique(mat1, 'rows');
mat=mat1;
```

```

[values, order] = sort(mat(:,2));
smat = mat(order,:);
sortmat=zeros(size(smat,1),3);
sortmat(1,:) = smat(1,:);
for ii=2:size(mat,1)
    if smat(ii,2) <= smat(ii-1,2)
        if smat(ii,1) <= smat(ii-1,1)
            sortmat(ii,:)=smat(ii-1,:);
            sortmat(ii-1,:)=smat(ii,:);
        else
            sortmat(ii,:)=smat(ii,:);
        end
    else
        sortmat(ii,:)=smat(ii,:);
    end
end
x=sortmat(:,1);
y=sortmat(:,2);
z=sortmat(:,3);
end

```

### Polynomial regression

```

function [P,xl,y1] = polyRegression (x,y,z);
a='X';
b='Y';
fun='P(1)';
P='P';
xw='XY(:, :, 1)';
yw='XY(:, :, 2)';

counter=2;
check=1;
checkcount=1;
RESIDUAL=[];

```



```

while check==1
    n=[1:checkcount];
    n=char(n);
    for ii=1:(length(n))
        count=ii;
        jj=0;
        while ii+jj <= count && ii>=0 && ii<length(n)
            fun=[fun '+' P '(' num2str(counter) ')' '.*' xw...
                '.*' n(1,ii+1) '.*' yw '.*' n(1,jj+1)];
            jj=jj+1;
            ii=ii-1;
            counter=counter+1;
        end
    end
    XY(:, :, 1) = x;
    XY(:, :, 2) = y;
    func=@(P,XY) eval(fun);
    [P,residual] = lsqcurvefit(func, zeros(counter,1), XY, z);
    X=linspace(min(min(x)),max(max(x)),size(x,1));
    Y=linspace(min(min(y)),max(max(y)),size(x,2));
    RESIDUAL=[RESIDUAL residual];
    [x1 y1]=meshgrid(X,Y);
    if (checkcount > 1) && (norm(RESIDUAL(checkcount))...
        -RESIDUAL(checkcount-1))<threshold)
        check=2;
        return
    end
    checkcount=checkcount+1;
end

```

### Interface with finite element analysis

```

function [z] = femPrediction(x,xmax,ymax)
load('NodeLabel.mat');
load('NodeX.mat');

```

```

load('NodeY.mat');
tmpi=[];
for ii=1:length(x)
tmpii = abs(NodeX(:,ii)-x(ii));
[idxiidxii] = min(tmpii);
closesti = NodeX(idxii);
nodeModi=NodeLabel(find(NodeX==closesti));
xfem=[0:5:xmax];
yfem=[0:5:ymax];
nodeValxi=fyi(ii);

[values, orderi] = sort(NodeY(nodeModi));
sortedNodei = nodeModi(orderi,:);
nodeValxi(ismember(sortedNodei,sortedNodei))=[];
end

fid = fopen('C:\Users\LUCA\Desktop\Tesi\Main\PatchRoutine.inp');
cac = textscan( fid, '%s', 'Delimiter','\n', 'CollectOutput',true );
fid = fopen('C:\Users\LUCA\Desktop\Tesi\Main\PatchRoutineMod.inp', 'wt' );

%write the input of the analysis with the prescribed nodal displacement

%% run job
delete('NodalDisplacement.rpt');
command='abq6141 job=PatchRoutineMod inp=PatchRoutineMod.inp interactive';
system('cd C:\Users\LUCA\Desktop\Tesi\Main');
status = system(command);
system('abq6141 cae noGUI=C:\Users\public\abaqusMacros.py');

%% import nodal displacement

fid = fopen('NodalDisplacement.rpt')
RPT = textscan( fid, '%s');
fclose(fid)

```

```
S = sprintf('%s*', RPT{1}{:,1});
Key  = '*1.*';
Index = strfind(S, Key);
NodalDisp=[];
for ii=1:numel(Index)
    nod= sscanf(S(Index(ii) + length(Key):end), '%g', 1);
    NodalDisp=[NodalDisp nod];
end
z=NodalDisp;
end
```

### Python macro needed to dynamically update FEM report

```
from abaqus import *
from abaqusConstants import *
import __main__
import section
import regionToolset
import displayGroupMdbToolset as dgm
import part
import material
import assembly
import step
import interaction
import load
import mesh
import optimization
import job
import sketch
import visualization
import xyPlot
import displayGroupOdbToolset as dgo
import connectorBehavior
import os
os.chdir(r"C:\Users\public\Main")
```

```
session.mdbData.summary()
o1 = session.openOdb(
    name='C:/Users/public/Main/PatchRoutineMod.odb')
session.viewports['Viewport: 1'].setValues(displayedObject=o1)
odb = session.odbs['C:/Users/public/Main/PatchRoutineMod.odb']
session.xyDataListFromField(odb=odb, outputPosition=NODAL, variable= (('U',
    NODAL, ((COMPONENT, 'U3'), )), ), nodePick= (('PART-1-1', 5551, (
    '#ffffffff:173 #7fff ]', )), ), )
#writing the prescribed nodal displacements
x0 = session.xyDataObjects['U:U3 PI: PART-1-1 N: 1']
x1 = session.xyDataObjects['U:U3 PI: PART-1-1 N: 2']
x2 = session.xyDataObjects['U:U3 PI: PART-1-1 N: 3']
x3 = session.xyDataObjects['U:U3 PI: PART-1-1 N: 4']
x4 = session.xyDataObjects['U:U3 PI: PART-1-1 N: 5']
x5 = session.xyDataObjects['U:U3 PI: PART-1-1 N: 6']
#...
#ending the writing phase
#saving now the report file
session.xyReportOptions.setValues(pageWidthLimited=SPECIFY,
    layout=SEPARATE_TABLES)
session.writeXYReport(fileName='NodalDisplacement.rpt', xyData=(x0, x1, x2, x3,
    x4, x5, x6, x7, x8, x9, x10, x11, x12, #...
    x5550))
```

# C

## Technical drawings

Here are reported main technical drawings of the prototype module

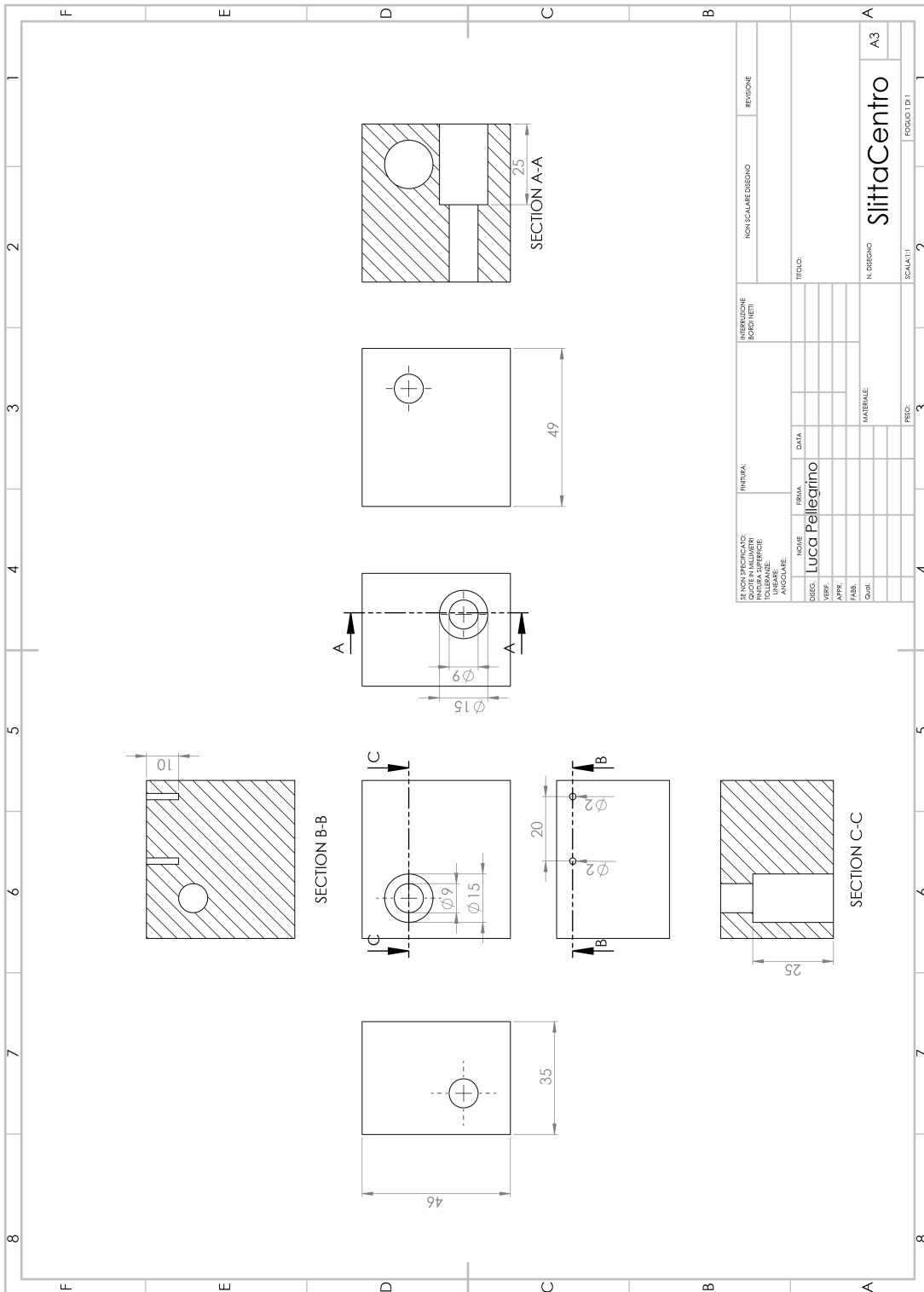


Figure C.1: Mechanical slide

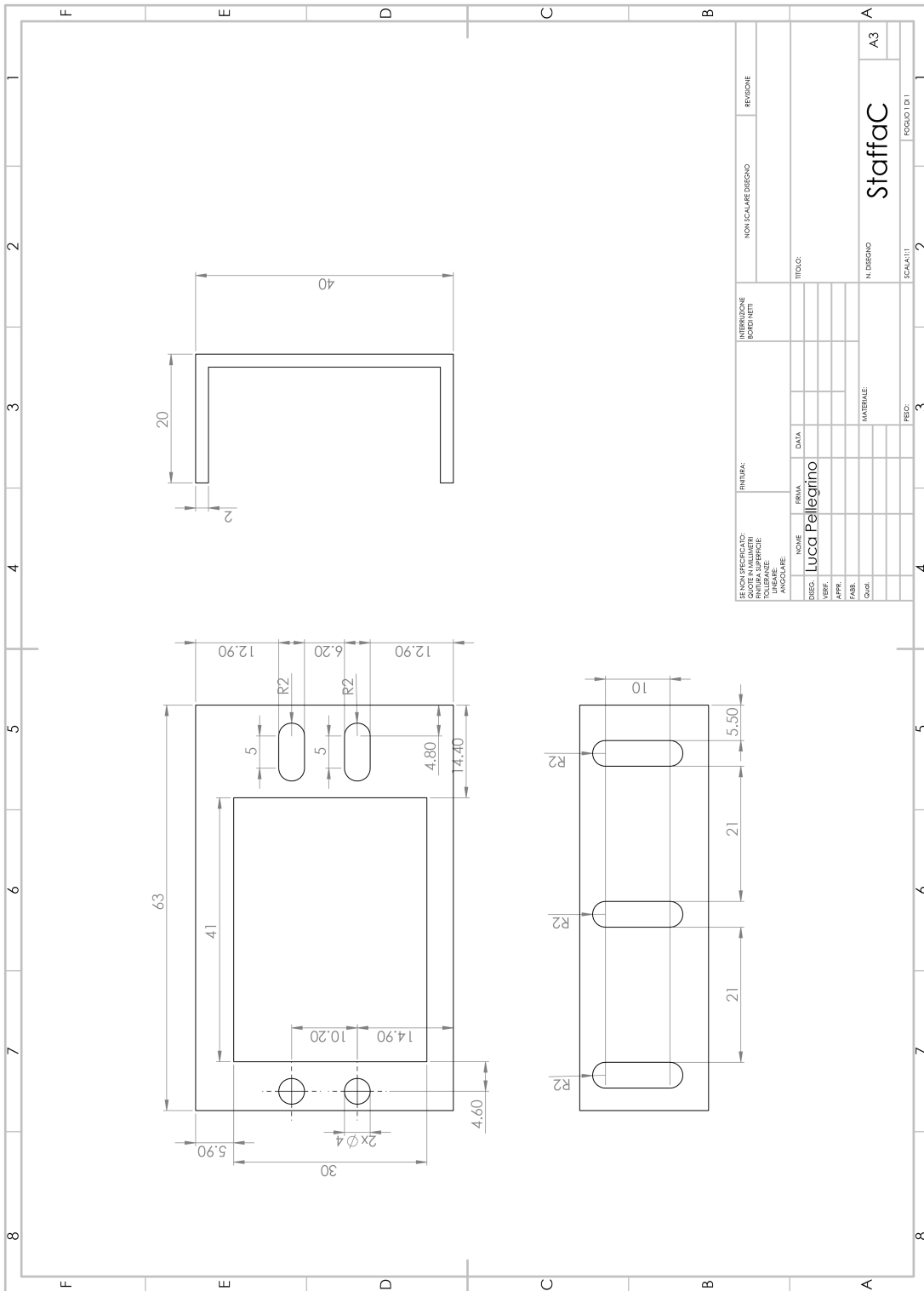


Figure C.2: C-section IPE beam

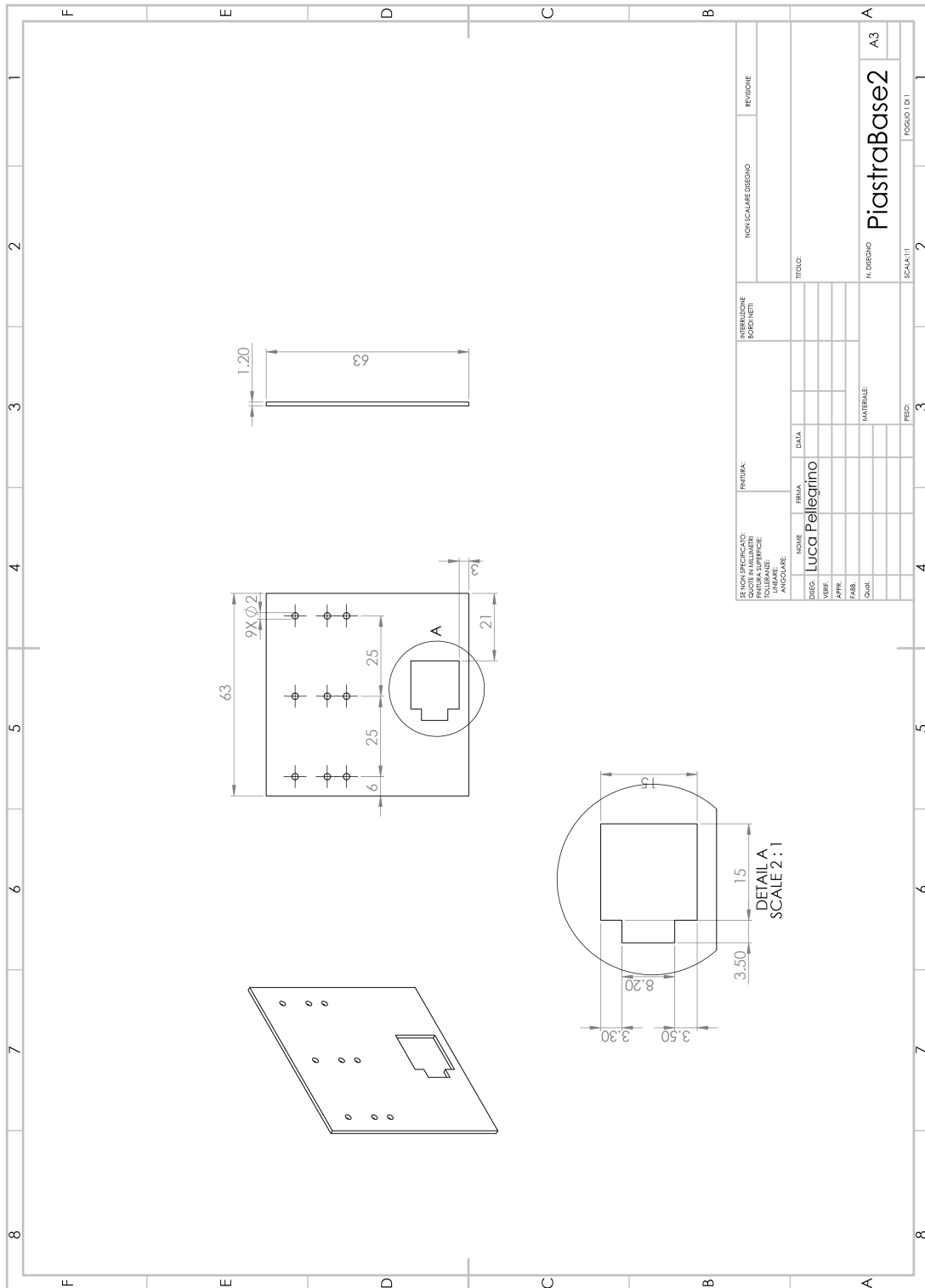


Figure C.3: Glide Plate



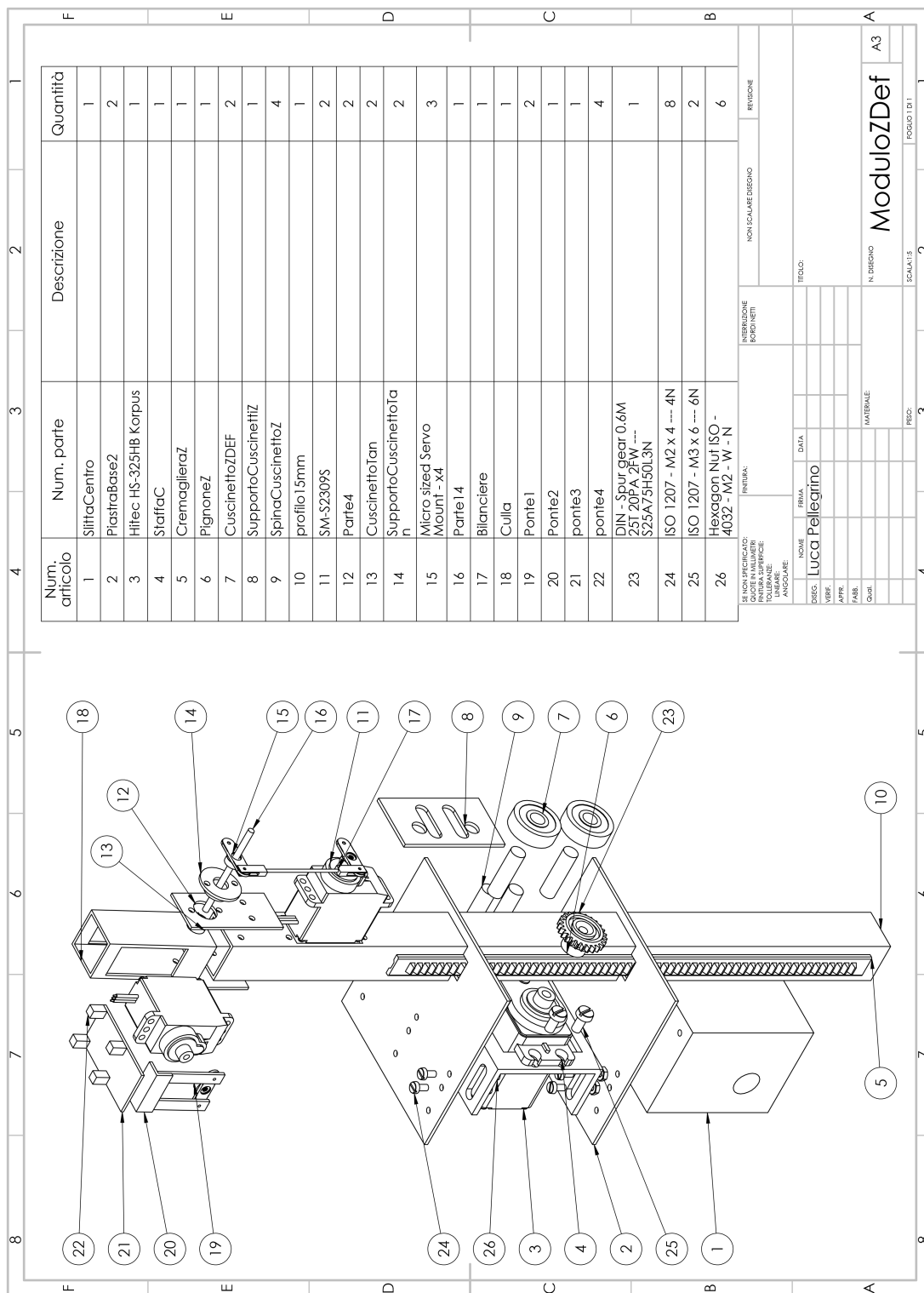


Figure C.4: Module exploded view: Bill Of Material (BOM)



# Bibliography

- [1] S. Agarwal, N. Snavely, S. Seitz, and R. Szeliski. Bundle Adjustment in the Large Computer Vision. In *Eccv*, volume 6312, pages 29–42, 2010.
- [2] C. Anurag, A. S. Harsha, and C. K. Anvesh. Auxetic materials. *International Journal for Trends in Engineering & Technology*, 5(2):156–160, 2015.
- [3] E. P. Baltsavias. A comparison between photogrammetry and laser scanning. *ISPRS Journal of Photogrammetry and Remote Sensing*, 54(2-3):83–94, 1999.
- [4] M. Bordegoni, F. Ferrise, M. Covarrubias, and M. Antolini. Haptic and sound interface for shape rendering. *Presence: Teleoperators and Virtual Environments*, 19(4):341–363, 2010.
- [5] G. Champion, Q. Wang, and V. Hayward. The pantograph Mk-II: A haptic instrument. In *2005 IEEE/RSJ International Conference on Intelligent Robots and Systems, IROS*, pages 723–728, 2005.
- [6] B. Cao, E. M. Bringa, and M. A. Meyers. Shock compression of monocrystalline copper: Atomistic simulations. In *Metallurgical and Materials Transactions A: Physical Metallurgy and Materials Science*, volume 38 A, pages 2681–2688, 2007.
- [7] B. Cao, D. H. Lassila, C. Huang, Y. Xu, and M. A. Meyers. Shock compression of monocrystalline copper: Experiments, characterization, and analysis. *Materials Science and Engineering A*, 527(3):424–434, 2010.
- [8] Y.-K. Chang and A. P. Rockwood. A generalized de Casteljau approach to {3D} free-form deformation. In *Proceedings of SIGGRAPH 94*, pages 257–260, 1994.
- [9] Z. Q. Cheng and R. C. Batra. Deflection relationships between the homogeneous Kirchhoff plate theory and different functionally graded plate theories. *Archives of Mechanics*, 52(1):143–158, 2000.

- [10] M. Covarrubias, M. Bordegoni, U. Cugini, and M. Antolini. Desktop haptic Strip for exploration of virtual objects. In *3DUI 2011 - IEEE Symposium on 3D User Interfaces 2011, Proceedings*, pages 101–102, 2011.
- [11] H. Decker. Analytical photogrammetry, 1980.
- [12] K. E. Evans. Auxetic polymers: a new range of materials. *Endeavour*, 15(4):170–174, 1991.
- [13] R.-D.-L.-T. Gabriel and V. Hayward. Virtual surfaces and haptic shape perception. In *Proceedings ASME IMECE Symposium on Haptic Interfaces for Virtual Environments and Teleoperator Systems*. 2000.
- [14] V. Hayward. Survey of Haptic Interface Research at McGill University. In *Workshop in Interactive Multimodal Telepresence Systems*, pages 91–98, 2001.
- [15] Hexcel Composites. Honeycomb Attributes and Properties, A comprehensive guide to standard Hexcel honeycomb materials, configurations, and mechanical properties. *Honeycomb Data Sheets*, pages 1–40, 1999.
- [16] Iwata, Yano, Nakaizumi, and Kawamura. Project FEELEX: adding haptic surface to graphics. *Proceedings of SIGGRAPH 2001*, (1):469–475, 2001.
- [17] a. M. L. Kappers. Human perception of shape from touch. *Philosophical Transactions of the Royal Society B: Biological Sciences*, 366(1581):3106–3114, 2011.
- [18] S. Klare, D. Forssilow, and A. Peer. Formable object - A new haptic interface for shape rendering. In *2013 World Haptics Conference, WHC 2013*, pages 61–66, 2013.
- [19] W. T. Koiter. The Stability of Elastic Equilibrium, 1945.
- [20] A. Krishnamoorthy and D. Menon. Matrix Inversion Using Cholesky Decomposition. *CoRR*, (3):10–12, 2011.
- [21] S. J. Lederman and L. a. Jones. Tactile and Haptic Illusions. *IEEE Transactions on Haptics*, 4(4):273–294, 2011.
- [22] S. J. Lederman and R. L. Klatzky. Lederman&Klatzky1987 Handmovements.pdf. *Cognitive Psychology*, 19:342–368, 1987.
- [23] D. Leithinger and H. Ishii. Relief: a scalable actuated shape display. *Proceedings of the fourth international conference on Tangible, embedded, and embodied interaction*, pages 221–222, 2010.

- [24] M. I. A. Lourakis and A. A. Argyros. SBA: A Software Package for Generic Sparse Bundle Adjustment. *ACM TOMS*, 36(1):30 pp, 2009.
- [25] A. Mansutti. *Tactile Display for virtual 3D shape rendering*. PhD thesis, 2014.
- [26] U. Mansutti, Alessandro, Covarrubias, Mario, Bordegoni, Monica, Cugini. Haptic strip based on modular independent actuators for virtual shapes rendering. In *IEEE Haptic Symposium*, Houston, Texas, USA, 2014.
- [27] K. Morgan, O. Hassan, and N. P. Weatherill. The Finite Element Method. *Academy of Engineering Polish Academy of Science Chinese Academy of Sciences National Academy of Science Italy (Accademia dei Lincei)*, 35(4):110–114, 1981.
- [28] Y. Nakagawa, S. Yonekura, and Y. Kawaguchi. Super thin 3D form display for multimodal user experiences using vertically deformation of leaf spring and SMA. In *ISVRI 2011 - IEEE International Symposium on Virtual Reality Innovations 2011, Proceedings*, pages 63–66, 2011.
- [29] E. Nava-Yazdani and K. Polthier. De Casteljau algorithm on manifolds. *Computer Aided Geometric Design*, 30(7):722–732, 2013.
- [30] Niu Ming Qi and E. Pennestr?? Optimum balancing of four-bar linkages. *Mechanism and Machine Theory*, 26(3):337–348, 1991.
- [31] K. Ogata. *Modern Control Engineering*, volume 17. 2002.
- [32] A. M. Okamura. Uniting Haptic Exploration and Display. In *Robotics Research: The Tenth International Symposium on Robotics Research*, number Vol. 6, pages 225–238. 2003.
- [33] G. Pahl and W. Beitz. *Engineering design: a systematic approach*, volume 34. 1996.
- [34] L. Piegl and W. Tiller. *The NURBS Book*, 1996.
- [35] W. R. Provancher, M. R. Cutkosky, K. J. Kuchenbecker, and G. Niemeyer. Contact Location Display for Haptic Perception of Curvature and Object Motion. *The International Journal of Robotics Research*, 24(9):691–702, 2005.
- [36] C. Ramstein and V. Hayward. The pantograph: a large workspace haptic device for multimodal human computer interaction. *Conference companion on Human factors in ...*, pages 57–58, 1994.

- [37] G. Robles-de-la torre and V. Hayward. Virtual surfaces and haptic shape perception. In *Haptic Interfaces for Virtual Environment and Teleoperator Systems Symposium, ASME International Mechanical Engineering Congress & Exposition*, 2000.
- [38] D. Salomon. *Curves and surfaces for computer graphics*. 2006.
- [39] R. Schellingerhout, a. W. Smitsman, and G. P. van Galen. Exploration of surface-textures in congenitally blind infants. *Child: care, health and development*, 23(3):247–64, 1997.
- [40] R. Schellingerhout, A. W. Smitsman, and G. P. Van Galen. Haptic object exploration in congenitally blind infants. *Journal of Visual Impairment & Blindness*, 92(9):674—, 1998.
- [41] E. Schweikardt and M. D. Gross. Digital clay: Deriving digital models from freehand sketches. *Automation in construction*, 9(1):107–115, 2000.
- [42] M. Solazzi, A. Frisoli, F. Salsedo, and M. Bergamasco. A fingertip haptic display for improving local perception of shape cues. In *Proceedings - Second Joint EuroHaptics Conference and Symposium on Haptic Interfaces for Virtual Environment and Teleoperator Systems, World Haptics 2007*, pages 409–414, 2007.
- [43] R. H. Sturges, K. O’Shaughnessy, , and R. G. others Reed. A systematic approach to conceptual design. *Concurrent Engineering*, 1, 1993.
- [44] S. Subramanian, C. Gutwin, M. N. M. Sanchez, C. Power, and J. Liu. Haptic and Tactile Feedback in Directed Movements. *Proceedings of Guidelines On Tactile and Haptic Interactions*, 2:37–42, 2005.
- [45] E. A. Thompson. Linkage Analysis. In *Handbook of Statistical Genetics*, pages 1141–1167. 2008.
- [46] R. a. van den Berg, H. C. J. Hoefsloot, J. a. Westerhuis, A. K. Smilde, and M. J. van der Werf. Centering, scaling, and transformations: improving the biological information content of metabolomics data. *BMC genomics*, 7:142, 2006.
- [47] D. S. Watkins. *Gaussian Elimination and Its Variants*. 2005.
- [48] G. Y. G. Ye, J. J. Corso, G. D. Hager, and A. M. Okamura. VisHap: augmented reality combining haptics and vision. *SMC03 Conference Proceedings 2003 IEEE International Conference on Systems Man and Cybernetics Conference Theme System Security and Assurance Cat No03CH37483*, 4:3425–3431, 2003.

- 
- [49] Z. W. Yin. Direct generation of extended STL file from unorganized point data. *CAD Computer Aided Design*, 43(6):699–706, 2011.